63-3-1

SOLAR ENERGY MEASUREMENT TECHNIQUES

TECHNICAL DOCUMENTARY REPORT ASD-TDR-62-882

January 1963

Flight Accessories Laboratory
Aeronautical Systems Division
Air Force Systems Command
Wright-Patterson Air Force Base, Ohio

Project No. 8173, Task No. 817301-12

Prepared under Contract No. AF 33(616)-7946
by Hoffman Semiconductor Division
Hoffman Electronics Corporation
El Monte, California

Authors: Dr. Bernd Ross
D. B. Bickler

NOTICES

When Government drawings, specifications, or other data are used for any purpose other than in connection with a definitely related Government procurement operation, the United States Government thereby incurs no responsibility nor any obligation whatsoever; and the fact that the Government may have formulated, furnished, or in any way supplied the said drawings, specifications, or other data, is not to be regarded by implication or otherwise as in any manner licensing the holder or any other person or corporation, or conveying any rights or permission to manufacture, use, or sell any patented invention that may in any way be related thereto.

Qualified requesters may obtain copies of this report from the Armed Services Technical Information Agency, (ASTIA), Arlington Hall Station, Arlington 12, Virginia.

This report has been released to the Office of Technical Services, U.S. Department of Commerce, Washington 25, D.C., in stock quantities for sale to the general public.

Copies of this report should not be returned to the Aeronautical Systems Division unless return is required by security considerations, contractual obligations, or notice on a specific document.

23-540M, 200, 4-2-6

Aeronautical Systems Division, Dir/Aeromechanics, Flight Accessories Lab, Wright-Patterson AFB, Ohio.
Rpt Nr ASD-TDR-62-882. SOLAR ENERGY MEASUREMENT TECHNIQUES. Final report, Jan 63, 167p. incl illus., tables, 56 refs.
Unclassified Report

This report describes a broad investigation which has been made of the subject of solar cell measurements. A portable tester has been designed and built which will enable an operator to determine the output of a solar cell power supply in space by analyzing output under conditions existing at either laboratory or field test sites. Painstaking

(over)

experimentation and analysis of many alternatives has resulted in recommended optimum instrumentation and procedures for measuring solar cells and for performing the calibrations required. Calibrated primary standard solar cells have been provided in terms of their absolute spectral response. Data has been accumulated on the operational parameters of many solar cells using optimized measurement procedures.

1. Solar energy
2. Cell measurement techniques
3. Portable testers
I. AFSC Project 8173, Task 817301-12
II. Contract AF 33 (616)-7946
III. Hoffman Electronics Corp., El Monte, Calif.
IV. Dr. B. Ross, D. B. Bickler
V. Aval fr OTS
VI. In ASTIA collection

Aeronautical Systems Division, Dir/Aeromechanics, Flight Accessories Lab, Wright-Patterson AFB, Ohio.
Rpt Nr ASD-TDR-62-882. SOLAR ENERGY MEASUREMENT TECHNIQUES. Final report, Jan 63, 167p. incl illus., tables, 56 refs.
Unclassified Report

This report describes a broad investigation which has been made of the subject of solar cell measurements. A portable tester has been designed and built which will enable an operator to determine the output of a solar cell power supply in space by analyzing output under conditions existing at either laboratory or field test sites. Painstaking

(over)

experimentation and analysis of many alternatives has resulted in recommended optimum instrumentation and procedures for measuring solar cells and for performing the calibrations required. Calibrated primary standard solar cells have been provided in terms of their absolute spectral response. Data has been accumulated on the operational parameters of many solar cells using optimized measurement procedures.

1. Solar energy
2. Cell measurement techniques
3. Portable testers
I. AFSC Project 8173, Task 817301-12
II. Contract AF 33 (616)-7946
III. Hoffman Electronics Corp., El Monte, Calif.
IV. Dr. B. Ross, D. B. Bickler
V. Aval fr OTS
VI. In ASTIA collection

FOREWORD

This report was prepared by the Semiconductor Division of Hoffman Electronics Corporation, El Monte, California on Air Force Contract AF 33(616)-7946 under Project No. 8173, Task No. 817301-12, "Study and Applied Research on Measurement Techniques for Solar Energy Converters." The work was administered under the direction of the Flight Accessories Laboratory, Aeronautical Systems Division. Joseph F. Wise is the project engineer on this contract for ASD.

The studies presented began in March 1961 and continued until August 31, 1962. The effort was primarily the responsibility of the Research and Development Department under the direction of Dr. Warren Eriksen. Although the studies were a group effort, the chief contributors and their fields of interest were: Dr. Bernd Ross, Photo Devices; Mr. William Paterson, Computer Circuitry; Mr. Lawrence W. Schmidt, Measurements; Mr. James M. Palmer, Calibration Procedures and Data Reduction; and Mr. Donald Bickler, Spectroradiometric Procedures.

This Technical Documentary Report is a Final Report covering the construction and calibration phase of Contract AF 33(616)-7946. This report is unclassified.

TABLE OF CONTENTS

ABSTRACT

This report describes a broad investigation which has been made of the subject of solar cell measurements. A portable tester has been designed and built which will enable an operator to determine the output of a solar cell power supply in space by analyzing output under conditions existing at either laboratory or field test sites. Painstaking experimentation and analysis of many alternatives has resulted in recommended optimum instrumentation and procedures for measuring solar cells and for performing the calibrations required. Calibrated primary standard solar cells have been provided in terms of their absolute spectral response. Data has been accumulated on the operational parameters of many solar cells using optimized measurement procedures.

TABLE OF CONTENTS (Cont'd.)

LIST OF ILLUSTRATIONS

LIST OF ILLUSTRATIONS (Cont'd.)

LIST OF ILLUSTRATIONS (Cont'd.)

LIST OF ILLUSTRATIONS (Cont'd.)

LIST OF ILLUSTRATIONS (Cont'd.)

LIST OF TABLES

1.0 INTRODUCTION

This report describes the program of investigations of solar cell measurements which has been carried out following the guidelines laid down in Technical Note ASD-TN-61-156 (Design Study of Solar Energy Measurements Techniques).

The following sections summarize the work done in three major areas -- Solar Cell Tester Fabrication and Test, Calibration, and Procedure Standardization. Significant accomplishments and complications are pointed out in these sections, but more detailed technical information on all pertinent topics will be found in Appendixes I thru VII. Conclusions and recommendations are also to be found in these Appendixes.

Manuscript released by the authors 11-9-62 for publication as an ASD Technical Documentary Report.

2.0 SUMMARY OF EXPERIMENTAL FABRICATION AND TEST PHASE

A portable tester has been designed and built which represents a self-contained system that will enable the operator to determine the output of a solar cell power supply in space by analyzing the output of the power supply under conditions existing at either laboratory or field test sites.

The tester consists of four main pieces of equipment, the curve-tracer, the computer, a sensor head and an associated pyrheliometer system mounted on a tripod. See Figs. 1 and 2.

Light striking the panel under test also strikes the sensor head which rapidly indexes through 13 positions, allowing light to strike standard cells through 13 different spectral filter windows. The resulting signals are fed into a computer which is programmed in accordance with the spectrum of sunlight in space and with spectral response of the solar cell panel being measured. The computer produces an output which can be utilized by the curve-tracer unit to produce a smooth I-V curve of the panel under both the test conditions and the conditions of space.

2.1 CURVE-TRACING UNIT OF PORTABLE TESTER

2.1.1 PERFORMANCE REQUIREMENTS

Projecting the state-of-the-art of solar panels into the next few years, it was decided to build the tester with a capability of testing a 1000 watt panel. This decision was based upon the data presented in Fig. 3. Figure 3 is a log-log plot of the current-voltage characteristics of several existing solar power systems presently available. The labeled points represent the respective peak power points for each supply. The arrows represent the current and voltage range necessary to achieve a reading as low as 2% of peak value. This plot shows that it is necessary for the curve-tracing load circuit to operate over a range of four orders of magnitude. The curve-tracing apparatus in use at Hoffman utilizes a manually varied resistance as the variable load when recording an I-V curve. This apparatus requires a degree of operator skill in order to prevent an overshoot of the recorder in the vicinity of peak power when an effort is being made to record the data as rapidly as possible. Rapid recording is desirable because it minimizes

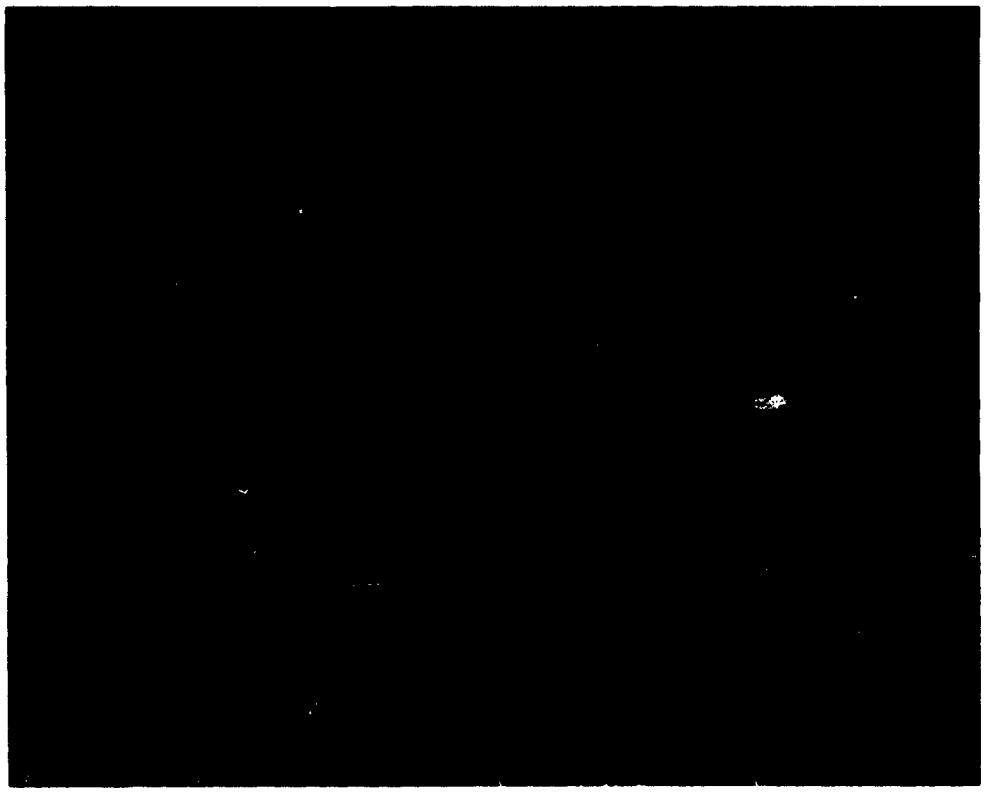

FIGURE 1 COMPUTER & CURVE-TRACER

FIGURE 2 PYRHELIOMETER AND MOUNT

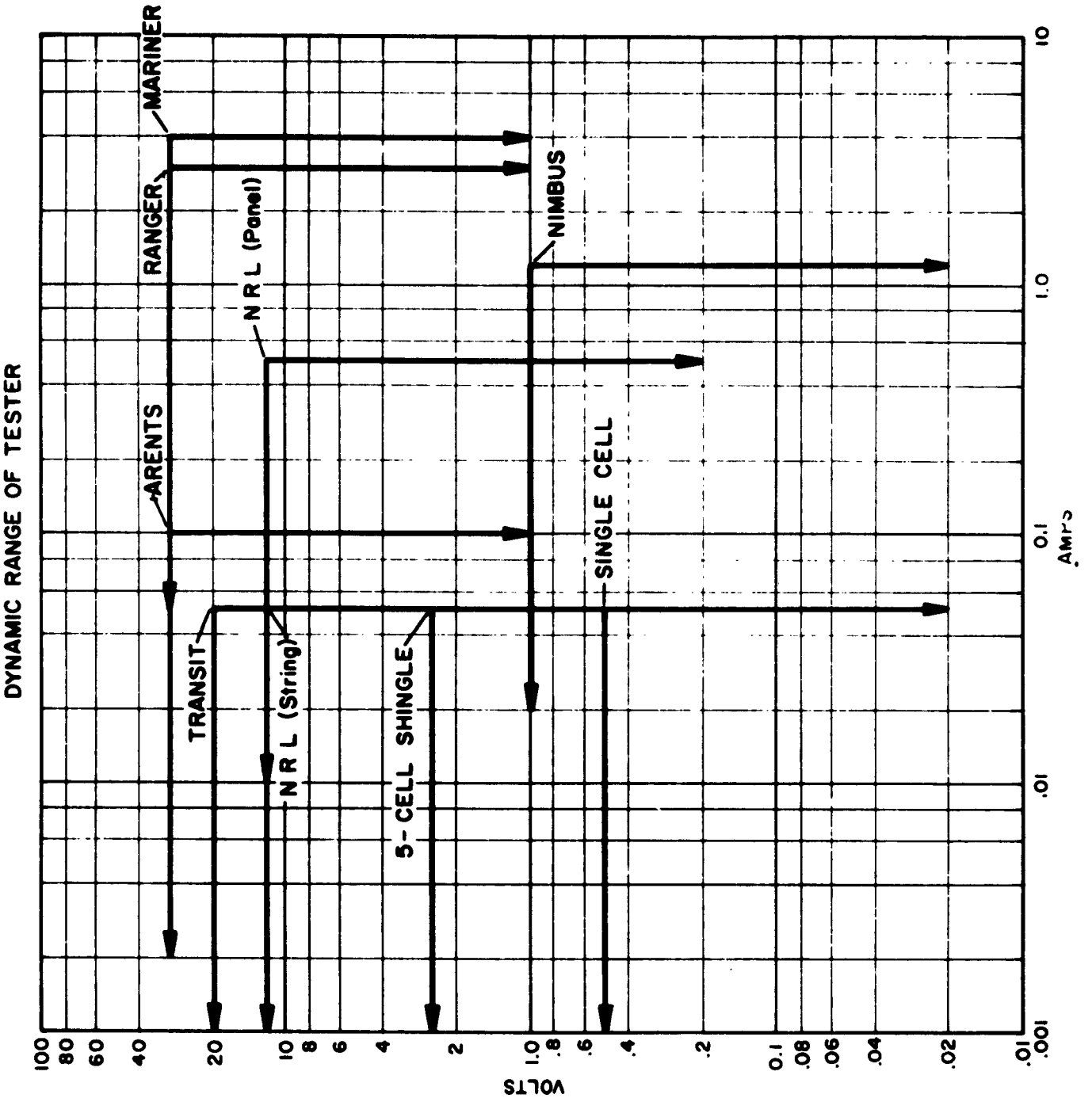

Figure 3. Dynamic Range of Tester

the effect of light source variations. In order to eliminate the operator, the portable tester is built with an automatically controlled transistor load circuit. This circuit is designed to hold constant the sum of the velocities in both the x direction and the y direction. The pen-tracing speed is variable, by means of a panel control, from zero to approximately 4 inches per second. Overshooting was found to occur at the knee in the curve near the peak power range with velocities in excess of approximately 2 inches per second.

2.1.2 FINAL CURVE-TRACING CIRCUIT DESIGN

With this combination of sensitivity and capacity, the load circuit was designed and breadboarded. Breadboarding served to optimize individual component values and determine local heat transfer loads. The heat exchanger for the 1000 watt transistor load was made compact by designing the system for a low continuous load and providing energy surge storage. The transistors are mounted on approximately 1-1/2 lbs. of copper for the purpose of absorbing heat surges.

A schematic of the curve-tracing portion of the tester is shown in Fig. 4.

2.2 COMPUTER UNIT OF PORTABLE TESTER

2.2.1 SENSOR UNIT OF COMPUTER

2.2.1.1 PERFORMANCE REQUIREMENTS

The spectral characteristics of the optical filters were altered from the characteristics listed in ASD TN-61-156. The study and planning phase showed that it is necessary to analyze the region between .850μ and 1.150μ with greater resolution than other regions. The original filter specifications were based upon this information and the fact that interference filters fall into bandwidth groups based upon the bandwidth expressed as a percentage of peak transmission wavelength.

The filter manufacturers agreed to the specifications but were unable to meet them in practice. After several attempts, a set of filters was made covering the desired range of the spectrum with the necessary resolution in the near infrared

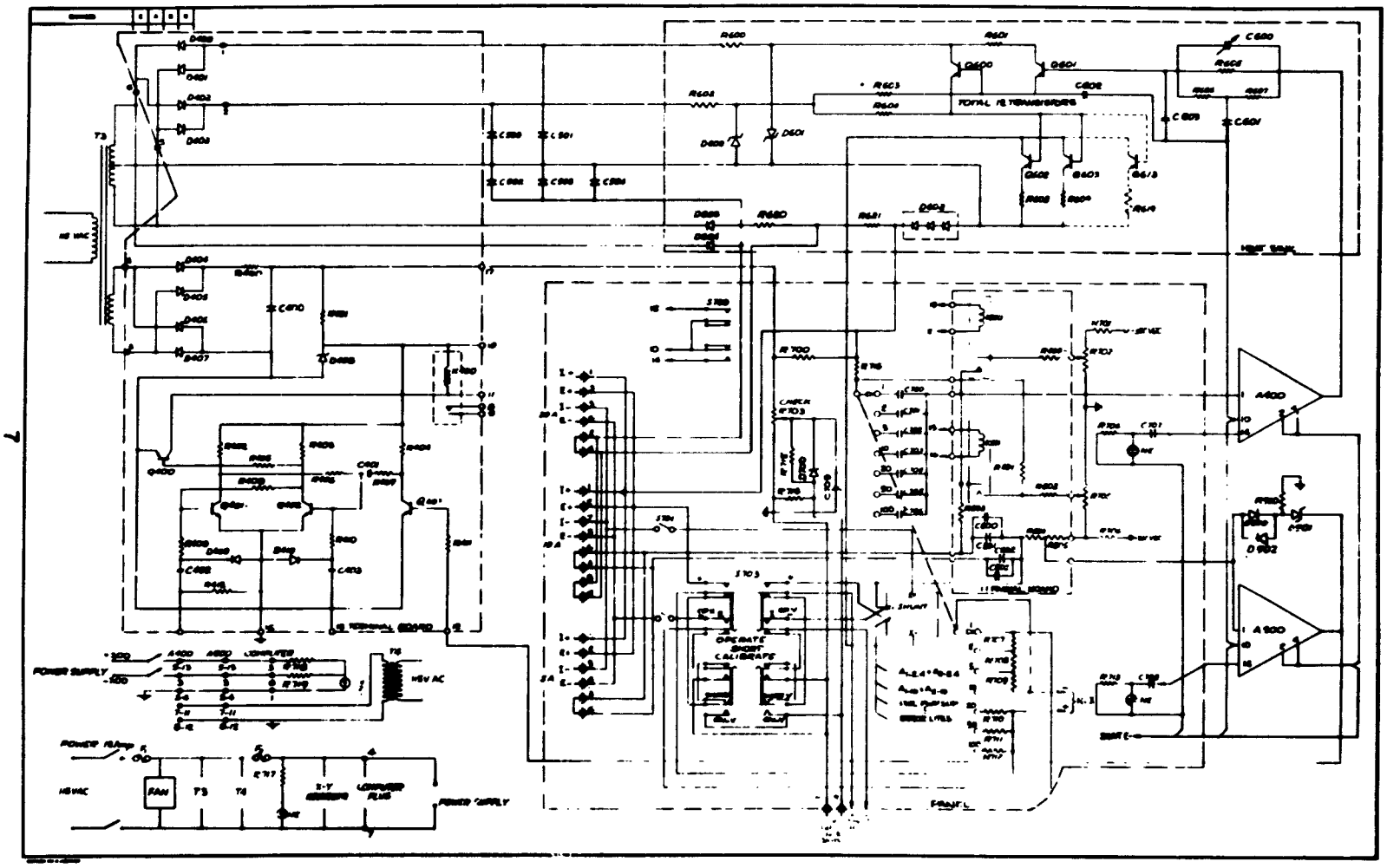

Figure 4. Curve Tracer Circuit

but differing from the spectral grouping detailed in ASD TN-61-156. For the sake of expediency these filters were accepted. The spectral response of all the channels is shown in Fig. 5. This data is for the filter and sensor combinations due to the fact that the channel response would be different if measured with a sensor of different spectral response. The response for each channel has been normalized to a common peak value. Early experiments with the spectral filters showed that it is necessary to prevent light from entering the filter glass from the edge, on the sensor side of the interference film. If light is allowed to bypass the interference film by this means, an error occurs which can be of the same order of magnitude as the desired signal strength.

The absolute transmission of the filter used in channel #1 is sufficiently high to allow the use of a silicon sensor. This eliminates the problems associated with a selenium sensor.

A small germanium cell is mounted over the center of the silicon sensor for sensing the infrared beyond the wavelengths where silicon responds. The spectral response of this germanium cell is shown in Fig. 6.

2.2.1.2 OPERATION

The filter channels in the sensor are synchronized with the amplifier channels in the computer by means of a switch pulse. This switch is cam operated by the filter wheel. A second cam energizes the filter wheel drive motor in all positions of operation except the "at rest" position. Due to this second cam, the wheel will return to the "at rest" position when power is supplied to the tester. The initial synchronization of the stepper switch in the computer is accomplished by manually operating the stepper switch until it corresponds to the starting position. An indicator light on the panel shows when the switch is on starting position. Another indicator light shows when the scanning cycle is complete.

After initial synchronization, the sensor wheel and the stepping switch will remain synchronized.

The timing for the synchronizing cam was made adjustable. The completion of the amplifier signal cycle for each channel is timed electronically by mono-stable flip-flop circuits.

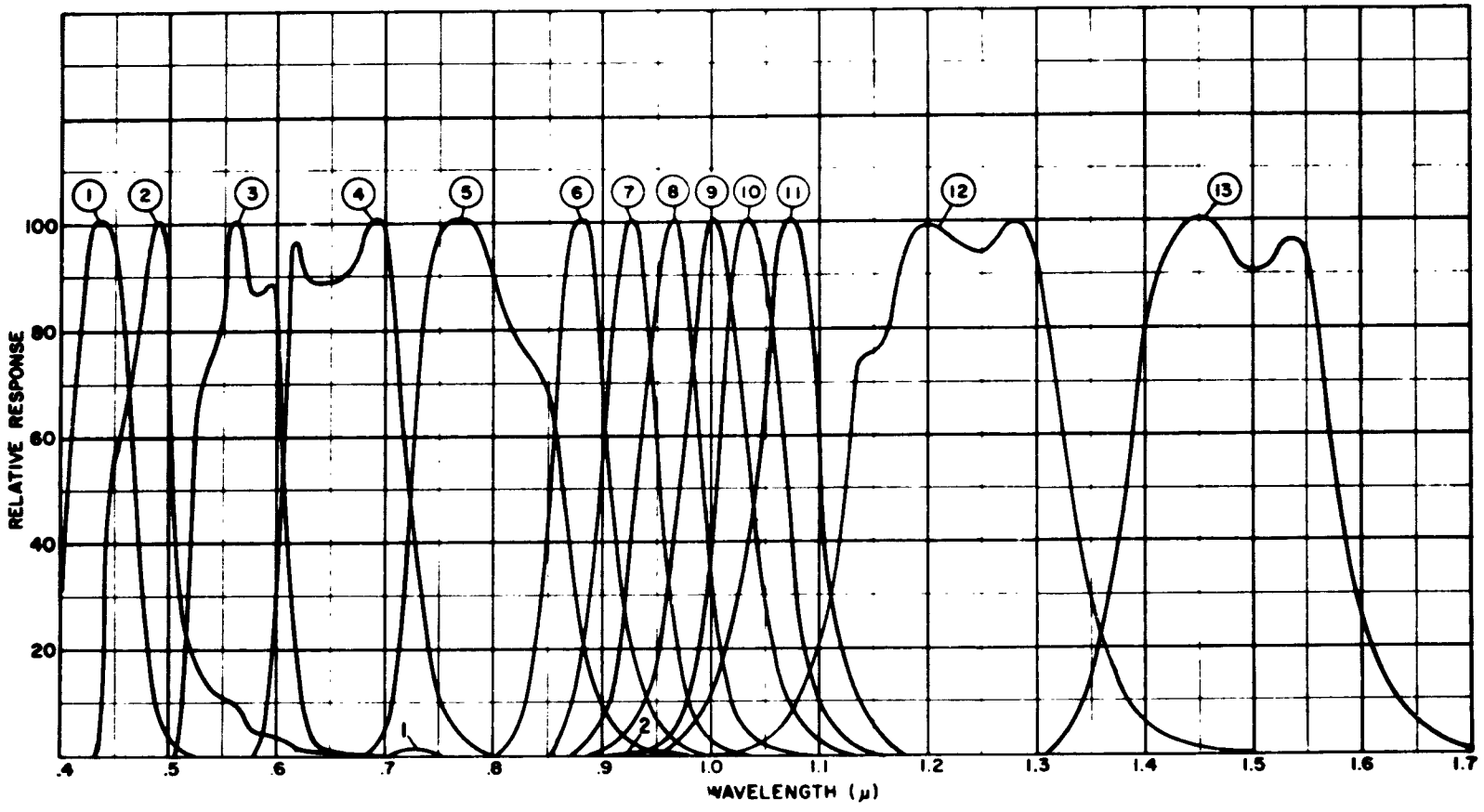

FIGURE 5 - SPECTRAL RESPONSE OF TESTER CHANNELS

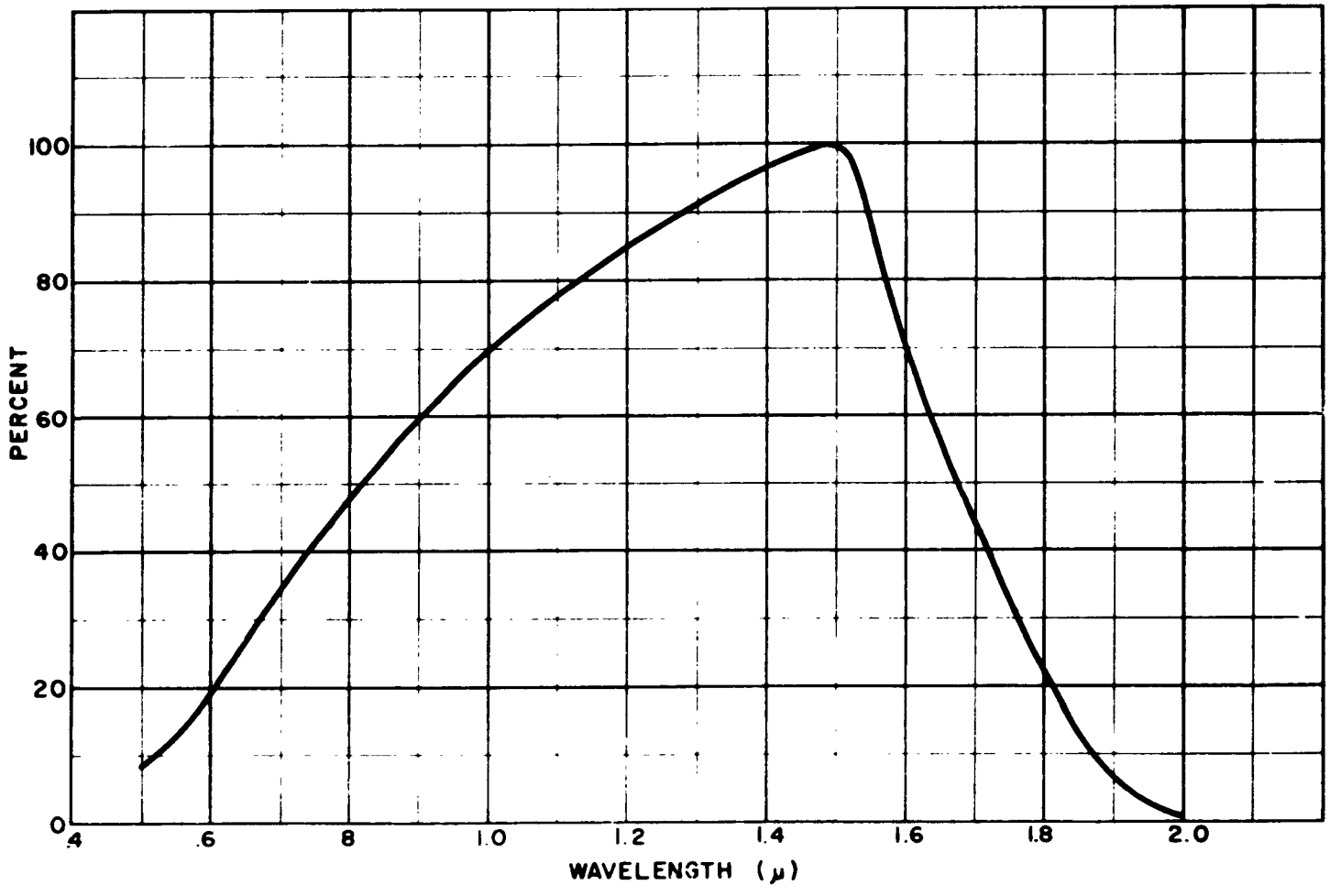

FIGURE 6- RELATIVE SPECTRAL RESPONSE
GERMANIUM SOLAR CELL

2.2.2 OPERATIONAL AND READOUT UNIT OF COMPUTER

The first amplifier operates on the signals from either the sensor or the space substitution circuit. The mode of operation is selected by a switch on the front panel.

In the "measure" mode, the sensor is illuminated by the light source under test. The signals from the sensor are amplified to provide a signal output which is proportional to the energy input in each channel. Each channel is provided with a variable feedback network which is adjusted to achieve this proportionality.

The space substitution circuit consists of a stable voltage source and individual resistive dividers for each channel. When the space substitution mode is in operation, the voltage from the resistive dividers are fed into the input of the first amplifier. These voltages represents the outputs that the sensor channels would have if the sensor were exposed to solar illumination in earth space.

It was necessary to build a conductance decade in order to function as the "scaler" mentioned in ASD TN-61-156. A simple voltage divider would be non-linear due to loading of the circuit. An additional stage of amplification would accomplish the scaler function, but the additional circuitry and power supply requirements would make the unit unnecessarily bulky. The scaler is inserted between the first and second amplifiers.

The second amplifier controls the spectral response function generator. With the front panel control in the "intensity" mode, the input spectral distribution is multiplied by a constant corresponding to a flat detector. In the "response product" mode the spectral distribution is multiplied by the detector spectral response that is programmed on the spectral response display panel. In addition, the potentiometers may be set to be equivalent to the inverse bandwidths of the channels to allow direct energy plots to be made.

The third amplifier functions as the totalizer. This section sums the signals from the thirteen channels. This process is not instantaneous, but takes approximately three seconds, corresponding to the time of completion of the sensor cycle. The switch leakage problems in the totalizing circuit have been

solved by the use of glass-sealed reed relays. These relays combine the advantages of rapid switching time, low leakage and low contact resistance.

The schematic diagram of the computer is shown in Fig. 7.

2.3 PYRHELIOMETER READOUT

The pyrheliometer electrical signals require a chopper stabilized amplifier for readout instrumentation. The vacuum tube voltmeter selected satisfies this amplification requirement. This unit was found to be the most accurate, commensurate with bulk and weight. Because it is a complete readout system, the pyrheliometer, equatorial mount and tripod, and VTVM readout unit comprise an integral system which may be operated independently of the tester. As an additional feature, the meter is available for field use as a normal volt-ohm-amp meter.

Provisions were made in the portable tester to crosscheck the voltage read on the x-y recorder, the digital voltmeter and the vacuum tube voltmeter. This check voltage is variable by means of a panel control on the curve tracing unit.

3.0 SUMMARY OF CALIBRATION PHASE

The calibration phase of this study has resulted in refinement of measurements due to certain critical areas which had previously not been recognized as critical. The problems incurred in solar cell calibration can be divided into two major categories. One category is that of relative spectral measurements, the other category is total radiation intensity measurement.

3.1 RELATIVE SPECTRAL MEASUREMENT

For purposes of this discussion relative spectral measurement includes the relative spectral response of solar cells as well as the relative spectral distribution of light sources. Both measurements are subject to errors arising from stray radiation in the monochromator. It was necessary to determine whether or not the system was subject to stray radiation errors and if so to eliminate them.

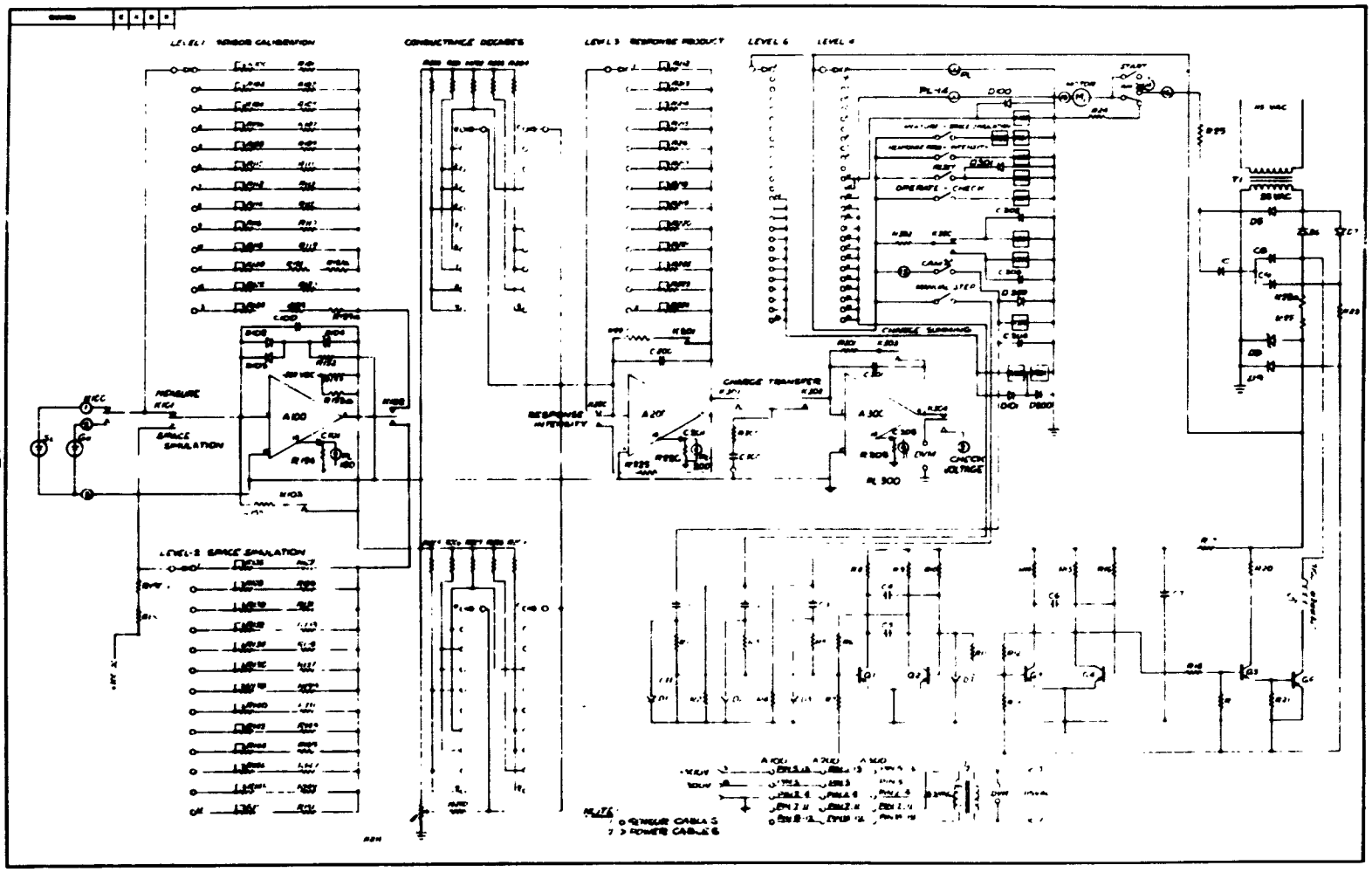

Figure 7. Special Computer Circuit

3.1.1 RELATIVE RESPONSE ERRORS

Stray radiation influence upon relative spectral response measurements was investigated by varying the range of the spectrum used as the monochromator input signal. Measurements were performed with the following light sources:

A. Bare tungsten lamp.

B. Tungsten lamp with infrared attenuating filter.

C. Tungsten lamp with infrared eliminating filter.

The infrared attenuating filter used is a 2" square of Corning glass CS-1-56 lapped to approximately .025" thickness and then polished. The thinner section was necessary to avoid a complete cutoff in the vicinity of 0.8 microns and to reduce the absorption in the near ultraviolet.

The infrared eliminating filter blocked out all radiation beyond 0.8μ. There was no measurable difference in the spectral response taken with the infrared eliminating filter and the infrared attenuating filter. Using the bare tungsten lamp reduces the measured spectral response at 0.45μ to 55% of the value when measured with infrared filters due to stray radiation. The conclusion drawn from these experiments is that the infrared attenuating filter used by Hoffman for the past year has reduced stray radiation and yielded correct spectral response measurements.

3.1.2 RELATIVE DISTRIBUTION ERRORS

When the spectral range is extended to include 0.3μ to 2.0μ, the possibility of stray radiation errors is increased. Measurements were made to determine if the calibration of light sources for use with solar cells was influenced by stray radiation in a single pass monochromator. The monochromator was calibrated with tungsten ribbon filament lamps supplied by the National Bureau of Standards. These lamps have been intensity calibrated with respect to their spectral radiation in the wavelength range from 0.25μ to 2.6μ.

3.1.3 SUNLIGHT SPECTRAL MEASUREMENTS

The monochromator was fitted with a heliostat of measured reflectivity. On June 23, 1960 the spectral distribution of the

sunlight on Table Mountain, California was measured with this apparatus. At the same time the spectrum was recorded by Dr. A. G. Froiland of the Smithsonian Institution, on the instrument which was at the time permanently installed on Table Mountain. For the purposes of this contract this data was received by Hoffman Electronics in April 1962, and reduced in May 1962. Data reduction consisted of generating the energy response function of the spectrometer by taking the inverse of the prism dispersion characteristic. The dispersion characteristic was listed in the Annals of the Smithsonian Institution and checked with the measured dispersion from the data. The data was in the form of an exposed glass photographic plate(1). The distance was measured between known atmospheric absorption bands and plotted as a dispersion characteristic. Three scale changes occurred in the exposure of the glass plate. These scale changes were evaluated by equating the energy on both sides of the change. The energy response function was then modified by the reflectivity of the coelostat mirrors and the transmission of the quartz prism. This correction data was found in the Annals of the Smithsonian. The results of this data reduction are shown in Fig. 8. The agreement between the two curves at the red and blue ends of the spectra shows that there was an equal amount of stray radiation, if any, in both instruments.

A disagreement was pointed out in the wavelength range of 0.6μ to 0.9μ. The instruments disagree by approximately 8%. This disagreement occurs where the solar cell response is greatest. This problem has not yet been resolved. Because of this calibration problem, no attempts were made to measure relative spectral distributions for the purpose of calibrating primary standard cells.

3.1.4 SUNLIGHT SPECTRAL CALCULATIONS

Standard cells were calibrated by using evaluations to modify the spectrum above the atmosphere to conditions at the time of test. Primary standard #28 was calibrated by this method and was later found to have an 8% difference in absolute spectral response from standards calibrated at a later date in natural

---

(1) Annals of the Astrophysical Observator of the Smithsonian Institution, (1902), p. 57.

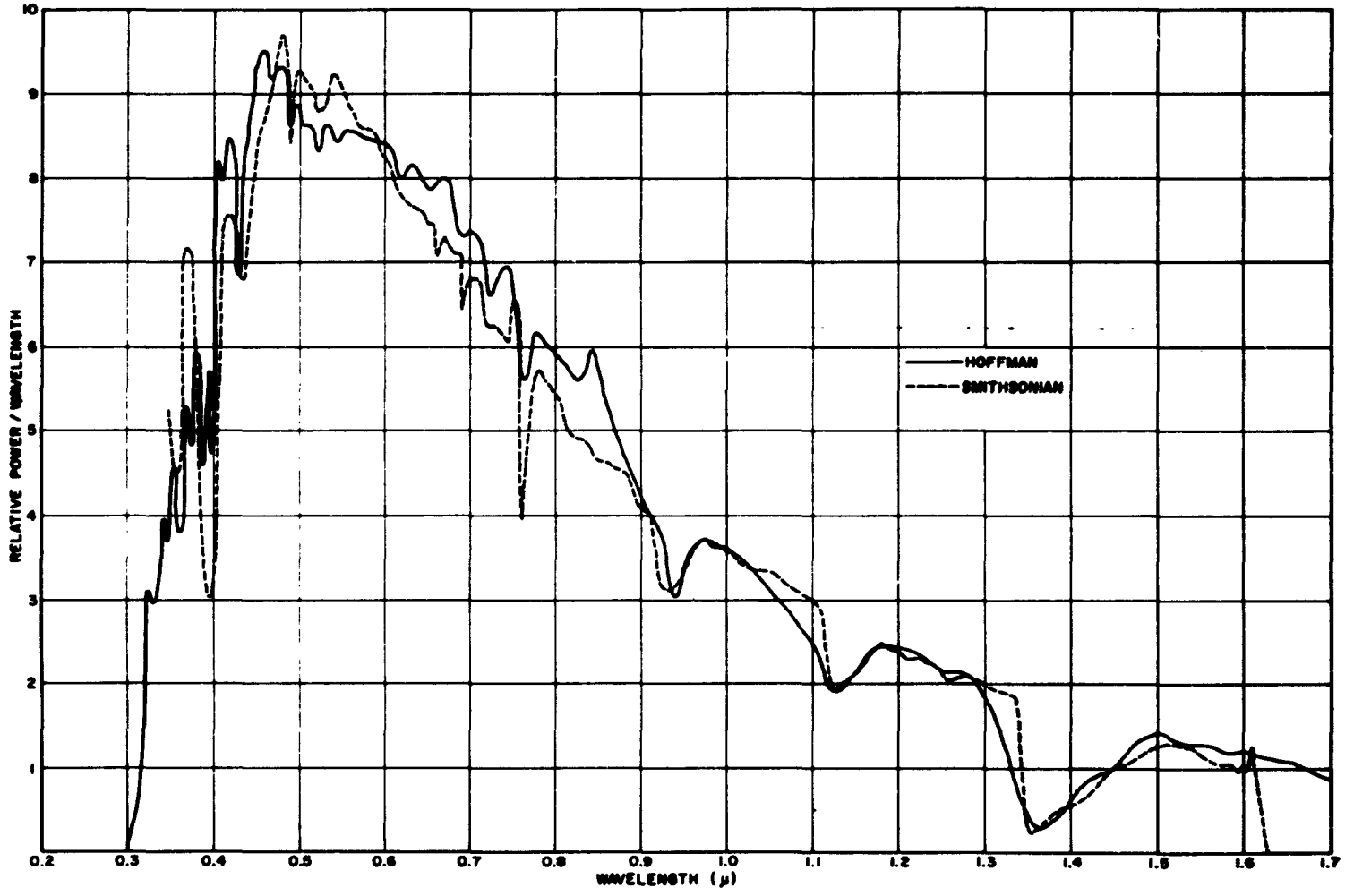

FIGURE 8 - INCIDENT SOLAR RADIATION SPECTRAL DISTRIBUTION, TABLE MOUNTAIN, CALIF., 6-23-60

sunlight. The 8% discrepancy between the calibration of primary #28 and standard #52 (internal std. of HSD) has been explained by the fact that an actual total atmospheric humidity measurement was not taken at the time of the #28 calibration. The calibration of #28 was based upon an assumption of 5mm of precipitable moisture. This amount agreed with both the average of moisture figures taken from the Annals of the Smithsonian Institution and with the measurements taken by Hoffman at Table Mountain several months previously. An analysis was made to find the accuracy dependence of this assumption. It was found that assuming no moisture at all would raise the cell output above the atmosphere by more than 17% over the output calculated for a 5 mm moisture assumption. The cells calibrated at a later time were calibrated by the method described in Appendix VII.

3.1.5 TUNGSTEN SPECTRAL MEASUREMENTS

The tungsten ribbon filament lamps which are calibrated by the National Bureau of Standards are calibrated in absolute spectral intensity at the filament surface. A device was constructed which used a curved mirror to focus the image of the lamp filament on a special cell with dimensions less than those of the filament image. The reflectivity of the curved mirror was measured by measuring the reflectivity of flat mirror samples which were aluminized at the same time as the curved mirror. The calculated space outputs of these cells, based upon this calibration, fell approximately 10% below the expected value obtained with older standard cells. Further investigation showed several errors were possible in this system due to focusing problems with the mirror because the ribbon filament is not a point source of light. This process was, therefore, abandoned for the more favorable one described in Appendix I.

Attempts to calibrate absolute spectral response of standard cells with tungsten lamps had proven faulty in the past. This was attributed to the inability of the 180° weather bureau type pyrheliometer to properly read the tungsten energy beyond 2μ wavelength. In order to eliminate this difficulty a 1/8 inch water filter was used in conjunction with a tungsten lamp calibrated for color temperature at given voltages. The transmission of the water filter was measured and applied to the published tungsten spectrum. Figure 9 is the relative

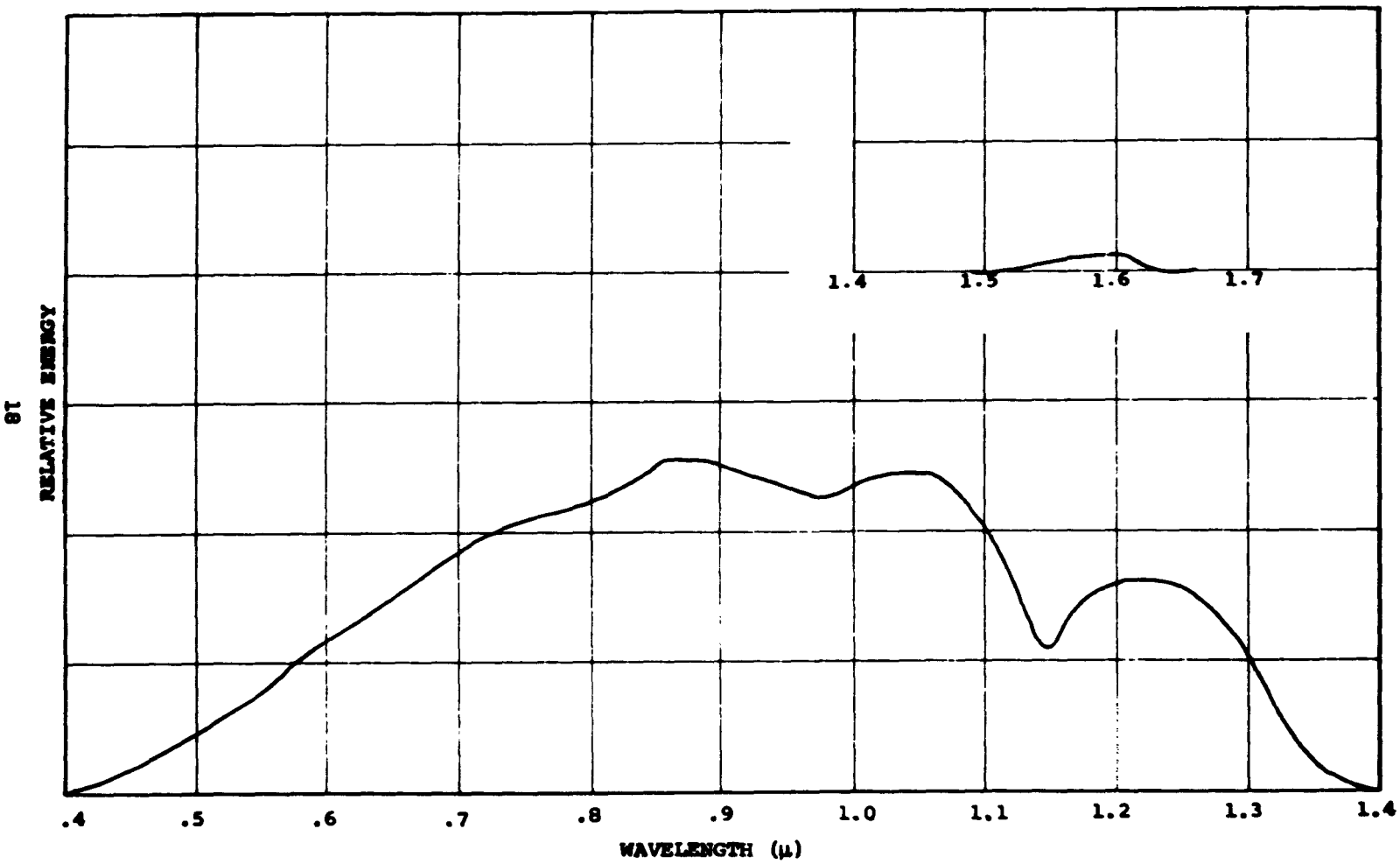

FIGURE 9 RELATIVE SPECTRAL DISTRIBUTION OF TUNGSTEN LAMP WITH WATER FILTER

spectral distribution of the combination of a 1/8" water filter and a tungsten lamp set at 2800°K. Because this spectrum is essentially limited to wavelength less than 1.4μ, the spectral difficulties with the 180° pyrheliometer were expected to be insignificant. The results proved approximately 10% low as compared to what was expected. The calibrated color temperature lamps used for calibration of the color temperature meter were compared to the ribbon filament standards from the NBS. The two NBS ribbon filament lamps read approximately 115°K lower than the three coiled filament lamps purchased as color temperature standards.

Calculations were made in an attempt to justify this color temperature difference on the basis of emissivity differences between the coiled filament and the ribbon filament. These calculations did not explain the 115°K color temperature difference. Tungsten spectral calculations are described in Appendix III.

The accepted method for measuring color temperature utilizes a Lummer-Brodhun contrast photometer in which the human eye is used as the criterion of comparison between the test source and an equivalent black body radiation source. When the human eye declares the test source and the black body of equivalent chromaticity, the black body temperature is the color temperature of the test source.

The Hoffman color temperature meter described in Appendix V utilizes solar cells and filters which compare the long wavelength distribution band (peak at .98μ) and short wavelength distribution band (peak at .58μ), see Fig. 10, of the test source and arrive at an equivalent color temperature. Due to the fact that the human eye has a significantly different spectral response from the solar cell, a difference in distribution seen as a small error by the solar cell, may be interpreted as a major error by the human eye. Since the silicon solar cell is the basic device to be measured under this contract, it was felt that the HEC color temperature meter is a useful device to assure repeatability in light source settings. However, since the absolute accuracy is questionable in the light of the above, the proposed light source setting is made independent of the color temperature meter (see Appendix I) and based entirely on NBS ribbon lamps utilizing NBS recommended settings.

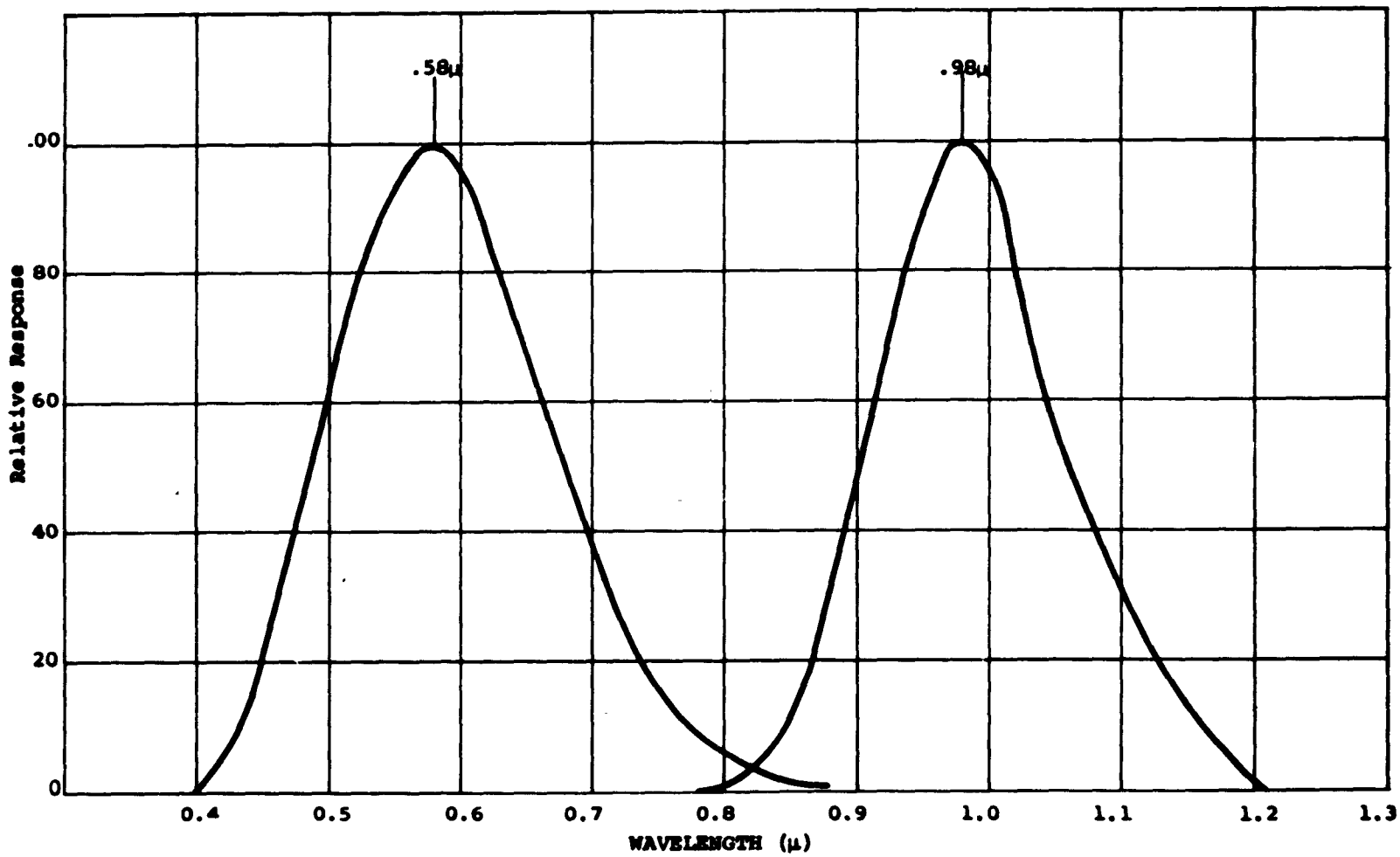

FIGURE 10 SPECTRAL RESPONSE - COLOR TEMPERATURE TARGET "B"

3.2 ABSOLUTE SPECTRAL MEASUREMENTS

The problems of absolute spectral measurement contain, in addition to those of relative spectral measurement, the problems of total radiation intensity measurement. Experiments performed with the two 180° weather bureau type pyrheliometer at Hoffman have shown a difference in excess of 20% between the ratios of signals under red lights and blue lights. This data agrees with data published by Gier & Dunkle[2] which shows a significant variation in reflectance at 1.0μ-2.5μ as a function of thickness of MgO. The thickness varied from 0.02 in. to 0.04 in. The pyrheliometer MgO coating is certainly less than 0.04 in. thick, and is therefore subject to spectral inaccuracy due to insufficient thickness. The absorptivity of MgO is listed by McAdams[3] as 0.08 at 6000°K and 0.14 at 3000°K. The conclusion drawn from these experiments and publications was that the pyrheliometers which are accurate to within 3/4% agreement with the Smithsonian Astrophysical Laboratory under sunlight, cannot be used to read the intensity of tungsten or other light sources, if a known accuracy is required.

An analysis was made of the linearity of the pyrheliometer with intensity. Calculations based upon thermocouple data supplied by Eppley showed a temperature difference of 7.25°C between hot junctions and cold junctions under 100mW/cm^2 solar radiation. The voltage output as a function of temperature difference is within 0.1% of linear throughout this range. The hot junction heat transfer by conduction is linear with temperature difference. The hot junction heat loss by radiation is a function of the fourth power of the absolute temperatures and as a result is less than 1% from linear through this range. The hot junction heat transfer by convection is a function of the temperature difference to the one-fourth power. It is necessary to know the total magnitude of the convection heat losses in order to determine the effect upon pyrheliometer linearity.

---

(2) R. V. Dunkle, "Spectral Reflectance Measurements", First Symposium Surface Effects on Spacecraft Materials, Ed. F. J. Clauss, Wiley & Sons, (1960), p. 117.

(3) McAdams, "Heat Transmission", McGraw-Hill, (1954), p. 62.

The relationship between radiation intensity and pyrheliometer output has been demonstrated, under natural conditions and in the laboratory, to be linear to within $\pm$ 1 percent over the intensity range 0.1 to 1.5 cal.cm^{-2}min.$^{-1}$ (4).

In July 1962 an Eppley normal incidence pyrheliometer was received and total intensity measurements were made. Standard cells were calibrated using the NBS ribbon filament lamps as relative spectral intensity sources only and reading total intensity with the normal incidence pyrheliometer. Standard cells calibrated by these means agreed with expected values within 4%. The primary standard cells for this contract were calibrated by these means. The detailed procedure is described in Appendix I.

4.0 SUMMARY OF STANDARDIZATION OF PROCEDURES PHASE

4.1 STANDARD REFERENCE SOLAR CELLS

710 solar cells were examined. The results of these measurements reported in ASD-TN-61-156 and Appendix VI were utilized in selecting primary and secondary standard cells. Calibration and measurement procedures were developed based upon the above findings. These calibration procedures are detailed in Appendices I and II. As a result of the studies inherent in this work, certain parameters were found to be considerably more critical than expected.

4.2 SINGLE LIGHT SOURCES

Artificial light sources comprising tungsten, tungsten-iodine, xenon, xenon-mercury, and carbon were experimentally investigated. In addition, data was gathered on commercially marketed space sun simulators. This data appears in Appendix III. Tungsten is spectrally not suited for solar cells measurements, but it has the advantages of good stability and universal availability. Tungsten-Iodine lamps are not recommended due

---

(4) "Performance Characteristics of Eppley 180° 10- and 50- Junction Pyrheliometers (Pyranometers). The Eppley Laboratory, Inc., March 25, 1960.

to their short life under conditions of continuous use. Xenon is a good light source in the blue portion of the spectrum but is not recommended for solar cell measurements unless steps are taken to suppress the strong spectral lines in the infrared region. Due to discrete spectral lines throughout the total range of emission of the xenon-mercury lamp, combined with a more rapid degradation rate, these lamps are not recommended for solar cell measurements.

Carbon arcs are spectrally best suited for single source space sun duplication; however, provisions must be made to compensate for the inherent lack of stability.

An analysis of the effect of short term stability is included in Appendix III which shows the importance of utilizing low ripple power supplies for light sources.

4.3 COMBINATION AND MODIFIED LIGHT SOURCES

Several combination and modified light sources have been investigated through a literature survey (See Appendix III). In all of these units, the attempt has been made to have the spectral distribution equivalent to that of space as indicated by the NRL curve[5].

A subcommittee, formed by the AIEE, has recommended acceptable deviations[6] from the NRL curve for the solar simulators. According to the literature search, none of the units has spectral distributions within these tolerances. The present state-of-the-art of spectral intensity measurement makes it extremely difficult to permit confinement of measurement error to limits as narrow as the tolerances prescribed in the AIEE proposed specification.

4.4 PORTABLE TESTER

The portable tester described in section 2.0 may be used for the standardization of measurements of solar cells and solar

---

(5) Johnson, F. S., "The Solar Constant," J. Meteorol., Vol. 11, No. 6, p. 431 (1954).

(6) Solar Cell Measurements Standardization, Lockheed Aircraft Corp., LMSD-288184 (1960).

cell power supplies. A summary of the operation of the tester follows.

An I-V curve of the converter being tested is drawn with the plotter portion of the tester.

The sensor head is placed in a position such that it receives energy identical to the converter being tested.

An assumed spectral response is programmed into the spectral response portion of the computer. The digital readout is reset to zero and the channels are scanned. The digital reading is compared to the I_{sc} of the converter and the scaler set to a multiplier which will bring the digital reading to equal the I_{sc} of the converter. The digital is reset and the channels scanned to check this scaler setting.

The converter and the sensor are exposed to energy of a different spectral distribution if it is desired to check the assumed spectral response. The previous process is then repeated without changing the scale settings.

If the proper spectral response was assumed, the readings will remain identical. If, however, the computer reading is greater than the new I_{sc} of the converter, it means that the assumed spectral response is too great for the wavelength range being examined. By a series of successive approximations, the programmed spectral response may be adjusted to equal the equivalent spectral response of the converter being tested. The possible variations in the spectral response of the solar cell converter are sufficiently defined in Appendix VI to allow accurate initial estimation of spectral response and sufficient knowledge of response variation to minimize the number of approximations.

When the short circuit current readings agree under different conditions of illumination, the computer setting is adjusted to agree with the converter spectral response.

The computer is then switched from the sensor circuit to the space substitution circuit. The totalizer is reset and channels are scanned to yield the I_{sc} of space.

With the I_{sc} value for space, the plotter axes are altered to yield the I-V curve of the converter under the anticipated conditions.

In order to spectrally analyze a light source, the spectral response channels are set, one at a time, to 100% response. The tester is cycled and the digital reads the energy for that particular channel.

APPENDIX I

PROCEDURES FOR CALIBRATING AND CHECKING PRIMARY REFERENCE SOLAR CELLS UNDER ARTIFICIAL LIGHT

1.0 INITIAL PARAMETERS

Four parameters are required to accurately calibrate standard solar cells in terms of absolute spectral response. The information obtained from these measurements and their associated calculations form a basis for determining the absolute spectral response of the solar cell.

1.1 RELATIVE SPECTRAL RESPONSE

The relative spectral response of a solar cell is measured on a modified Perkin-Elmer Model 98 monochromator, shown in Fig. 11. This instrument has been calibrated for wavelengths from 0.3 to 1.5μ, using the known wavelengths of the line spectra of neon, mercury, helium, and hydrogen.

The energy received by the monochromator thermocouple is reflected by two first surface mirrors, M_6 and M_7, after the exit slit. The solar cell being measured is exposed directly to the energy behind the exit slit. In order to eliminate the spectral correction necessary with these mirrors, a thermopile, T', is inserted directly into the path of the energy directed onto the solar cell being measured. A thermopile is used behind the exit slit because a single thermocouple is not sufficiently sensitive without focusing mirrors.

The thermopile detector, Fig. 12, was specially modified for this application. The characteristics of the thermopile are as follows: Calcium fluoride window; 10 ohm resistive impedance; 3 microvolt per microwatt sensitivity at 13 cycles per second chopping frequency.

An energy vs. wavelength curve of a tungsten lamp is plotted on an X-Y recorder. The lamp is a type 9A/t8½/1 lamp operating at a color temperature of 2800°K ±10°K. The spectrum from the lamp is modified by a Corning glass filter CS-1-56

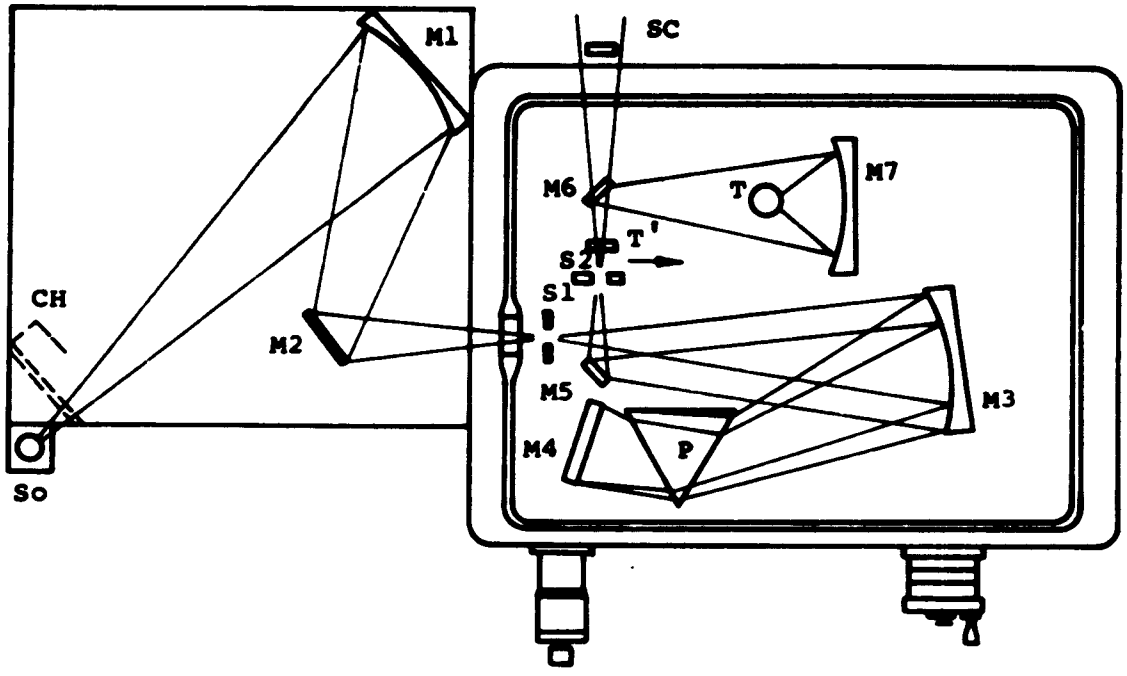

FIGURE 11 MODIFIED MODEL 98 MONOCHROMATOR

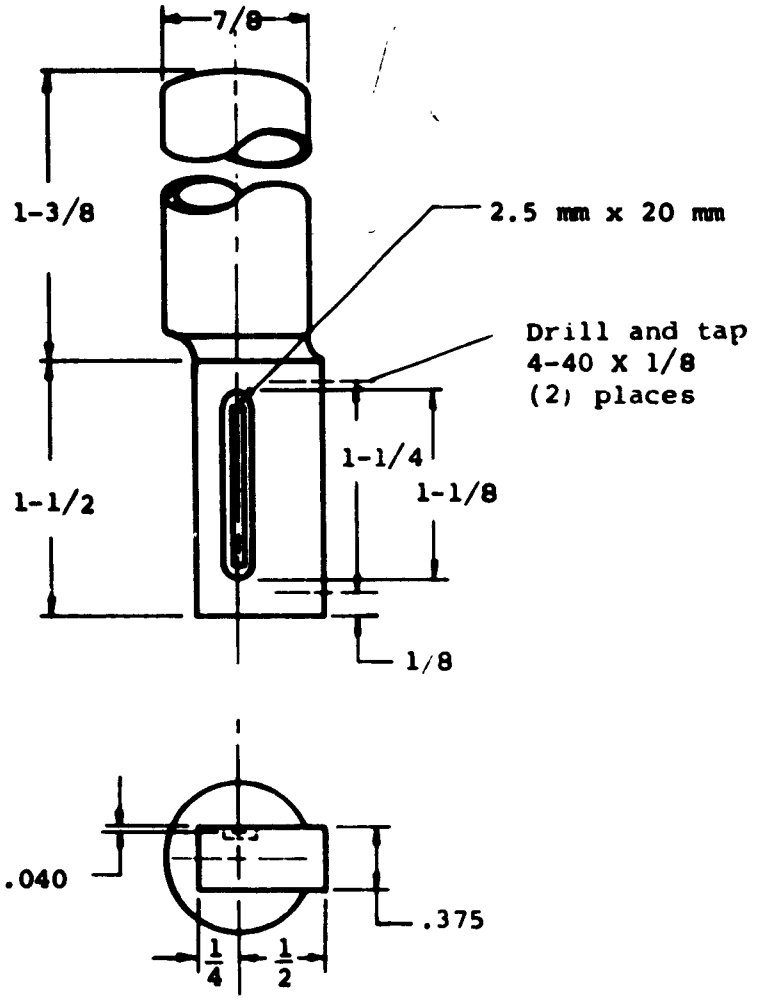

FIGURE 12 MODIFIED THERMOPILE

x .025 inch to remove excessive infrared energy and reduce stray radiation. The energy from the exit slit is recorded using the thermopile. The solar cell under test is then placed in the optical path and its output (short circuit current) is plotted as a function of wavelength on the same graph as the thermopile curve, as shown in Fig. 13. By dividing the cell output at each wavelength by the corresponding thermopile (flat detector) output, a relative spectral response curve is obtained, Fig. 14.

1.2 RELATIVE SPECTRAL DISTRIBUTION

The lamp chosen for the determination of absolute spectral distribution is the GE 30A/T24/7 obtained from the National Bureau of Standards as "standards of spectral irradiance." These lamps have a quartz window fused at the end of an extension which reduces the deposits formed as a result of filament evaporation. This extension causes light spots in the intensity pattern due to wall reflection. The effect of these reflections is eliminated by placing a one inch orifice at the end of the lamp extension.

The lamp was calibrated by using focusing mirrors which placed the unwanted wall reflections out of focus. Attempts to duplicate this type of procedure were unsuccessful due to the sensitivity of the mirror reflectivity measurements and the focus intensity relationship.

A 0.5 mm x 5 mm portion from the center of the filament is, rigorously, the only calibrated portion of the lamp. The filament is 44 mm long and 3 mm wide. When the lamp is operated at approximately 15 amps, no color gradient is noticeable in the center 25 mm of the filament. It is necessary to view the filament in a dark room to prevent reflections from the filament giving the illusion of color gradients. When the lamp is operated at 30 amps, the brightness prevents visual observation. At the higher current, end effects are reduced and the uniformity of filament temperature is improved.

1.3 TOTAL RADIATION INTENSITY

The total energy output of the lamp is measured with a normal incidence pyrheliometer, calibrated against a Smithsonian Angstrom secondary standard pyrheliometer located in Newport, R.I.

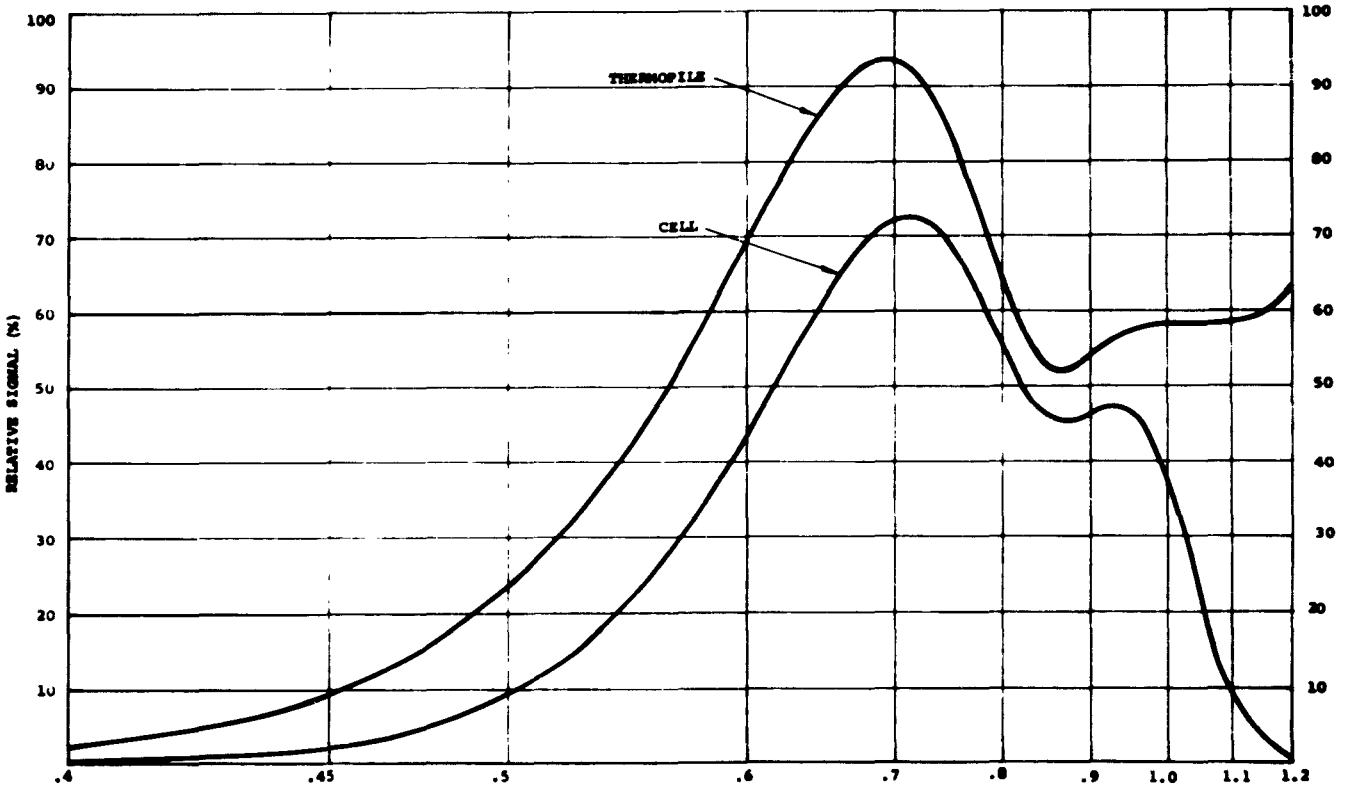

FIGURE 13 SOLAR CELL SPECTRAL RESPONSE

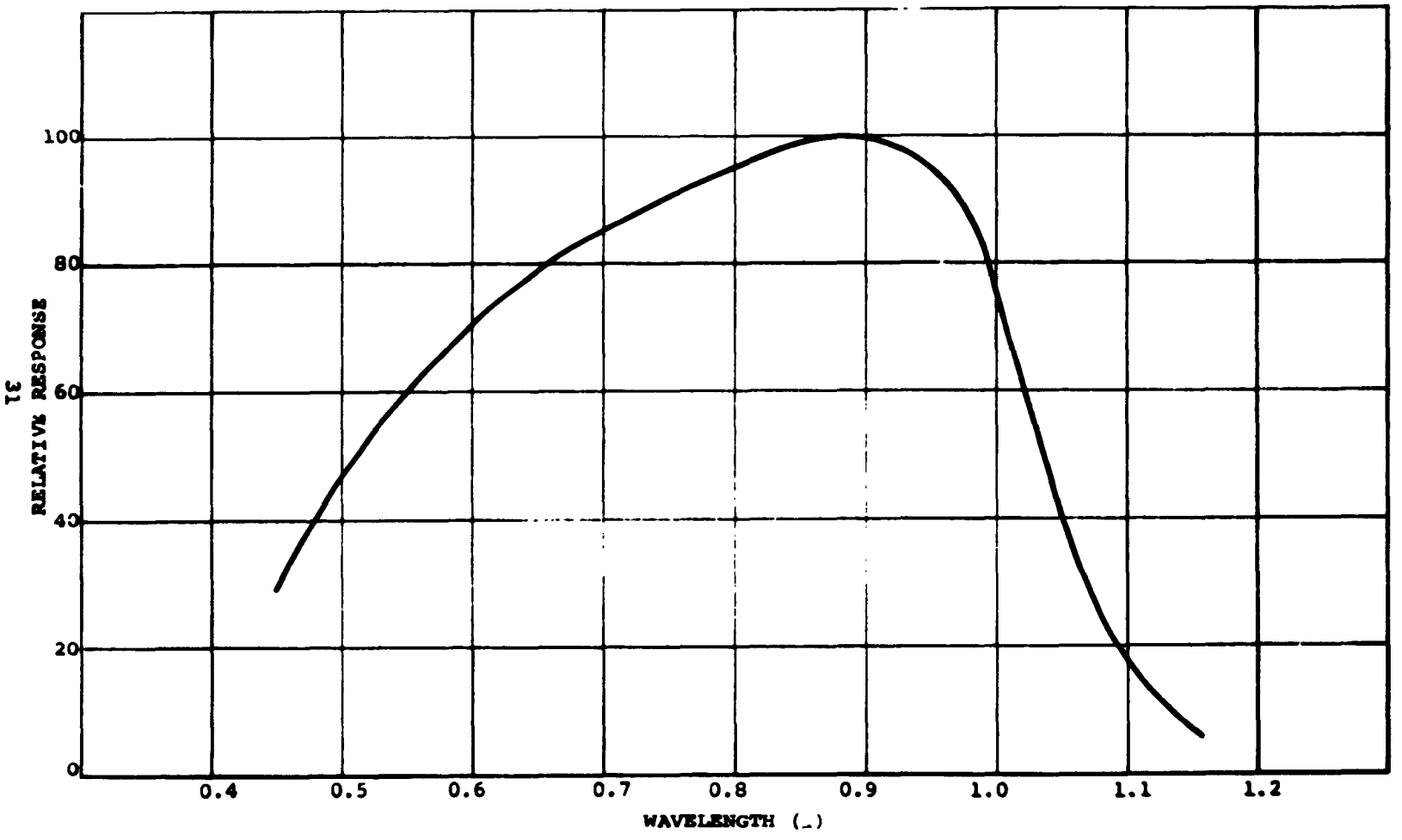

FIGURE 14 RELATIVE SPECTRAL RESPONSE

This energy is recorded in millivolts on a digital voltmeter and is converted to give intensity in mW/cm^2.

The relative spectral distribution is plotted to a convenient energy scale vs. a wavelength scale of 0.1μ/inch on the horizontal. The radiation is extrapolated from 2.6μ to 5.0μ by using data from General Electric[1]. The transmission of the quartz window is taken from Amersil Quartz[2] and applied from 3.6μ to 5.0μ. The area under this curve is integrated with a planimeter. This area is the graphical equivalent to the total energy as measured by the pyrheliometer. The vertical scale is multiplied by the ratio necessary to convert the scale into absolute units of $mW/cm^2/0.1\mu$.

1.4 SHORT CIRCUIT CURRENT

The short circuit current of the standard cell being calibrated must be measured at the same intensity indicated by the pyrheliometer. Precautions must be taken to assure that the cell is at the same distance from the filament as the pyrheliometer detector. The pyrheliometer detector is positioned 208 mm from the front collimation orifice. The uniformity of the intensity field must be scanned to assure that the intensity does not vary over the area of the cell or pyrheliometer.

2.0 ABSOLUTE SPECTRAL RESPONSE

The relative spectral response curve is multiplied by the absolute spectral distribution curve point-by-point for each wavelength interval. This is plotted and the area under this curve is integrated with a planimeter.

The short circuit current (I_{SC}) of the cell under test corresponds to the area under the curve of the spectral response-spectral distribution product.

---

(1) General Electric Radiation Calculator GEN-15B.

(2) "Optical Quartz Glass Grades Suprasil and Infrasil" Engelhard Industries, Amersil Quartz Division Brochure.

A vertical scale (mA/.1μ) is selected such that the area under the curve equals I_{sc}. Since any point on the response-distribution product curve is the product of the readings at the same wavelength of the two curves, the response curve is evaluated by dividing the reading of the product curve at the given wavelength by the reading of the distribution curve at the same wavelength. Mathematically this is expressed by:

$$E = T \int_0^\infty D(\lambda)\, d\lambda \qquad \text{Evaluation of T} \qquad (1)$$

and

$$I_{sc} = S \int_0^\infty R(\lambda)\, T\, D(\lambda)\, d\lambda \qquad (2)$$

$$S = \frac{I_{sc}}{\int_0^\infty R(\lambda) \cdot T \cdot D(\lambda)\, d\lambda} \qquad \text{Evaluation of S} \qquad (3)$$

where:

$R(\lambda)$ = relative spectral response (dimensionless)

$D(\lambda)$ = relative spectral distribution (dimensionless)

S = scale factor to make spectral response absolute ($mA/mW/cm^2/\mu^2$)

T = scale factor to make spectral distribution absolute ($mW/cm^2/\mu$)

I_{sc} = short circuit current under calibration conditions (mA)

E = energy of calibration illumination (mW/cm^2)

λ = wavelength (μ)

$SR(\lambda)$ = absolute spectral response

3.0 EXPERIMENTAL DETAILS

Figure 15 shows the preferred placement of the apparatus. It was found that intensity measurements taken with the pyrheliometer on the NBS lamp did not follow the square law of intensity at

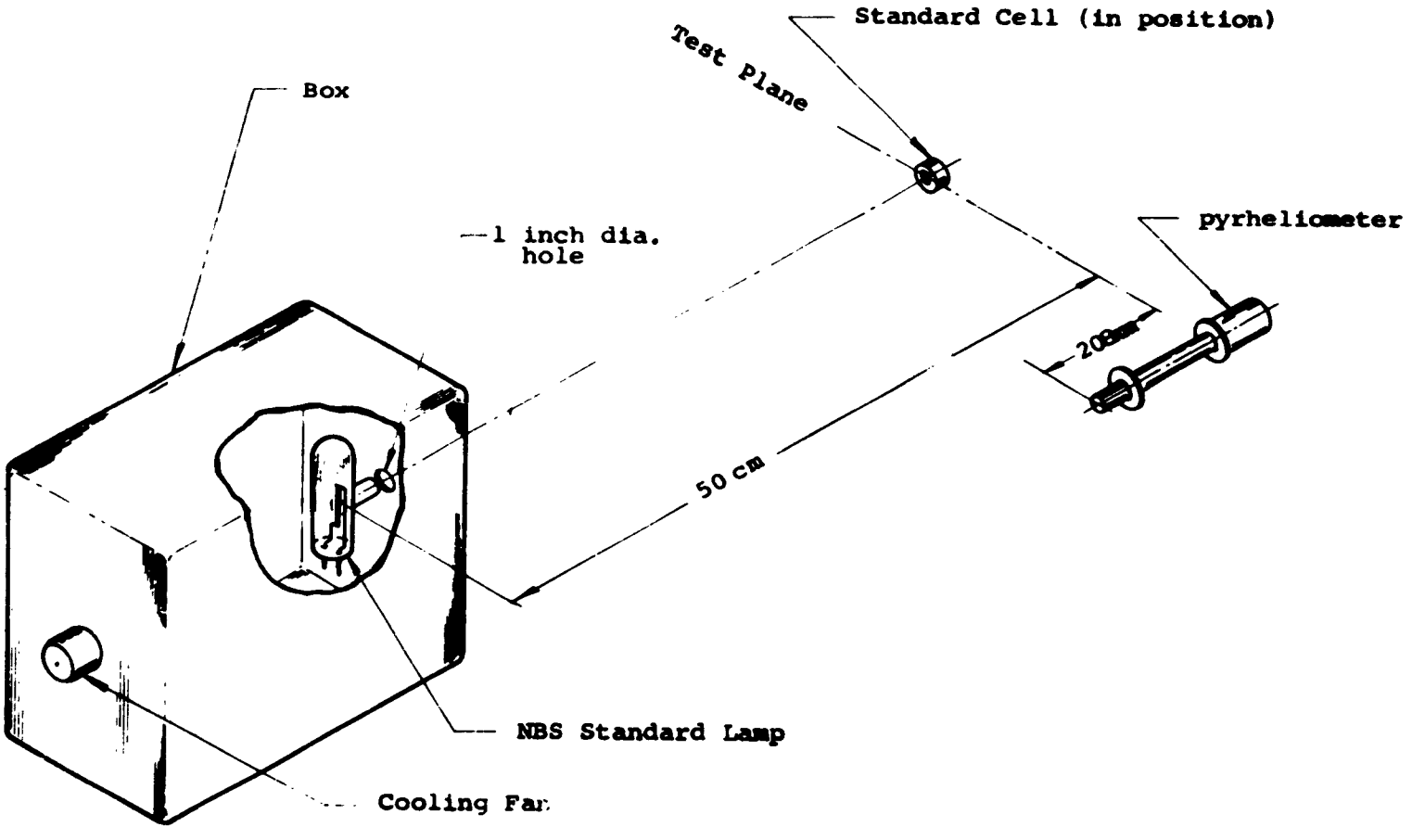

FIGURE 15 STANDARD CELL CALIBRATION APPARATUS

distances less than 50 cm from the filament. Greater distances reduce the signal and cause a reduction in accuracy.

The pyrheliometer was read with a Fitgo DC amplifier multiplying the signal by 1000 and a NLS digital voltmeter.

The standard cell short circuit current was measured with the same DC amplifier and digital voltmeter across a 250 watt Dale resistor, 1 ohm 0.05%.

APPENDIX II

PROCEDURES FOR CALIBRATING SECONDARY REFERENCE SOLAR CELLS AND COMPARING THEM TO PRIMARY SOLAR CELLS

1.0 SECONDARY REFERENCE CELLS

A secondary reference solar cell is an encapsulated standard cell whose calibration is based upon its associated primary cell. The general requirements of primary cells, i.e., high stability and good forward diode characteristics are also prerequisites for secondary cells. The only specific requirement for a secondary reference solar cell is that it have the same spectral response as its associated primary. If the secondary cell has a relative spectral response characteristic that is identical to its associated primary, then the ratio of the short-circuit currents for the two cells will be identical under any light source.

The secondary reference solar cells prepared for this program are divided into two groups of four cells each. Each group of four cells is associated with one primary cell. The spectral responses of these cells are matched as closely as is possible such that the short circuit current ratios between the secondaries and their primaries are constant.

To be used as a standard cell, a secondary reference cell must have two parameters defined; the absolute spectral response of the cell and the tmperature coefficient of short circuit current. This specification is in the form of a graph for the absolute spectral response with the ordinate shown in mA $cm^2 mW^{-1} \mu^{-2}$ and the abscissa in μ, and a temperature coefficient of short circuit current in the units of percent change of short circuit current for unit temperature from a center of 28°C.

2.0 THE PROCEDURE FOR THE SELECTION AND CALIBRATION OF A SECONDARY REFERENCE CELL

2.1 SELECTION OF CELL

As in the procedure for the selection of a primary cell, a large number of cells from a uniform production lot are measured

for their spectral response characteristics. A group whose spectral response characteristics are uniform is selected and the mean cell is designated as primary. The cells are then encapsulated.

2.2 CALIBRATION OF CELL

The actual calibration takes place after the primary absolute response characteristics are determined. A tungsten source is provided, set at a color temperature of 2800°K for convenience. The short circuit current of the secondary cell is measured at a light level corresponding to 100 mW/cm^2 sunlight equivalent. The primary is measured under the same conditions. The ratio of I_{SCS}/I_{SCP} is multiplied by the absolute spectral response of the primary. This is then the absolute spectral response of that secondary.

The general temperature characteristics are of the same form as for primary cells. These temperature characteristics may be used with little error in the determinations using the absolute spectral response. The change in absolute spectral response is generally negligible when used in sunlight over a temperature span of 20°C, but becomes appreciable and must be compensated for when used with low temperature thermal radiation sources.

2.3 COMPARISON OF PRIMARY AND SECONDARY REFERENCE CELLS

Checks may be made on the absolute spectral response by comparing a secondary to its primary under various light sources. For this program, the cells were compared under 2800°K bare tungsten, the same tungsten using a sheet of Corning Glass 1-56 filter to eliminate the infrared, and a sheet of Corning Glass 7-56 filter to eliminate the blue end of the spectrum. No deviations of greater than 2% in the ratio of I_{SCS}/I_{SCP} under any of these conditions was observed on the secondary cells.

APPENDIX III

ARTIFICIAL LIGHT SOURCES

1.0 DISCUSSION

The following categories classify artificial light sources according to similar output characteristics:

(1) Band Spectra

Fluorescence

Electro-luminescence

(2) Line Spectra

Arcs

Glow discharges

Flames

(3) Continuous Spectra

Incandescence

The light sources tested for this program were either arcs or incandescent sources. Fluorescent, electro-luminescent and glow discharge sources have intensities which are too low to be considered for solar cell testing. The common flames are all of low color temperature and are unstable, making them undesirable as test sources. The arcs tested for this program were: Xenon, xenon-mercury and carbon. The incandescent sources tested were: Tungsten and tungsten-iodine.

The following categories classify artificial light sources according to their applicability as a standard source for solar energy conversion testing:

(1) National Bureau of Standards ribbon filament tungsten standard of spectral radiance.

(2) Other tungsten lamps

(3) Stabilized DC xenon arc

(4) Other sources

The major parameters concerning light sources for this program are as follows:

(1) Spectral distribution

(2) Power requirements

(3) Distance from lamp at required intensity and uniformity of illumination.

(4) Long-term variation

(5) Short-term variation

The dividing point between short-term and long-term variation is a function of the instrumentation used to read the current-voltage characteristics of the solar cells being measured. With the use of an X-Y recorder having a frequency response of approximately 20 cycles/sec, this becomes the dividing point. In the event that instruments are used which have other response speeds a corresponding dividing point must be considered.

An experiment was devised to determine the difference in I-V characteristics of a cell operating first under a source whose output is invariant (a tungsten source operating under direct current) and under a source whose output is periodically varying, (a mercury arc operated on 60 $\sim$ alternating current). It was proven by a previous experiment that the I-V characteristics (curve shape) are independent of radiation wavelength. In this experiment I-V curves were plotted for a cell, under tungsten, with red and blue filters.

The experiment to determine short-term variation effects was performed with the intensities of the lamps adjusted such that the short circuit current on the cell was equal under both lamps. The results of this experiment are shown in Fig. 16.

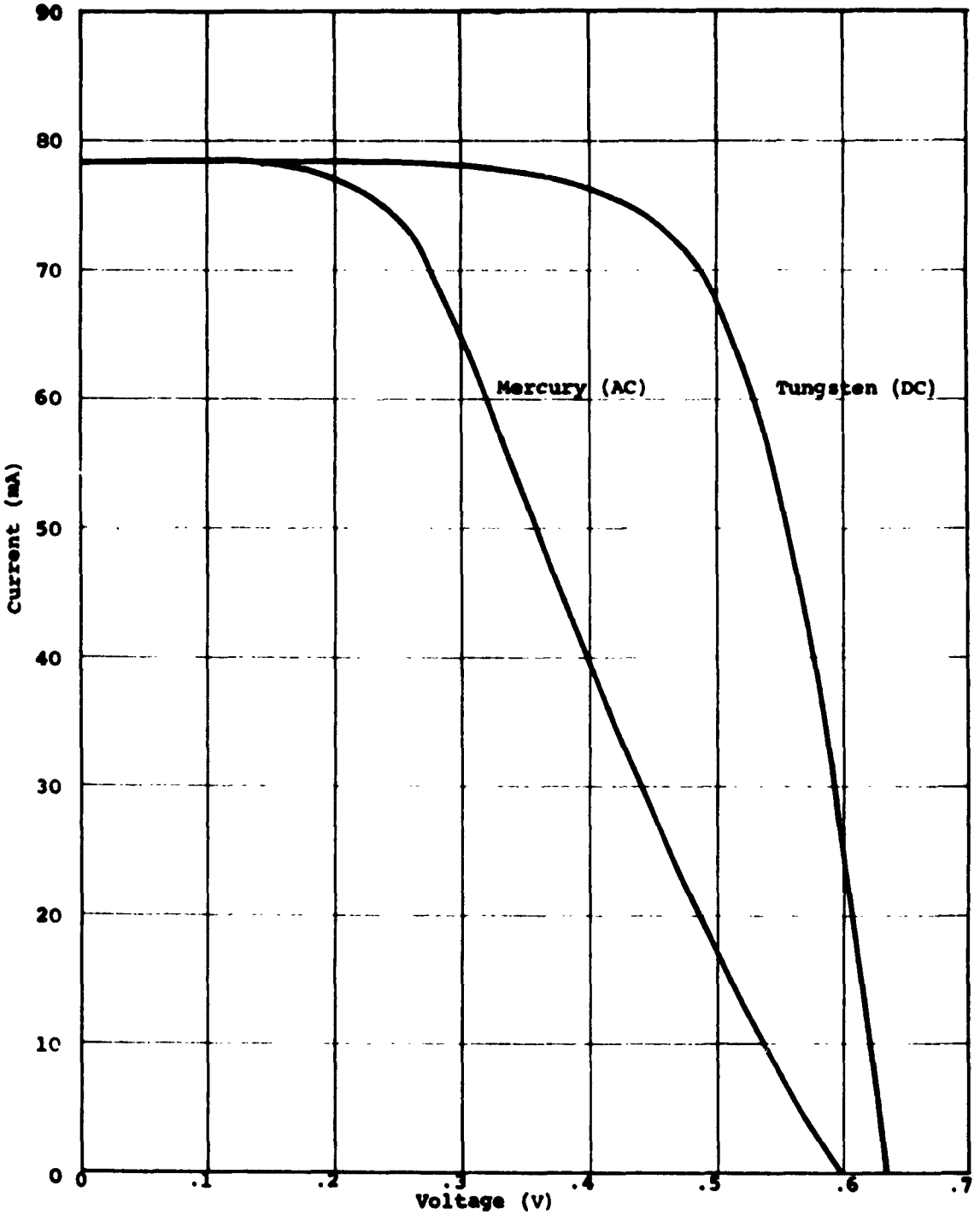

Fig.16 - I-V CURVES OF A STANDARD CELL UNDER DC AND AC LIGHT SOURCES

The change of curvature can be explained by considering a solar cell whose I-V curve is that of an ideal diode. Referring to Fig. 17, the characteristics of an ideal cell are shown for two different light levels. Because the short circuit current varies linearly and the open circuit voltage varies logarithmically with light intensity, the change in current is greater than the change in voltage at normal sunlight intensity levels.

Assuming that the short-term variation limits are represented by the upper and lower curves, the average characteristic is illustrated by the center curve. Since at any given time the cell "sees" a particular load resistance, the variation will follow this line of constant resistance. Should the instrumentation measure the rms value of the fluctuation rather than the average, a similar decaying effect at the knee will be produced.

2.0 LIGHT SOURCE CHARACTERISTICS

2.1 TUNGSTEN

Tungsten lamps are classified by type of filament, type of reflector and type of lens. Long-term degradation tests were performed on PAR 38 150W Flood as representative of reflector type lamps and on T20-500W display spotlights as representative of lamps with clear envelopes.

Distribution of intensity measurements were performed on ten different types of lamps, chosen as representative of light sources for solar cell testing.

2.1.1 SPECTRAL DISTRIBUTION

The spectral distribution of tungsten lamps is very nearly that of a black-body radiator.

The spectral distribution of a black-body is a function only of the absolute temperature and Planck's radiation constants. In practice, emissivities of 0.999 have been attained[1]. The

---

(1) Stair, Johnston, & Halbach, J. Res. NBS, 64A, #4, (1960), p.291.

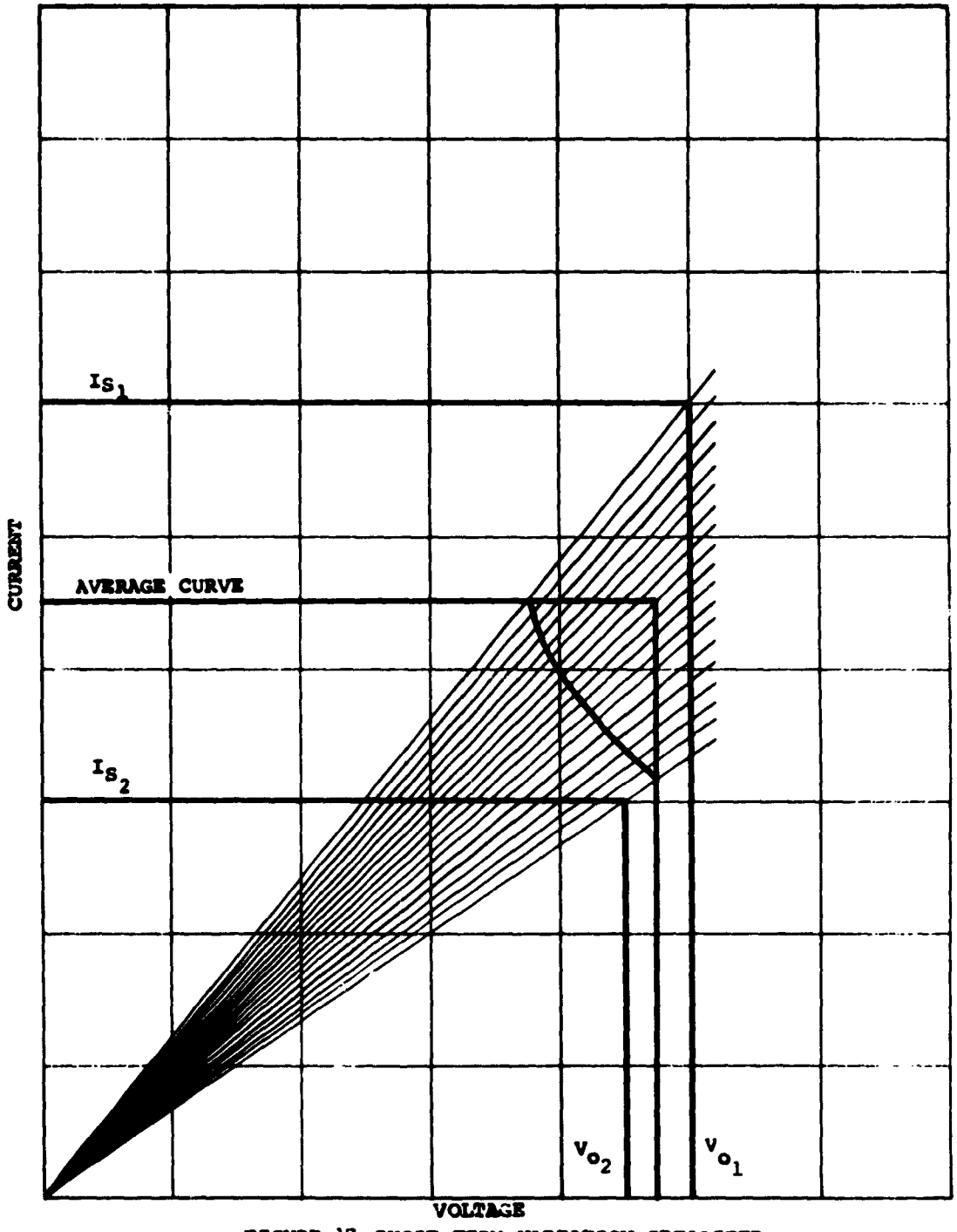

FIGURE 17 SHORT-TERM VARIATION IDEALIZED

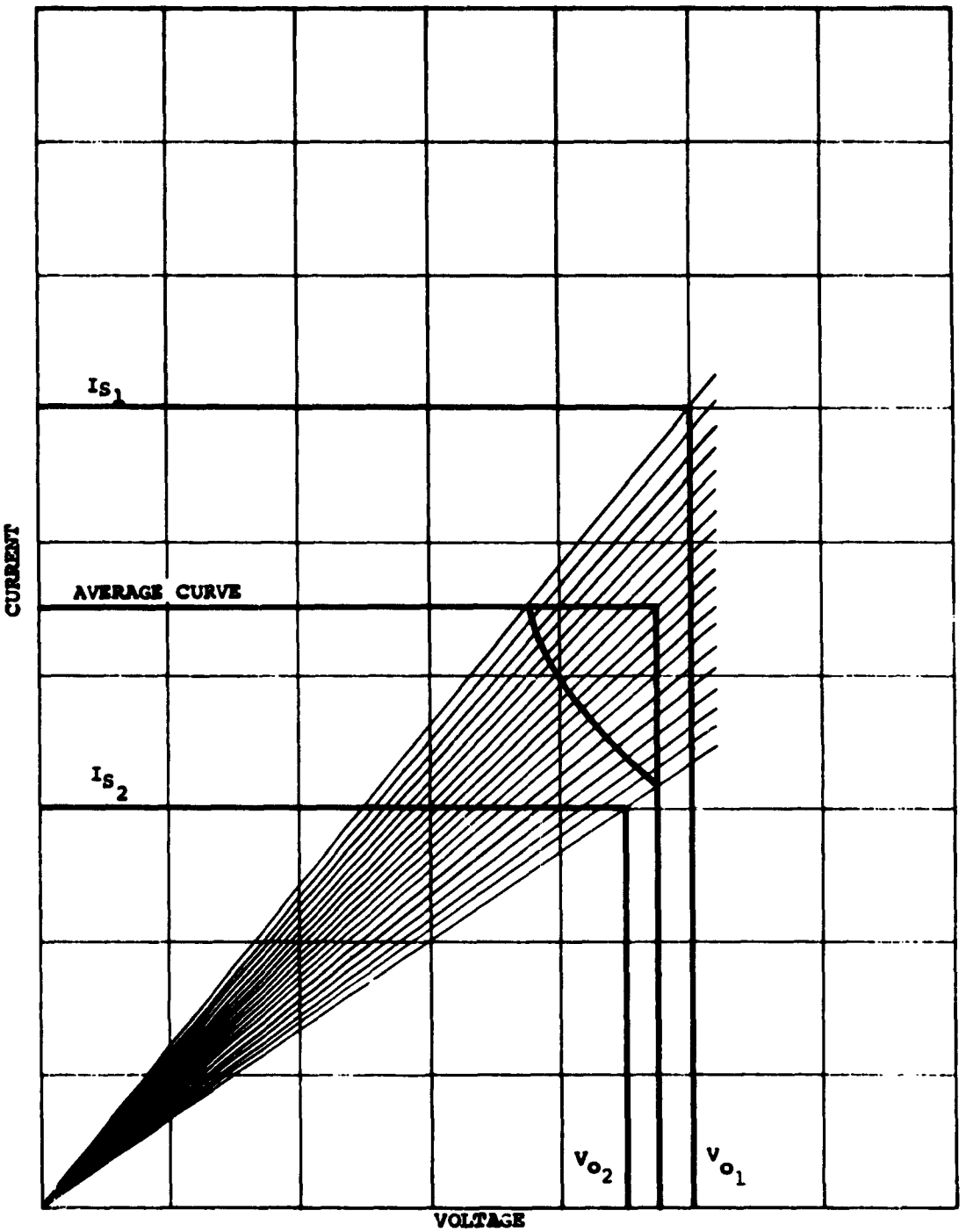

FIGURE 17 SHORT-TERM VARIATION IDEALIZED

equation of the spectral distribution of any incandescent source at a uniform temperature is:

$$J_\lambda = c_1 \lambda^{-5} \left(e^{\frac{c_2}{\lambda T}} - 1 \right)^{-1} \epsilon_\lambda$$

where J_λ = watts per cm^2 of surface per micron wavelength at wavelength λ

λ = wavelength in microns

T = temperature in °K

ϵ_λ = emissivity

c_2 = 14,388 μ°K

c_1 = 37,413 watts per cm^2 per μ^4

By using this equation, the spectral output of any incandescent source may be calculated provided the temperature and emissivity are known.

Tungsten has been the object of many optical studies. Numerous authors have studied the emissivity of tungsten, and the best work at this time is by DeVos[2].

This work has been used by the National Bureau of Standards[1] and is shown for 2800°K in Fig. 18. The color temperature as a function of true temperature is shown in Fig. 19 and is data from Forsythe & Worthing[3]. This data was presented on the Nela scale of color temperature of 1922. The difference between this scale and the presently used scale of 1949 is relatively insignificant. By measuring the color temperature, one obtains enough data to calculate the spectral distribution of the emission from a tungsten ribbon at that color temperature. A sample calculation sheet is shown in Fig. 20.

---

(2) DeVos, J. W., Physica, 20, 690, (1954).

(3) Forsythe, W. F., & Worthing, A. G., Astrophys. J., 61, 146, (1925).

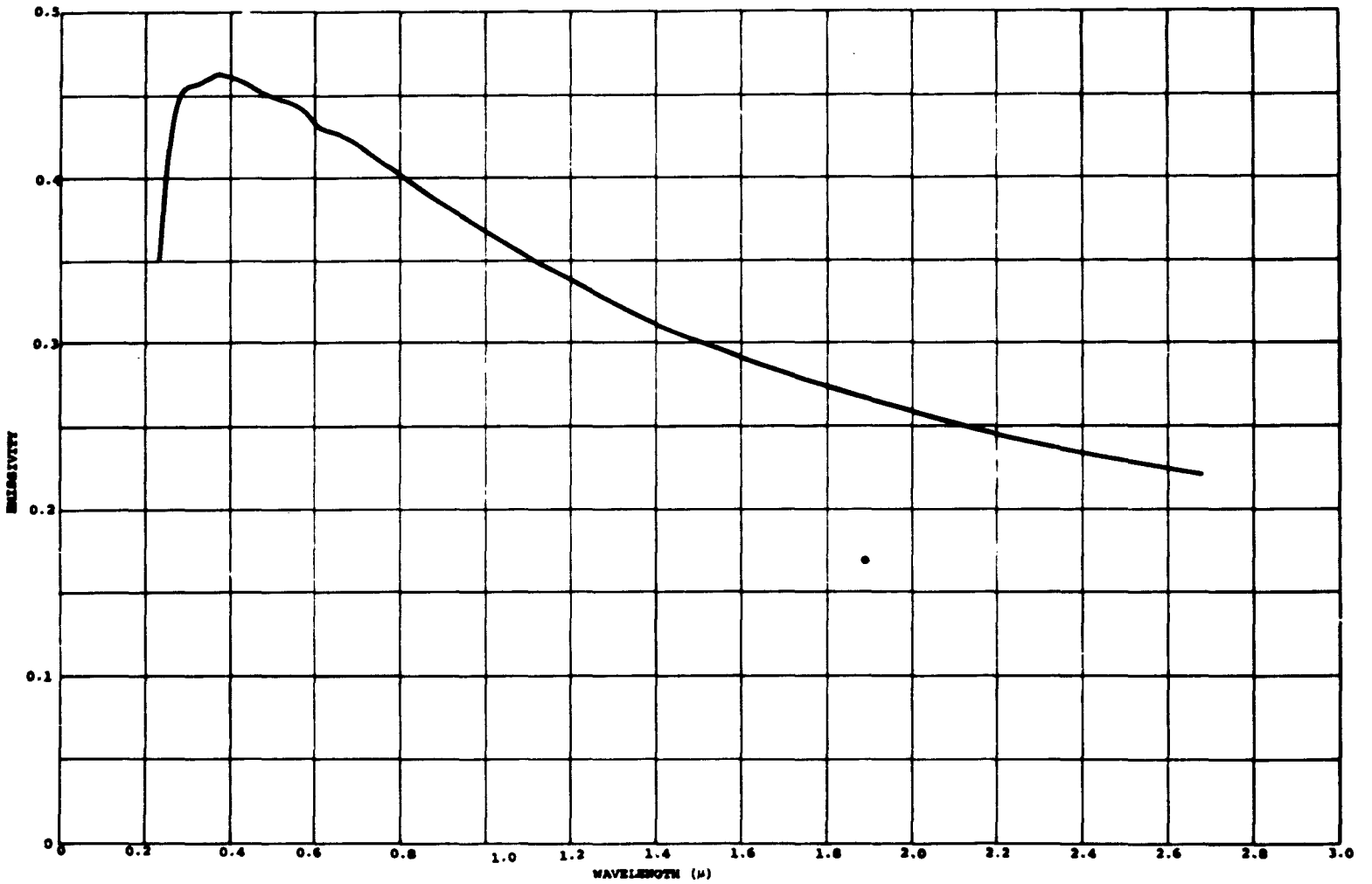

FIGURE 18 THE EMISSIVITY OF TUNGSTEN RIBBON VS. WAVELENGTH FOR 2800°K TEMPERATURE (DeVos, 1954)

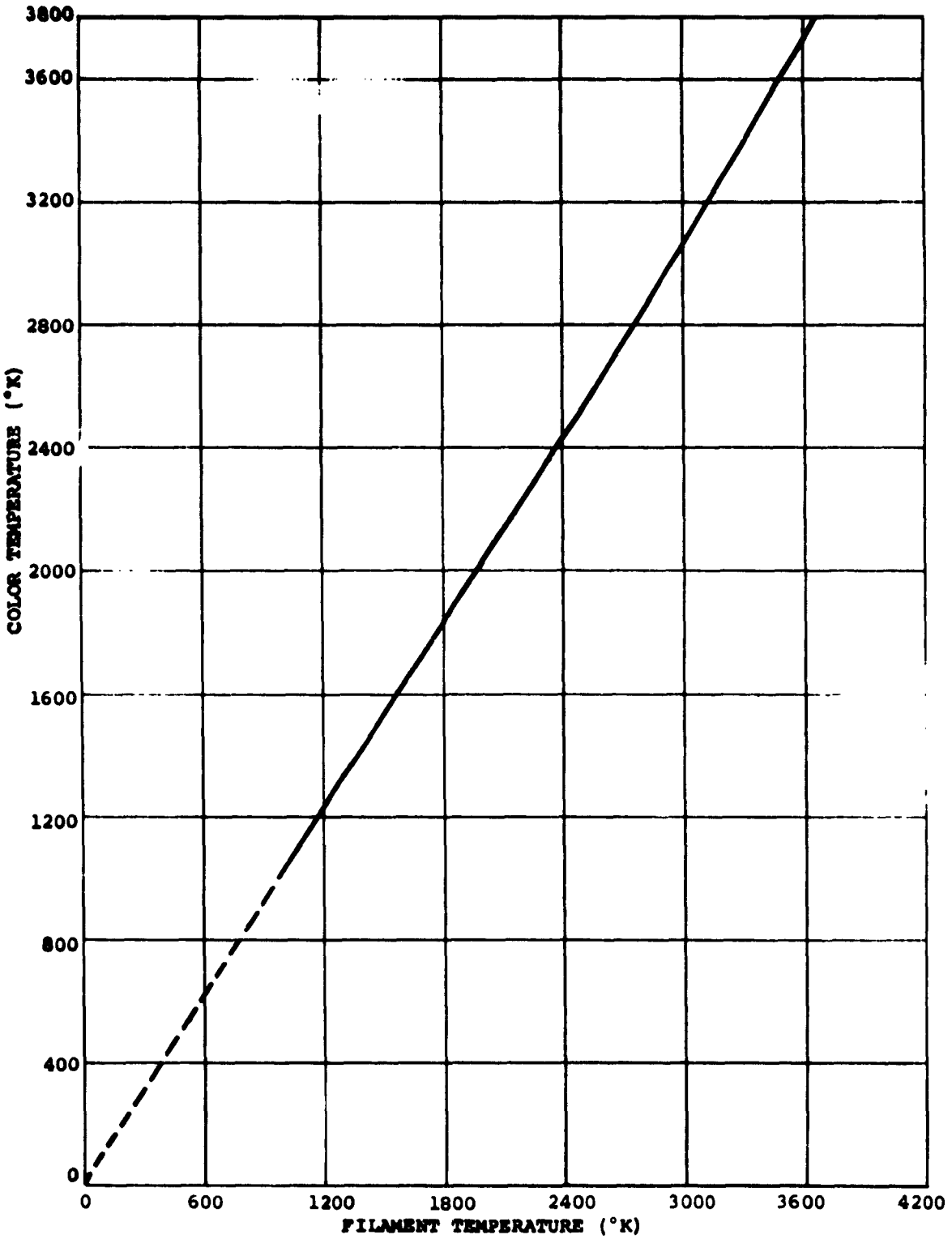

FIGURE 19 COLOR TEMPERATURE VS. FILAMENT TEMPERATURE
TUNGSTEN WIRE IN VACUUM

SPECTRAL DISTRIBUTION CALCULATION SHEET

$J_\lambda = \frac{C_1}{\lambda^5} \frac{1}{e^{\frac{C_2}{\lambda T}} - 1}$ $\quad C_1 = 36,970$ $\quad C_2 = 14,380$ $\quad J_\lambda = w\ cm^{-2}\ \mu^{-1}$

$T =$ _____ °K

λ_μ	λT	$\frac{14380}{\lambda T}$	$e^{\frac{14380}{\lambda T}}$	$\frac{14380}{\lambda T - 1}$	$\frac{1}{e^{\frac{14380}{\lambda T}} - 1}$	λ^5	$\frac{36970}{\lambda^5}$	J_λ	ϵ_λ	$J'\lambda$
.40						1.024^{-2}	3.610^{6}			
.45						1.845^{-2}	2.004^{6}			
.50						3.125^{-2}	1.183^{6}			
.55						5.033^{-2}	7.345^{5}			
.60						7.776^{-2}	4.754^{5}			
.65						1.160^{-1}	3.187^{5}			
.70						1.681^{-1}	2.199^{5}			
.75						2.373^{-1}	1.558^{5}			
.80						3.277^{-1}	1.128^{5}			
.85						4.437^{-1}	8.332^{4}			
.90						5.905^{-1}	6.261^{4}			
.95						7.738^{-1}	4.778^{4}			
1.00						1.000^{0}	3.697^{4}			
1.10						1.611^{0}	2.295^{4}			
1.20						2.488^{0}	1.486^{4}			
1.30						3.713^{0}	9.957^{3}			
1.40						5.378^{0}	6.874^{3}			
1.50						7.594^{0}	4.868^{3}			
1.60						1.049^{1}	3.524^{3}			
1.70						1.420^{1}	2.604^{3}			
1.80						1.890^{1}	1.956^{3}			
1.90						2.476^{1}	1.493^{3}			
2.00						3.200^{1}	1.155^{3}			
2.10						4.084^{1}	9.052^{2}			
2.20						5.154^{1}	7.173^{2}			
2.30						6.436^{1}	5.744^{2}			
2.40						7.962^{1}	4.643^{2}			
2.50						9.766^{1}	3.786^{2}			
2.60						1.188^{2}	3.112^{2}			
2.70						1.435^{2}	2.576^{2}			
2.80						1.721^{2}	2.148^{2}			
2.90						2.051^{2}	1.803^{2}			
3.00						2.430^{2}	1.521^{2}			

FIGURE 20 SPECTRAL DISTRIBUTION CALCULATION SHEET

The previous statements apply only to ribbon filament lamps with flat transmission envelopes. Either quartz or glass envelopes have sufficiently flat transmission through the range of interest that their presence may be neglected for relative spectral measurements.

When the filament is coiled, the emissivity vs. wavelength curve changes. This results from the fact that each element of area of the filament no longer looks at the cold surroundings. Some of the areas look at other portions of the filament, and the entire filament more closely resembles a black-body; the emissivity increases, and the slope of the emissivity vs. wavelength curve flattens.

2.1.2 POWER REQUIREMENTS

The power requirements of the ten lamp types tested are listed in Figs. 21 through 24.

2.1.3 DISTANCE FROM LAMP AT REQUIRED INTENSITY AND UNIFORMITY OF ILLUMINATION

The required intensity was set with an encapsulated cell manufactured early in 1959. The intensities were set at levels which produced the same short circuit current that was measured with this cell under 100 mW/cm^2 of earth surface sunlight. The distances from the lamps at this intensity are listed in Fig. 21 through 24. The uniformity of illumination is plotted full scale in Fig. 21 through 24 as the area enclosed by the 95% iso-intensity line. This area was scanned by a 3.5 mm diameter cell.

2.1.4 LONG-TERM VARIATION

Tungsten lamp degradation was studied by the National Bureau of Standards on various types of lamps[4]. The lamps were operated at constant voltage, and the change in color temperature and luminous flux was measured. The change in

---

(4) Judd, D. B., "Changes in Color Temperature of Tungsten-Filament Lamps at Constant Voltage", J.O.S.A. 26, 409, (1936).

COLOR TEMP 2800°K
INTENSITY 100mW/cm^2 "SUN EQUIV."
PROFILE INTENSITY $^{+0}_{-5}$%

500W DISPLAY SPOTLIGHT
— — VOLTAGE 106 VAC
LAMP TO TARGET DISTANCE 4 IN.

250 W AIRCRAFT LANDING REFLECTOR
——— VOLTAGE 11 VAC
LAMP TO TARGET DISTANCE 51.5 IN

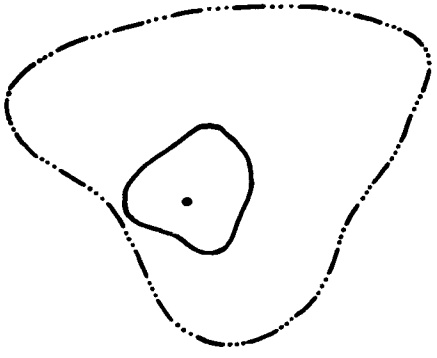

Fig. 21 - TUNGSTEN PROFILES

COLOR TEMP 2800°K
INTENSITY 100mW cm^2 "SUN EQUIV."
PROFILE INTENSITY $^{+0}_{-5}$ %

150W PAR 38 FLOOD
—— VOLTAGE 135V APPROX.
LAMP TO TARGET DISTANCE 15.5 IN.

150 W PAR 38 SPOT
—·—· VOLTAGE 124 VAC
LAMP TO TARGET DISTANCE 26.5 IN.

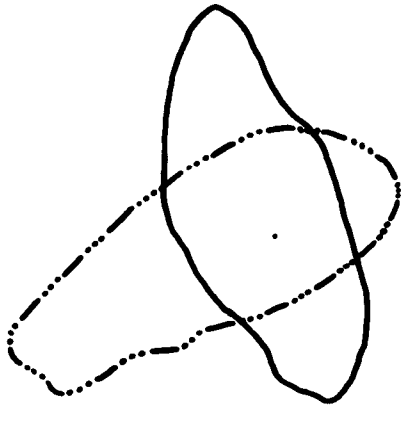

Fig. 22 TUNGSTEN PROFILES

COLOR TEMP 2800°K
INTENSITY 100mW/cm^2 "SUN EQUIV."
PROFILE INTENSITY $^{+0}_{-5}$ %

300W PAR 56 MFL MEDIUM FLOOD
—·—·— VOLTAGE 122.5 VAC
LAMP TO TARGET DISTANCE 35 IN.

300W PAR 56 WFL WIDE FLOOD
——— VOLTAGE APPROX. 133 VAC
LAMP TO TARGET DISTANCE 23 IN.

300W PAR 56 NSP NARROW SPOT
– – – VOLTAGE 124.5 VAC
LAMP TO TARGET DISTANCE 57 IN.

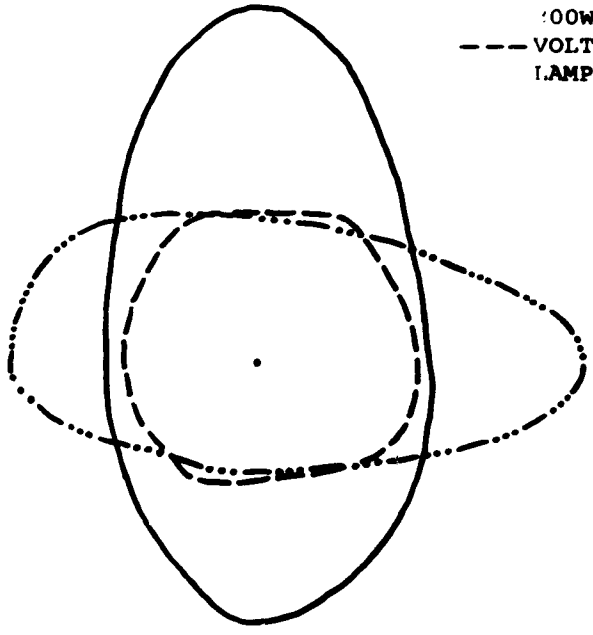

Fig. 23 TUNGSTEN PROFILES

COLOR TEMP. 2800°K
INTENSITY 100mW/cm^2 "SUN EQUIV."
PROFILE INTENSITY $^{+0}_{-5}$ %

500W PAR 64/WFL WIDE FLOOD
– – – VOLTAGE 135V AC
LAMP TO TARGET DIST. 27.5 IN.

500W PAR 64/MFL MEDIUM FLOOD
–·–·– VOLTAGE 135V AC
LAMP TO TARGET DIST. 44 IN.

500W PAR 64/NSP NARROW SPOT
——— VOLTAGE 120V AC
LAMP TO TARGET DIST. 68 IN.

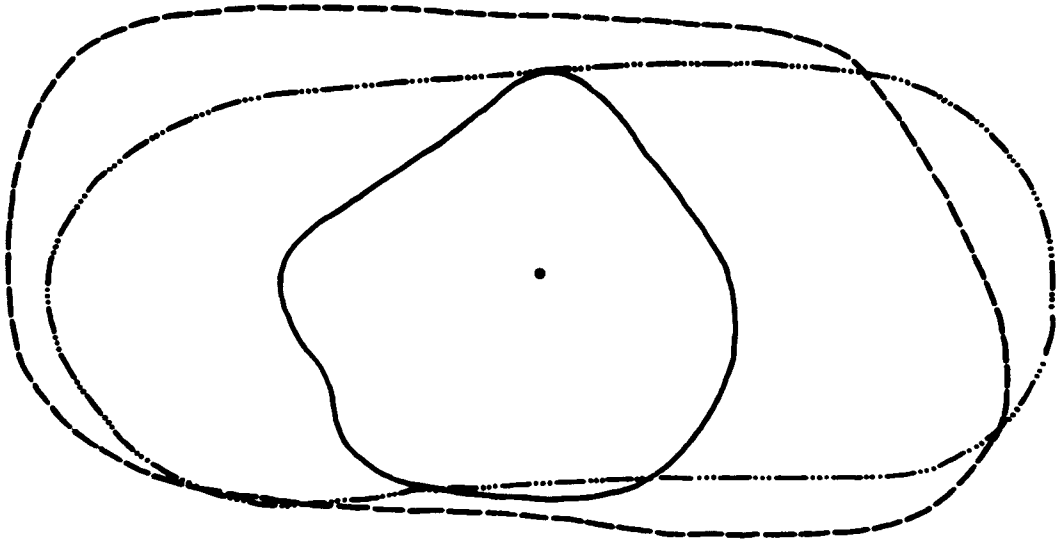

Fig. 24 TUNGSTEN PROFILES

color temperature was ascribed to two distinct phenomena:

(1) Evaporation of the filament

(2) A brown deposit on the bulbs being spectrally selective in nature.

It has been suggested that lamps be run on constant current rather than constant voltage.

Measurements made on a T20-500W lamp, shown in Fig. 25, indicate that a greater accuracy is obtained by measuring voltage rather than current as evidenced by the greater slope of the voltage curve.

It was expected that aged lamps measured at initial voltage would decrease in color temperature due to the increased resistance caused by filament evaporation. Conversely, lamps measured at the initial current would increase in color temperature due to the increased resistance.

For the purposes of this contract, fifteen of each of the two types of lamps (150 watt PAR/38 and 500 watt T-20) were operated in a life test to determine their degradation characteristics. Five of each type of lamp were operated on direct current, five on alternating current, and five on half-wave rectified alternating current. This was done to determine the proper power source for minimum long-term degradation. The voltages of the independent power supplies were adjusted to yield an average color temperature of approximately 2800°K for each group of five lamps.

During the aging of the lamps, color temperature measurements were taken at intervals.

Figure 26 is a curve of color temperature degradation for the 500W-T20 lamps operating on half-wave rectified current. These lamps showed the most severe degradation. Figures 27 through 31 show similar characteristics for the other lamps tested.

It may be noted that an increase in color temperature occurs in the first few hours of operation. This was investi-

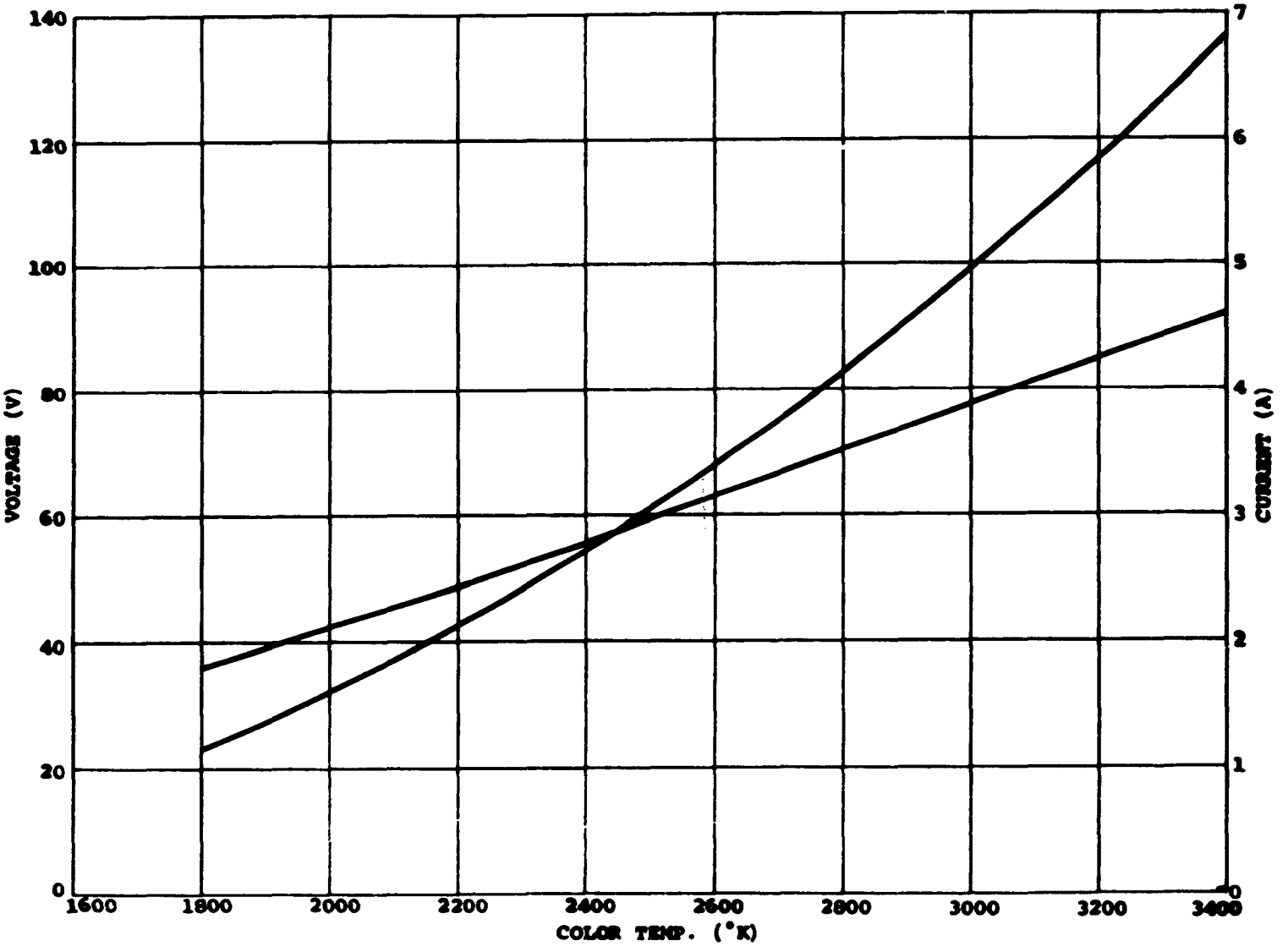

FIGURE 25 COLOR TEMPERATURE VS. LAMP VOLTAGE & CURRENT FOR 500W T20 LAMPS

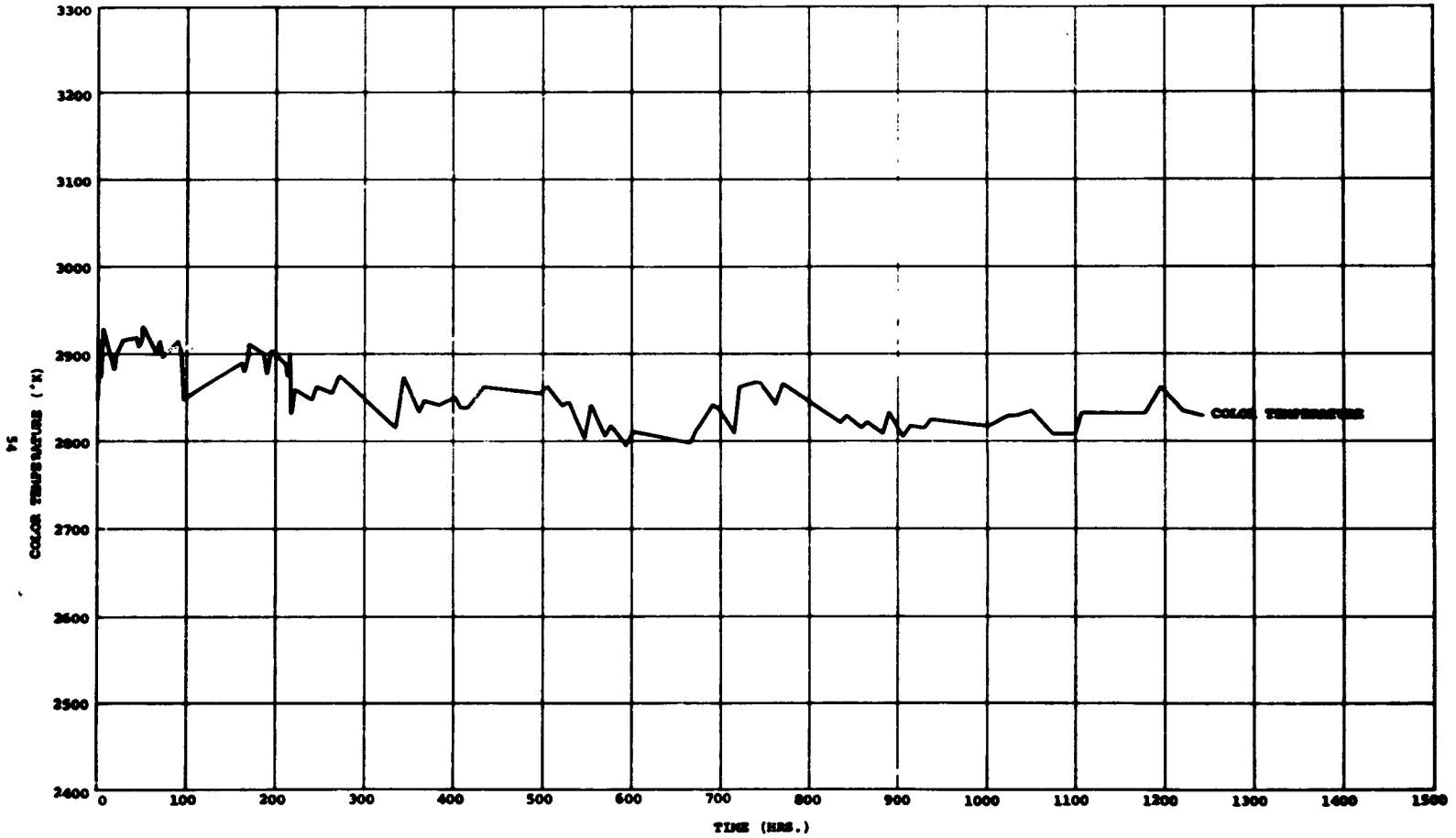

FIGURE 26 COLOR TEMPERATURE VS. TIME FOR T20 LAMP ON HALF-WAVE AC CURRENT

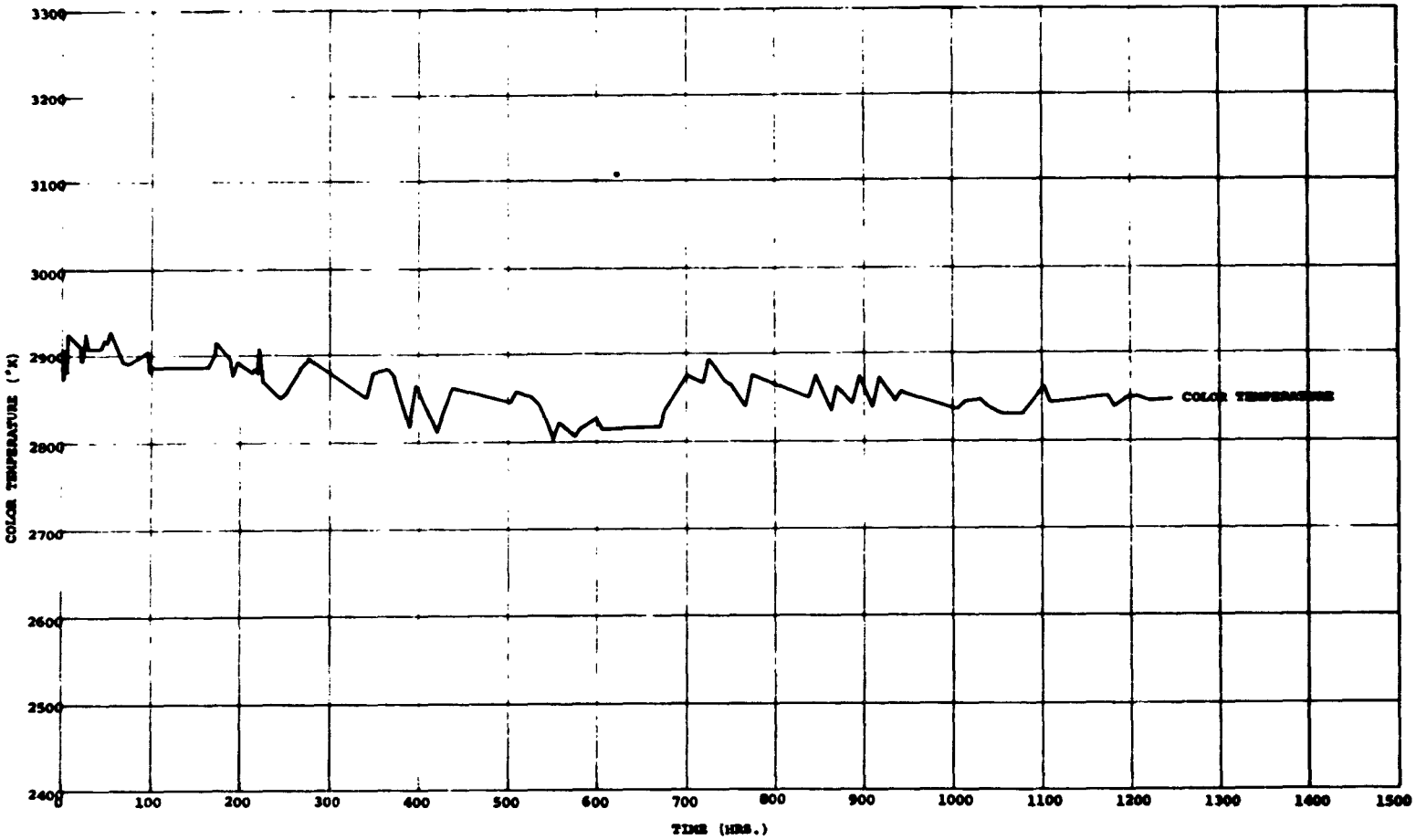

FIGURE 27 COLOR TEMPERATURE VS. TIME FOR F20 LAMP ON AC CURRENT

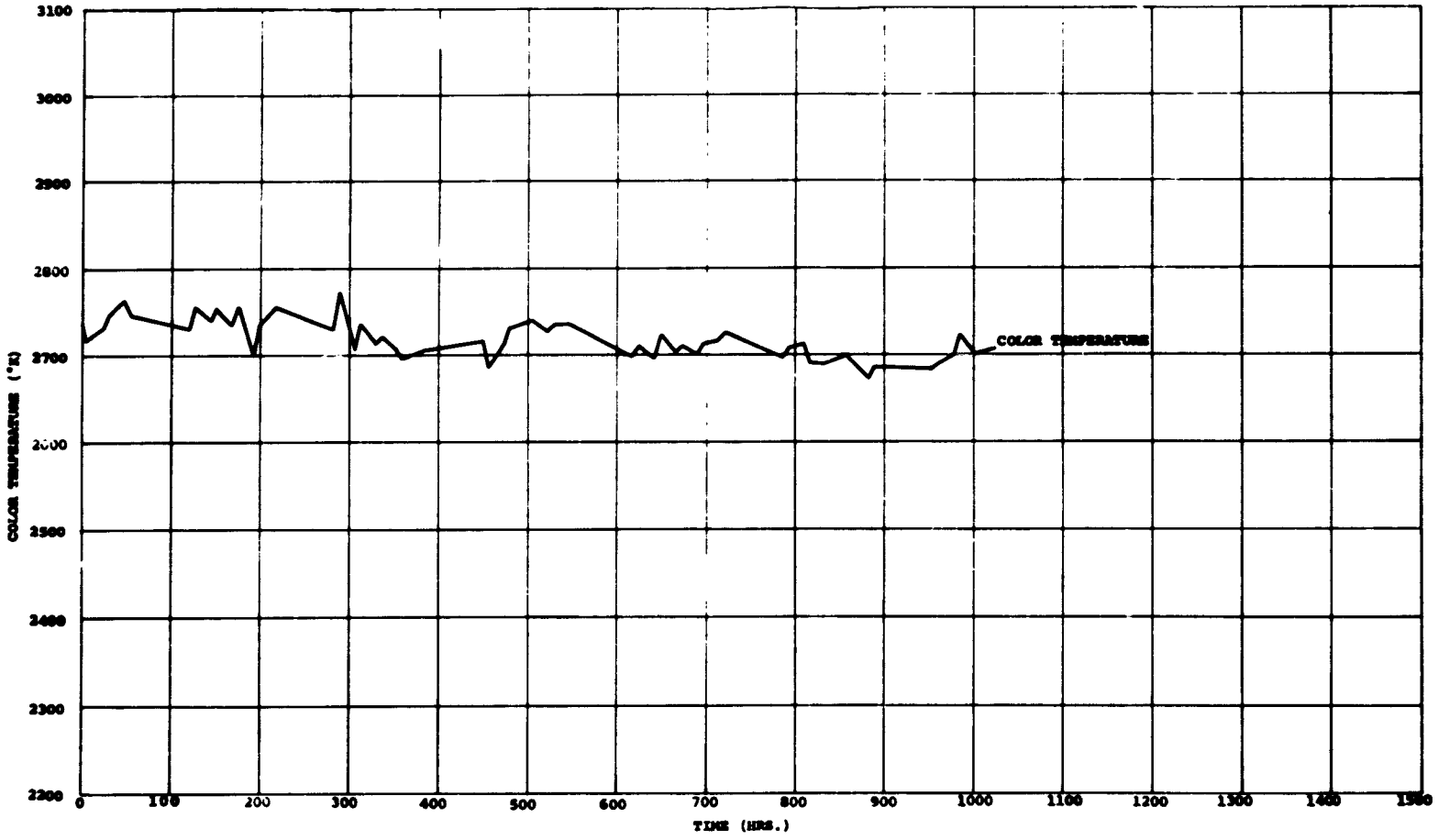

FIGURE 28 COLOR TEMPERATURE VS. TIME FOR T20 LAMP ON DC CURRENT

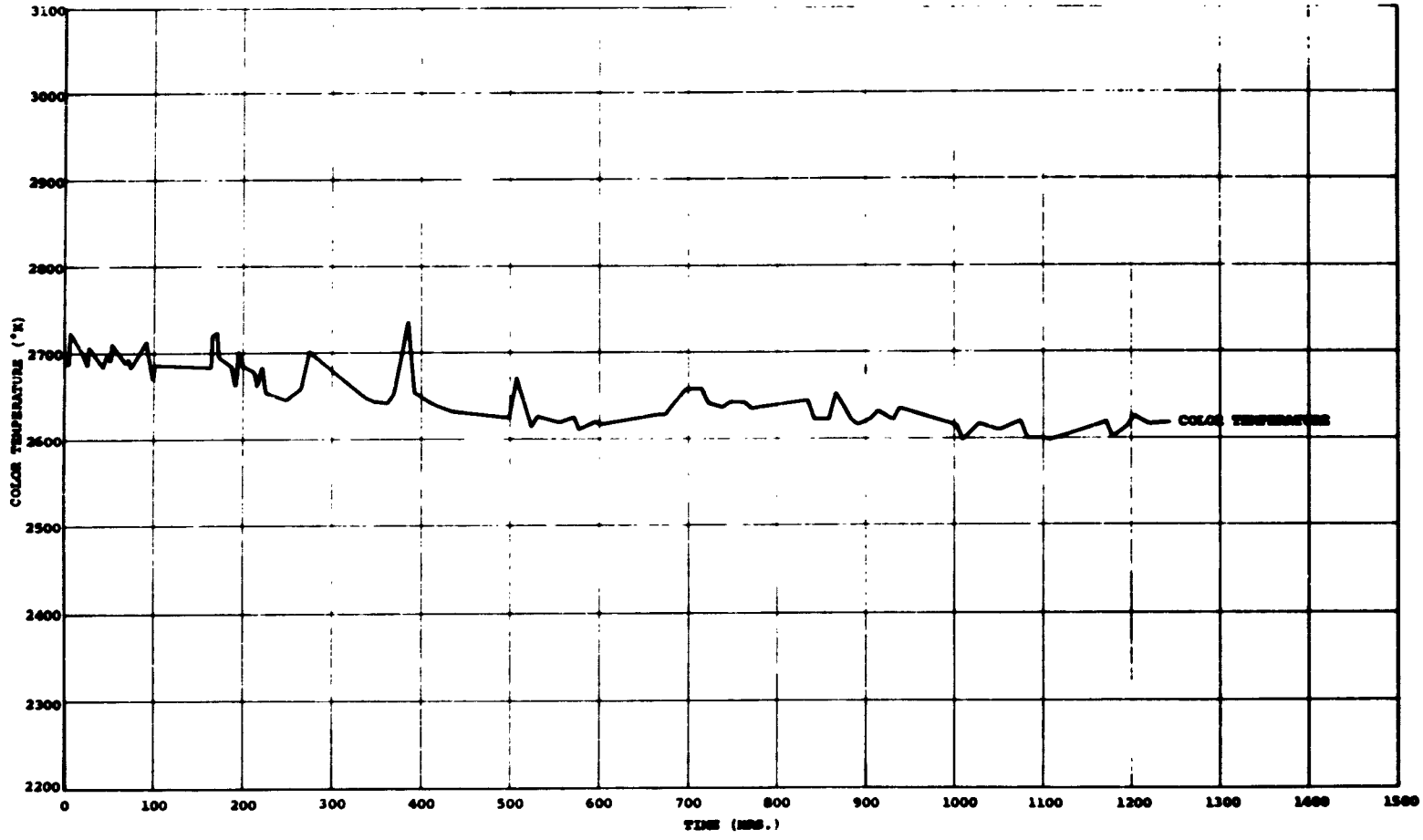

FIGURE 29 COLOR TEMPERATURE VS. TIME FOR PAR-38 LAMP ON HALF-WAVE AC CURRENT

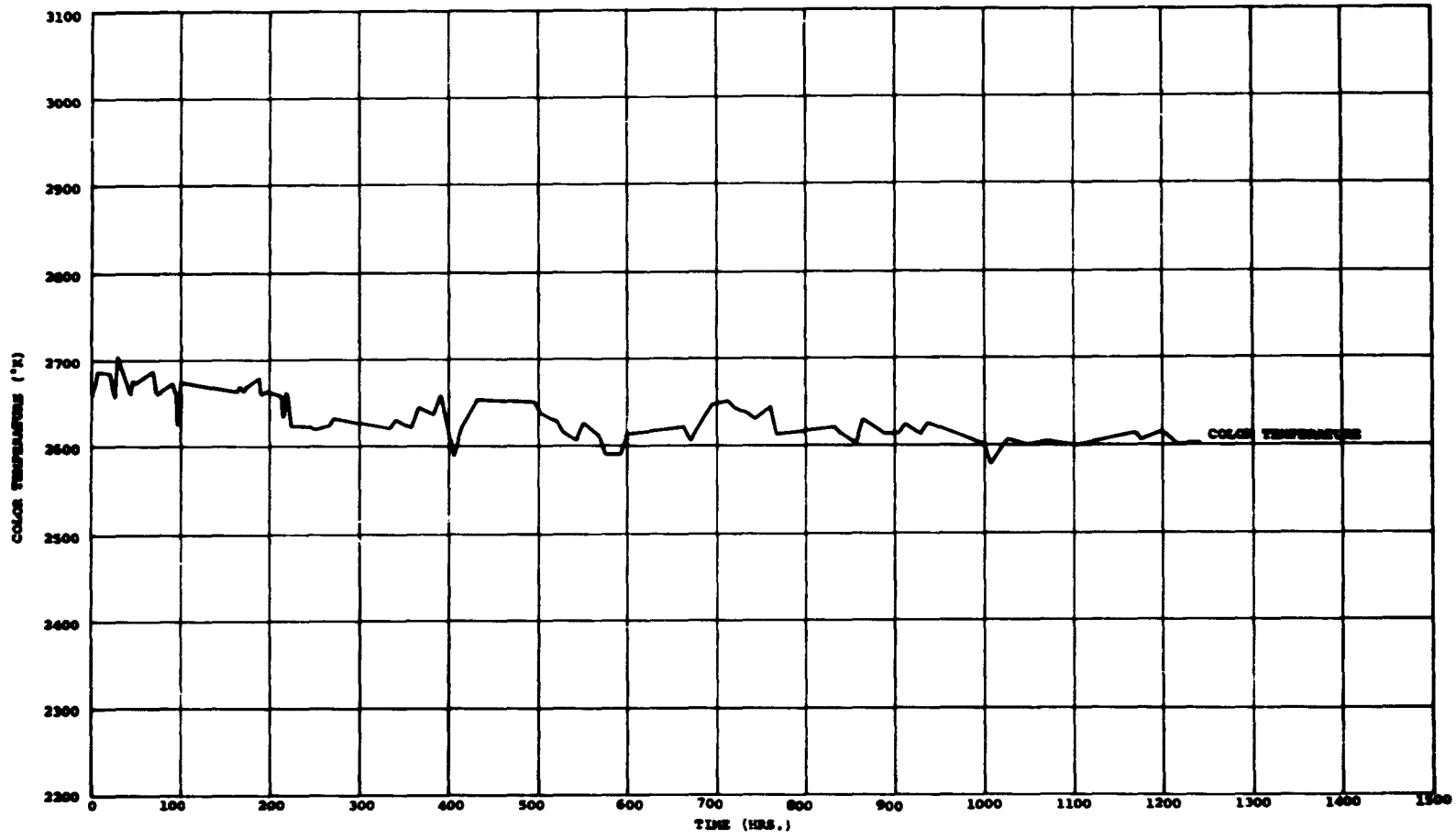

FIGURE 30 COLOR TEMPERATURE VS. TIME FOR PAR 38 LAMP ON AC CURRENT

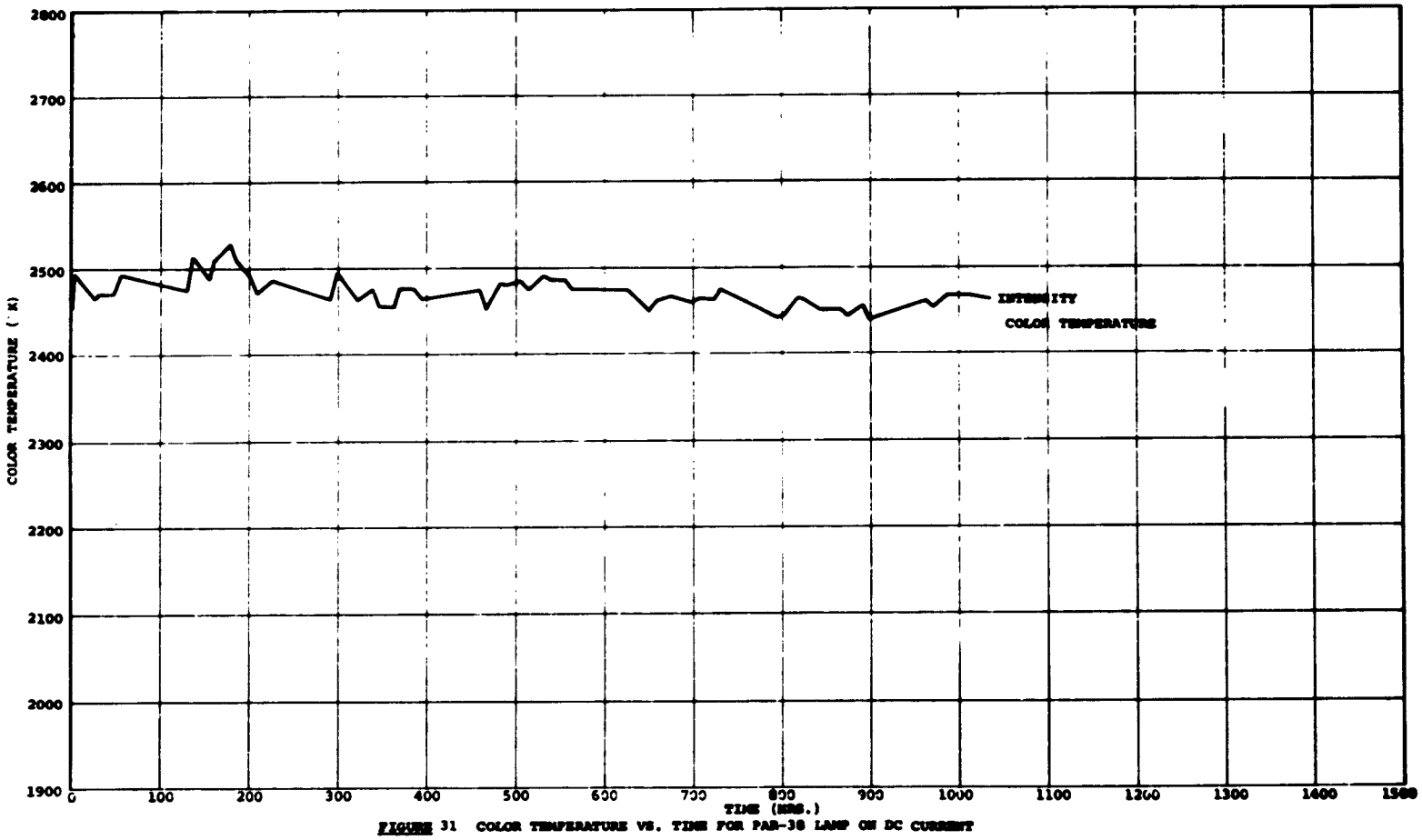

FIGURE 31 COLOR TEMPERATURE VS. TIME FOR PAR-38 LAMP ON DC CURRENT

gated under more closely controlled conditions which resulted in the data presented in Fig. 32.

Listing the results of Figs. 26 through 31, the following degradations are shown:

Lamp Type	Current	Initial Color Temp.	Final Color Temp.	Change Color Temp.
PAR 38	Half-wave	2705°K	2610°K	-95°K
150 watt	AC	2685°K	2600°K	-85°K
Flood	DC	2495°K	2465°K	-30°K
T20	Half-wave	2985°K	2925°K	-60°K
500 watt	AC	2985°K	2900°K	-85°K
	DC	2745°K	2700°K	-45°K

The average color temperature for the lamps operated on DC was lower than that of the lamps operated on either AC or half-wave.

According to the National Bureau of Standards[5], a typical 400 watt monoplanar filament lamp will degrade in color temperature about 1 degree per hour of operation at 3140°K, about 0.1 degree per hour at 2850°K and about 0.01 degree per hour at 2360°K. These 400 watt lamps are similar to the T20 lamps used in these tests.

Plotting this data results in the curve shown in Fig. 33. Interpolation of this curve indicates that the DC color temperature degradations should be multiplied by approximately 2.2 in order to be compared to the AC degradations. The resulting calculations show that lamps operated with DC degrade approximately twice as fast as those operated with AC. The results of these tests show no appreciable difference between lamps operated on AC and lamps operated on rectified half-wave current.

---

(5) Ibid, Ref. 4

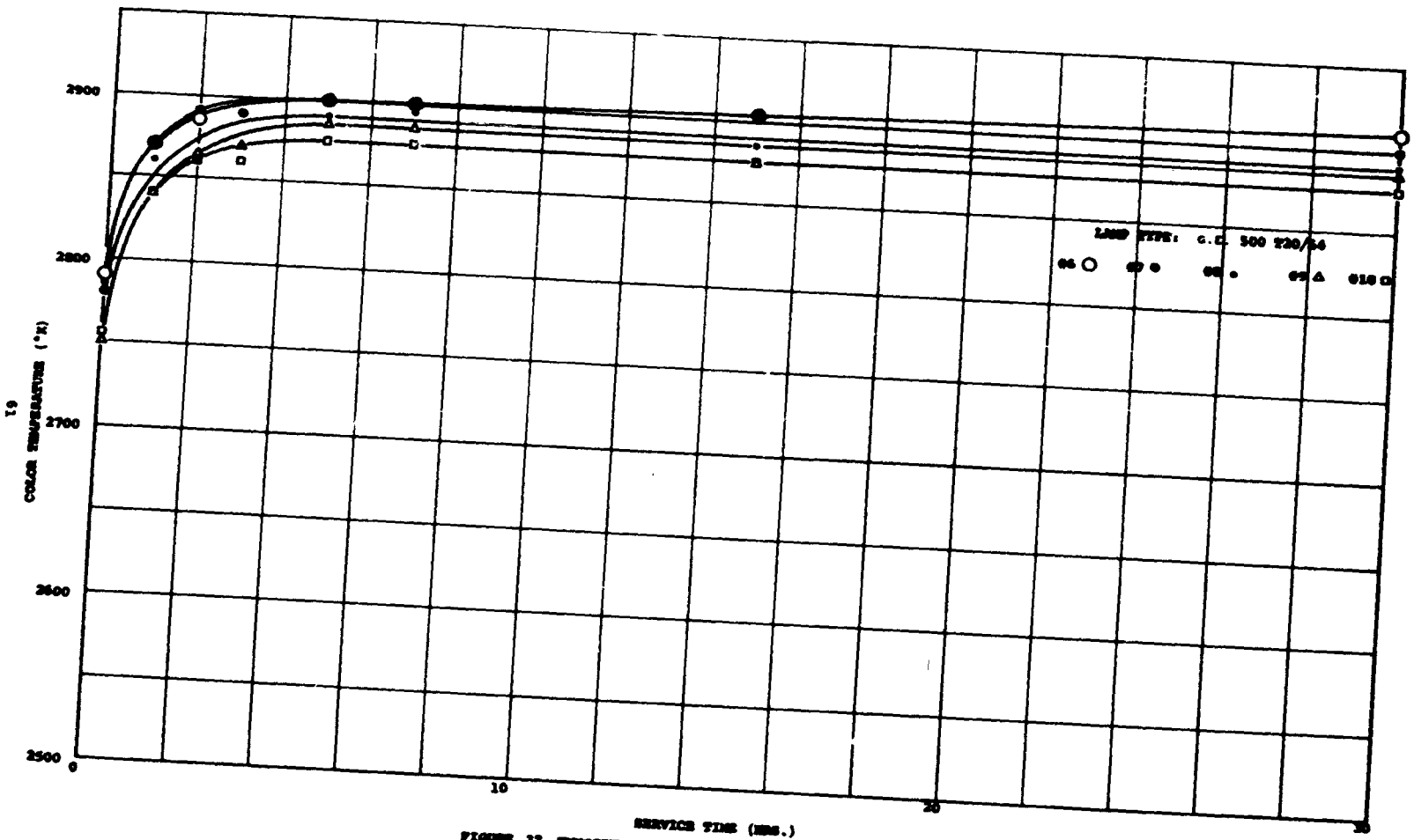

FIGURE 32 TUNGSTEN COLOR TEMPERATURE VS. SERVICE TIME

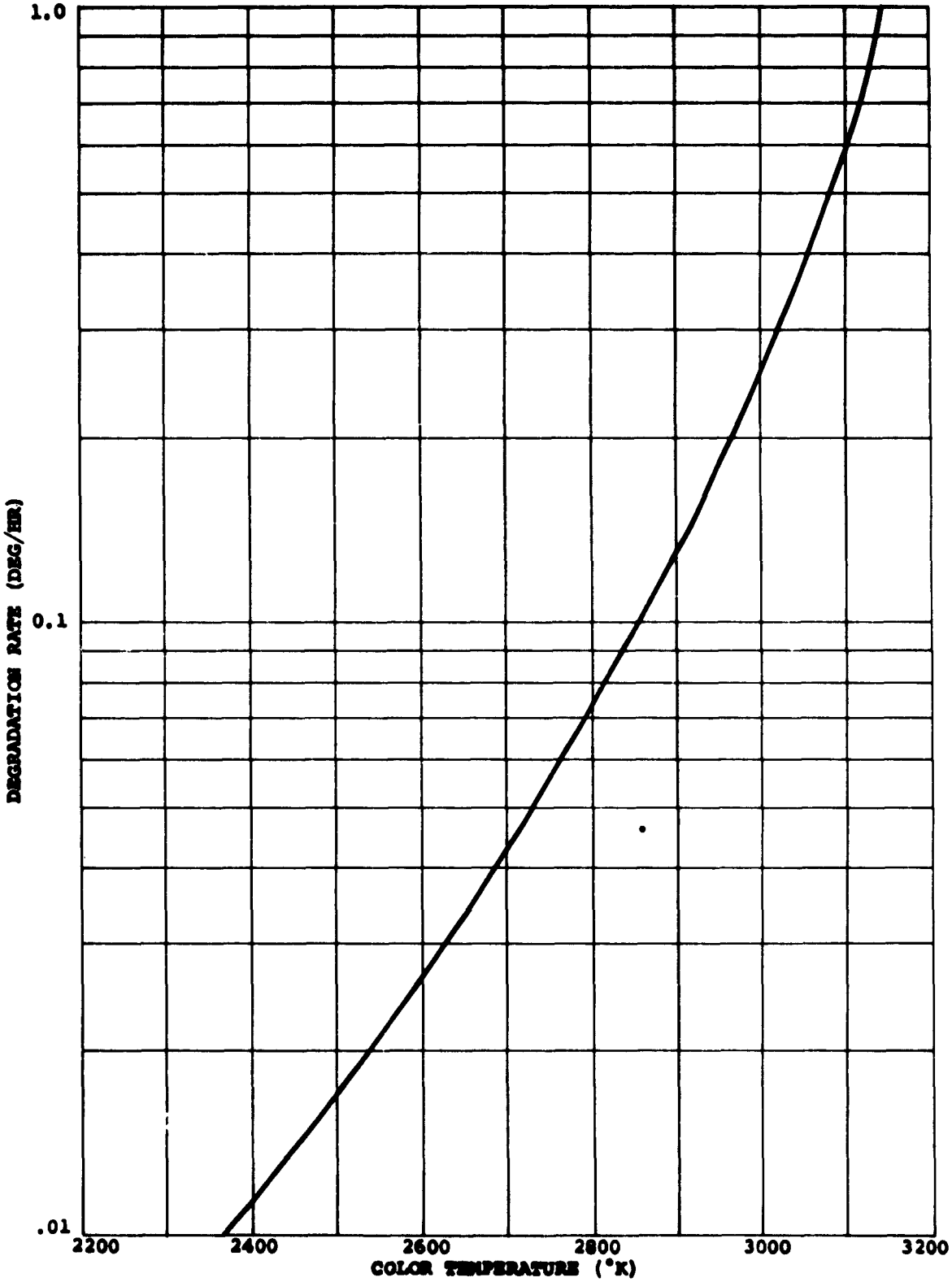

FIGURE 33 COLOR TEMP. DEGRADATION FOR A TYPICAL 400W MONOPLANAR FILAMENT LAMP

The effect of the brown film deposit on the inside of aged lamps was investigated. The transmission characteristics of the film were measured through an undisected lamp. As a result, the measurement was taken through two layers of film. Because of the curvature of the lamp, focusing prevented the taking of absolute transmission measurements. Figure 34 is the relative transmission of two film layers, front and back, from a 500W T20 lamp with over 1000 hours of operation. The measurements were taken into the infrared in order to include the spectral region affecting solar cells.

The smooth slope of this transmission curve explains the spectral shift which results in a color temperature decrease with bulb life.

As a result of this study, the following recommendations are made:

Direct current should be used for working with calibrated standard lamps on short-term calibrations, due to the more accurate instrumentation possible with DC.

Alternating current should be used for long-term operation to reduce lamp degradation.

Voltage measurements should be used to set lamps for the greatest precision.

Current measurements should be used to set lamps for long-term operation where a degradation may occur. The increased voltage required to maintain current on aging lamps tends to offset the degradation due to film deposits on the lamp.

2.2.0 TUNGSTEN IODINE

The tungsten iodine lamp is a relatively new development. It operates on the principle that the iodine reacts with the tungsten film deposited on the inside of the envelope when the quartz envelope is maintained at a temperature in excess of 600°C. The tungsten-iodine is gaseous at this temperature and is carried back to the filament, where, at a still higher temperature, it decomposes and deposits the tungsten back on the hot portion of the filament.

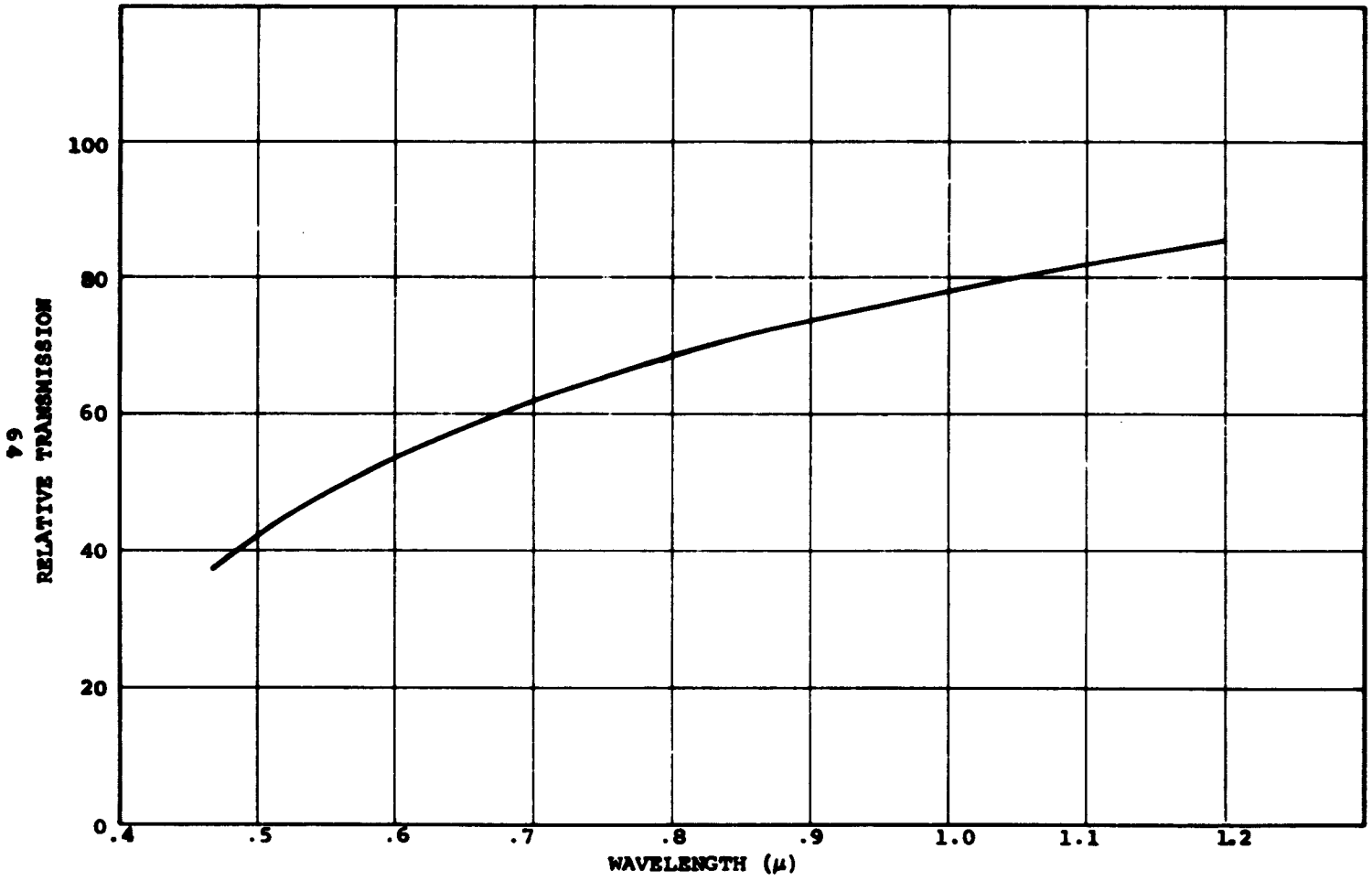

FIGURE 34 RELATIVE SPECTRAL TRANSMISSION "BROWN" TUNGSTEN LAMP

2.2.1 SPECTRAL DISTRIBUTION

Immediately after shutting the power off, the tungsten-iodine lamps tested have a purple color due to gaseous iodine. It was expected that the spectrum of the lamp would be shifted toward the blue as a result of this color. Careful measurements with the monochromator did not show any measurable difference between the spectrum of the tungsten-iodine lamps and the normal tungsten lamps. The spectral shift, if any, must be the result of a smooth absorption characteristic.

2.2.2 POWER REGULATOR

The lamps were operated at specified voltage rather than the reduced voltage required for a color temperature of approximately 2800°K. The reason for the higher power level was the fact that the design temperature is determined by power. The lamps were operated at 118 Volts and drew approximately 5.6 amperes.

2.2.3 DISTANCE FROM LAMP AT REQUIRED INTENSITY AND UNIFORMITY OF ILLUMINATION

The intensity was set in the same manner as in the tungsten measurements. The distance from the lamp was 28 inches, and the area enclosed by the 95% iso-intensity line is plotted full scale in Fig. 35.

2.2.4 LONG TERM VARIATION

Degradation tests were run with the lamps operating at rated voltage. The lamps were shut off at one hour intervals and color temperature was recorded at 5.6 amperes. Five lamps were tested in this manner, and the averages for each interval are plotted in Fig. 36.

After six hours of operation, the data showed that the lamps had been "seasoned", and they were left to burn continuously overnight. (These lamps were designed for intermittant duty in a home movie light system.) By morning all the lamps had failed by melting their quartz envelopes. The lamps were operated without reflectors and were accessible to air on all sides. They should have been cooler than with the reflector designed for use with them.

INTENSITY 100 mW/cm^2 "SUN EQUIV."
PROFILE AREA $\pm$ 5% OF MAXIMUM

TUNGSTEN IODINE LAMP DWY 625 WATTS
VOLTAGE SET AT 118V AC
LAMP TO TARGET DISTANCE 28 IN.

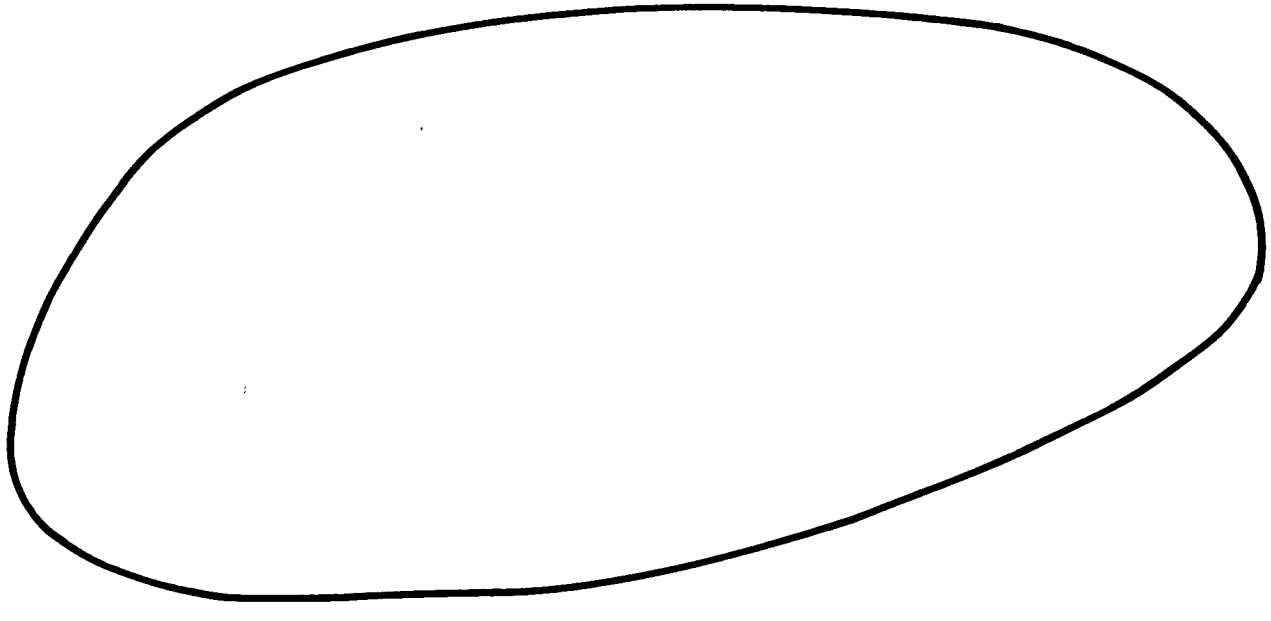

FIGURE 35 TUNGSTEN IODINE PROFILE

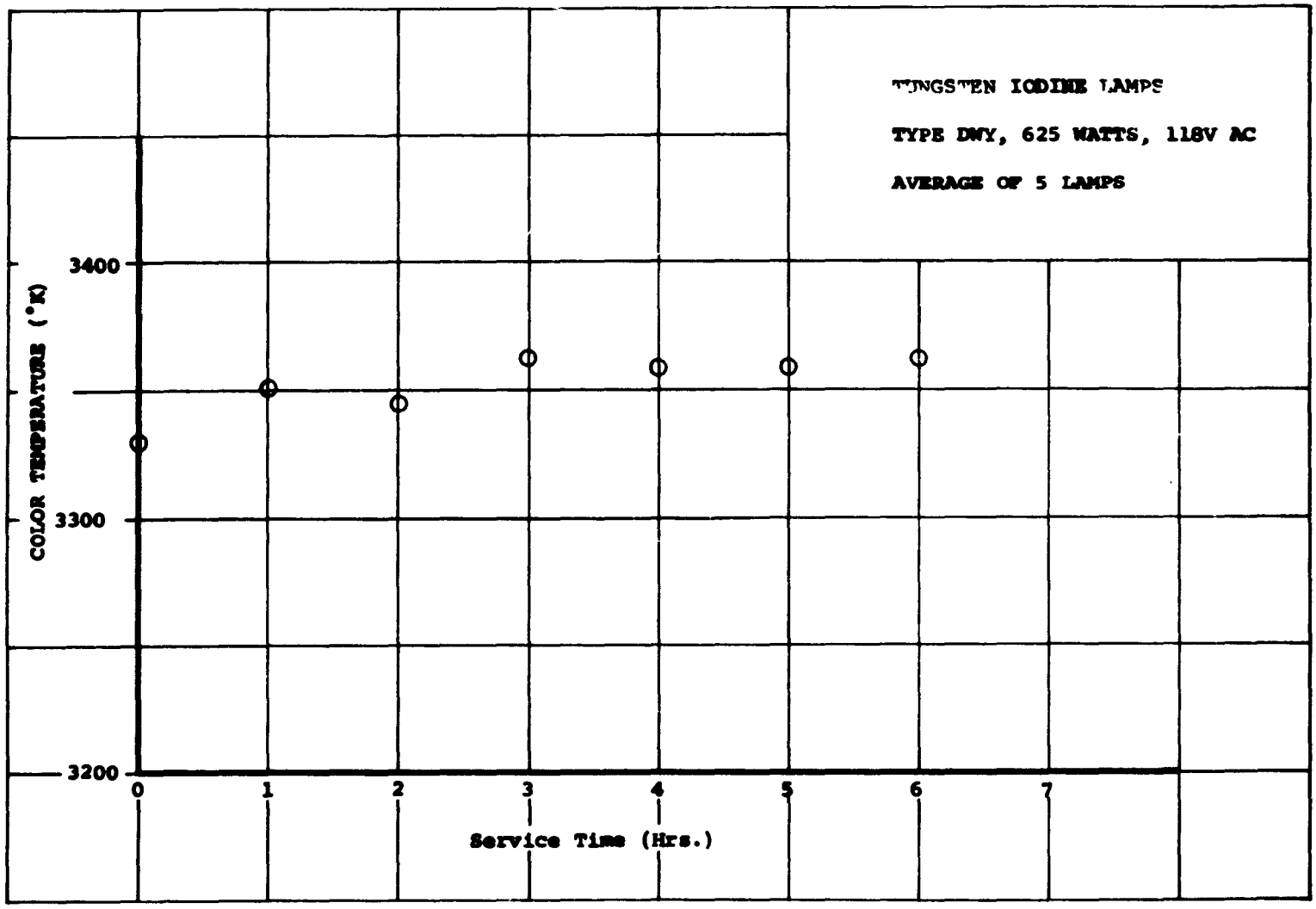

FIGURE 36 COLOR TEMPERATURE (°K) VS. SERVICE TIME (HRS.)

2.2.5 SHORT TERM VARIATION

I-V curves taken under the tungsten-iodine lamp, operating at rated voltage, exhibit none of the degradation shown in Fig. 1 for tungsten lamps.

2.3.0 XENON

Two lamps were chosen for these tests. The Osram XBO-162 lamp was selected as representative of compact short arc design, and the Osram XBF-6001 was selected as being representative of the long-arc lamps. These lamps have the following parameters:

	XBO-162	XBF-6001
Length of Arc	2.5 mm	110 mm
Average Life	1200 hrs	1000 hrs
Length	15 cm	33 cm
Diameter	5.8 cm	2.5 cm
Burning Position	Vertical ± 15°	any
Cooling	Forced Air	water

Both lamps were DC operated.

2.3.1 SPECTRAL DISTRIBUTION

The spectral distribution curve as presented by Osram for the XBF-6000 and XBF-6001 lamps is shown for reference in Fig. 37.

It has been found that the spectral distribution of xenon arcs is dependent upon lamp current. The radiation from a xenon arc is basically comprised of three components:[6] (1) The continuous spectrum from the gas itself, with a color temperature of approximately 6000°K; (2) a line spectrum due to the ionization of the xenon molecules; and (3) continuous radiation from the electrodes and envelope. The continuous spectrum from the quartz envelope on air cooled lamps at

---

(6) HANOVIA Chemical & Mfg. Co. (Engelhard Industries) brochure "Xenon and Xenon-Mercury Compact Arc Lamps"

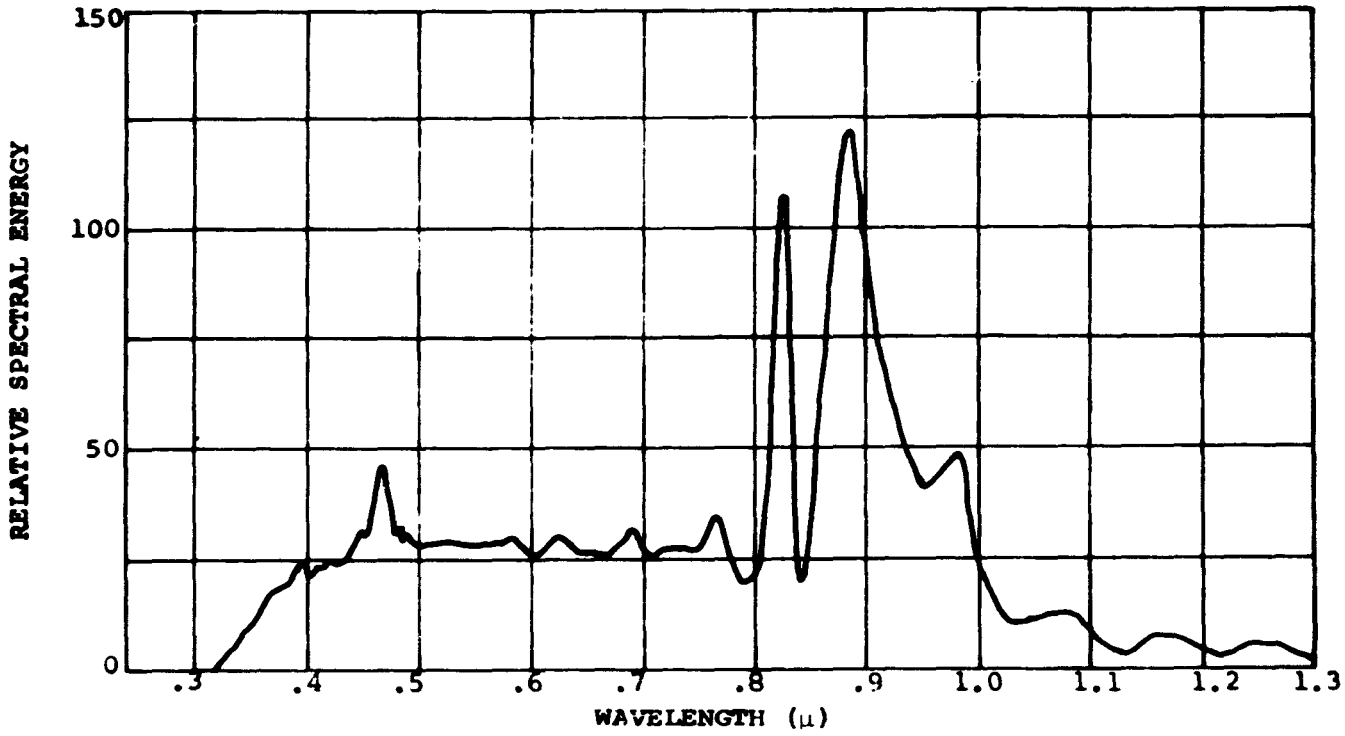

FIGURE 37 RELATIVE SPECTRAL ENERGY DISTRIBUTION OF HIGH-PRESSURE XENON LAMPS XBF 6000 & XBF 6001 (DATA FROM OSRAM)

operating current is essentially that of a black-body at 1100°K. This radiation varies with current but is primarily in the infrared beyond 2μ, and this does not affect solar cell measurements. The electrodes are incandescent having a color temperature of near 2800°K, and radiating about 70 watts per cm^2 of electrode surface.

Fig. 38 shows the relative spectral distribution of the XBO-162 air cooled lamp operating at 5 amp and at 7-1/2 amp. The curves have been normalized to the same output at .87μ.

2.3.2 POWER REQUIREMENTS

	XBO-162	XBF-6001
Supply Voltage	65-110 volts	220 volts
Operating Voltage	20 volts	165 volts
Current	7.5 amps	37 Amps
Wattage	150 watts	6000 watts

2.3.3 INTENSITY

It is impractical to operate arc lamps without reflectors. Because the lamp manufacturers do not recommend specific reflectors, and lamp geometries vary, the only comparison made is that of luminous flux. Attention is called to the fact that this specification pertains to the visible portion of the spectrum. The lamps tested were listed by the manufacturer.

XBO-162	3200 Lumens
XBF-6001	205,000 Lumens

2.3.4 LONG TERM VARIATION

The long-term degradation characteristics of the two different types of lamps is quite different. The air cooled arc lamps degrade through two mechanisms: (1) Erosion of the electrodes, greatly increased by the number of starts, and (2) through accumulation of dirt and electrode material on the bulb. As the electrodes erode with time, the short-term stability decreases. The dirt collected on the outside of the bulb burns into the quartz as the bulb temperature is quite

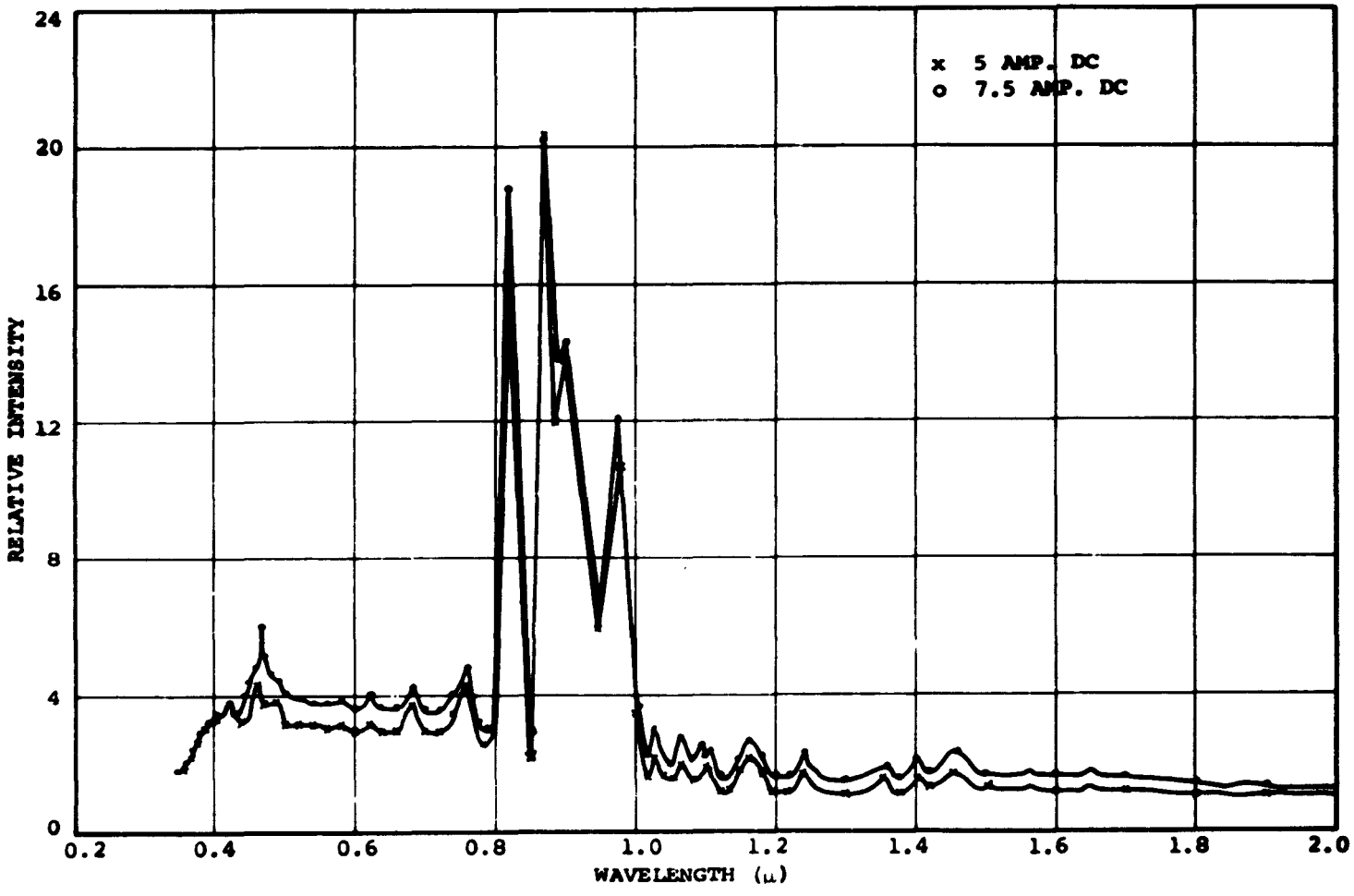

FIGURE 38 SPECTRAL DISTRIBUTION OF XENON XBO162 LAMP

high. The eroding electrodes deposit tungsten on the envelope, resulting in a gradual decrease in color temperature. Water cooled lamps suffer from the same electrode erosion, but foreign matter does not burn into the jackets as their temperature is low. However, contaminants in the cooling water darken the lamp.

Short-term stability of the long tube water-cooled arc is very good due to the contained nature of the arc. For greater than a 10 to 1 range in operating current, the arc fills the entire tube.

Stability measurements were made using a solar cell operating at short circuit current as a detector. Fig. 39 shows the stability of the XBF-6001 lamp operated over a 4 to 1 intensity range.

The lamp used had approximately 100 hours of operation out of a rated life of 1000 hours.

The compact arc lamp is less stable due to the unconfined nature of the arc. An excellent discussion of the stability is given in Ref. 1. Since the shape of the arc is a bow between the electrodes, this bow can move around the electrodes. With optical systems, this arc must therefore be out of focus. The blown glass bulb acts as a variable lens and distorts images when used in an optical system. An Osram XBO162 lamp was operated in the same manner as the XBF6001 lamp. The results are shown in Fig. 40. This lamp had been used for approximately 500 hours out of a rated life of 1200 hours.

Conclusions drawn from this study are that the water cooled line arc is the most suitable lamp with respect to stability. Also, because of the water absorption, changes in the spectral distribution beyond 1.4 microns are unnoticed.

2.3.5 SHORT-TERM VARIATION

The short-term variation of all arc lamps is a function of the power supply ripple. For the preceeding experiments the large arc was operated on full wave rectified three phase power. With balanced phases, this results in less than 5% ripple. I-V curves taken with this power supply coincide

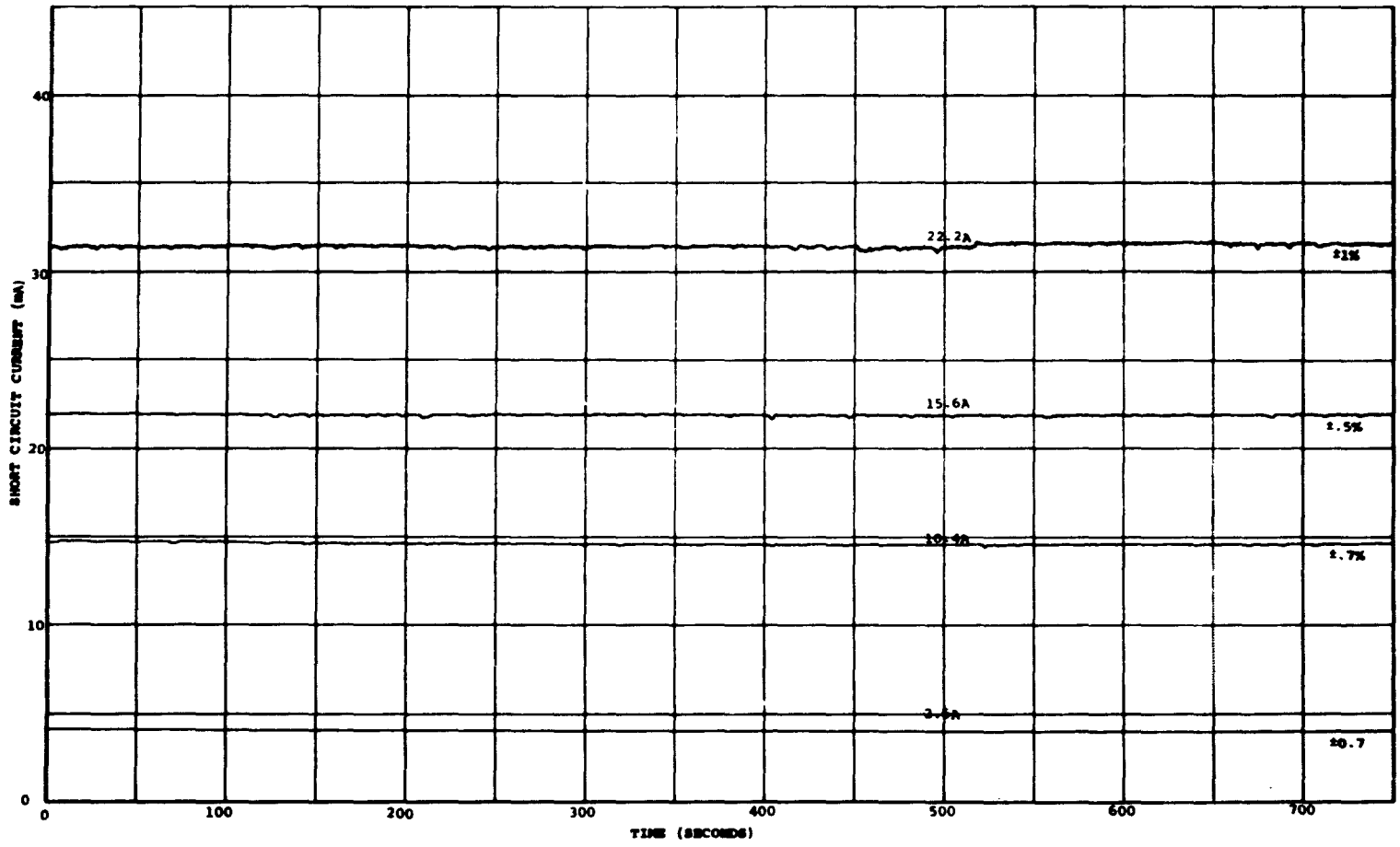

FIGURE 39 OSRAM XBP 6001 XENON ARC LAMP STABILITY TEST, 6000 WATT WATER COOLED - LONG ARC

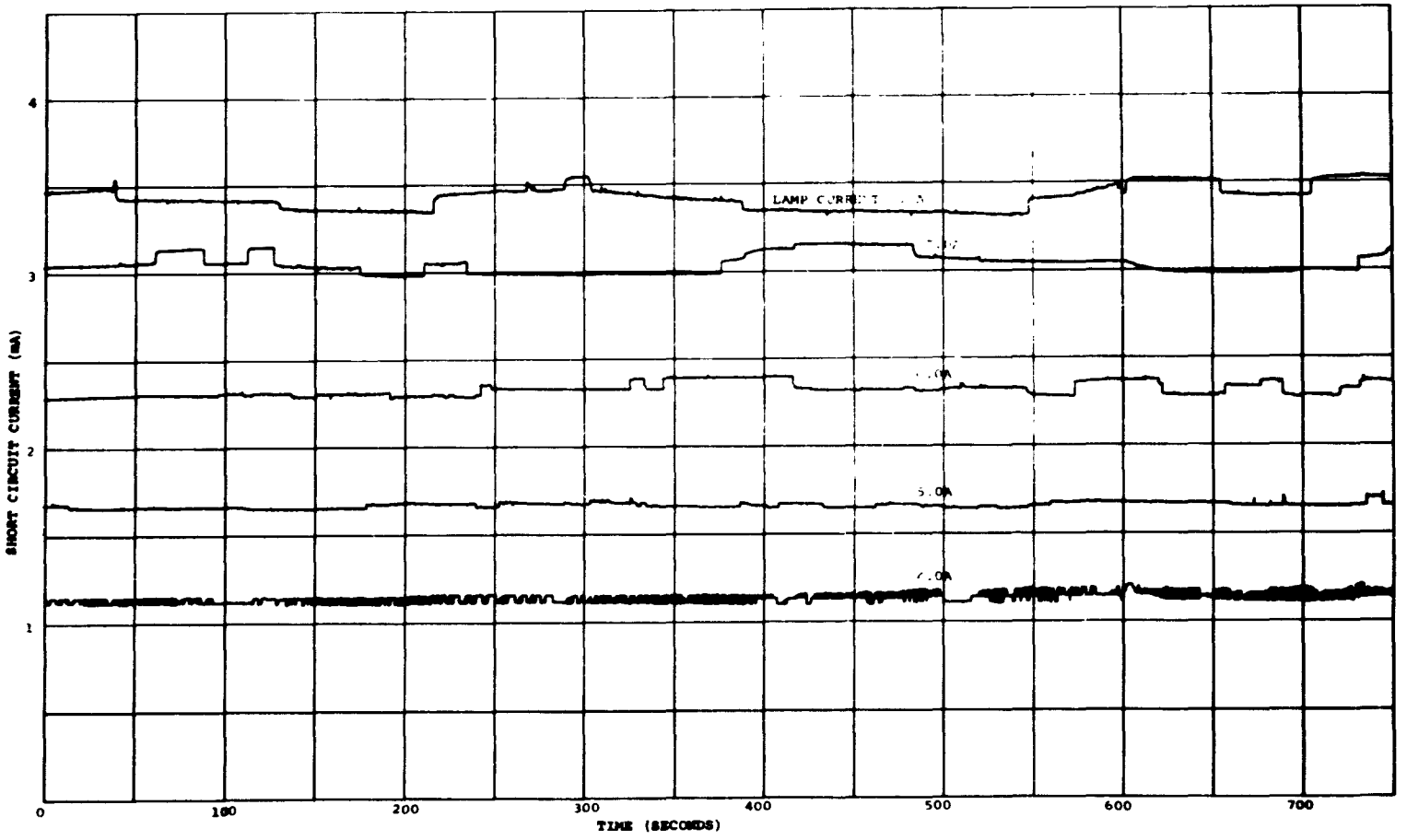

Fig. 40 OSRAM XBO 162 XENON ARC LAMP STABILITY TEST 150 WATT COMPACT ARC

exactly with curves taken with tungsten and show none of the degradation shown in Fig. 16.

2.4.0 XENON-MERCURY

The xenon-mercury data was taken from a Hanovia type 537B 1000 watt A.C. arc lamp with a 6.5 mm arc length.

2.4.1 SPECTRAL DISTRIBUTION

A xenon-mercury lamp is basically a mercury arc with xenon gas added to reduce starting and warm-up time. Consequently, the spectrum is predominantly that of the mercury arc with a background spectrum of xenon. At 0.7μ, for example, the xenon contributes approximately 25% to the total radiation. The spectral distribution variation with operating current is shown in Fig. 41. These curves have been normalized to show the spectral shift.

2.4.2 POWER REQUIREMENTS

The Hanovia 1000 watt lamp operates on 65 volts and 18 amperes.

2.4.3 INTENSITY

As with the xenon arcs, the xenon-mercury lamp intensity is rated in lumens. The Hanovia type 537B lamp puts out 52,000 lumens at rated power.

2.4.4 LONG-TERM VARIATION

The xenon-mercury arc lamps available are of the compact-arc variety. Consequently, they suffer from the same stability problem as those shown for xenon compact-arc lamps. A time plot was made using a solar cell operated at short circuit current as a detector and is shown in Fig. 42.

2.4.5 SHORT-TERM VARIATION

Because the lamp tested was an A.C. arc, the I-V curves of solar cells taken under this lamp show the full degradation of any 60 cycle arc. The difference between curves taken with

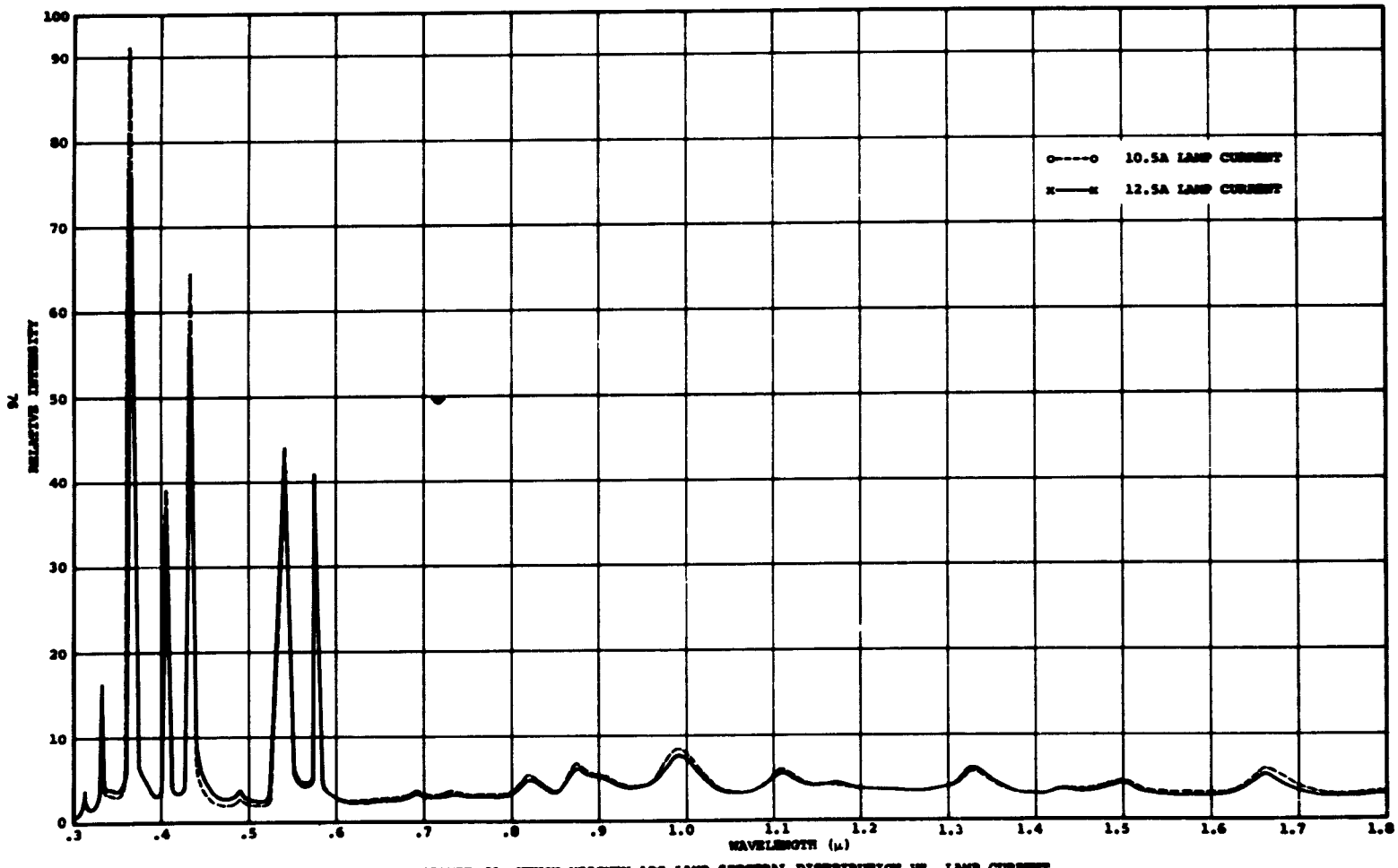

FIGURE 41 XENON-MERCURY ARC LAMP SPECTRAL DISTRIBUTION VS. LAMP CURRENT

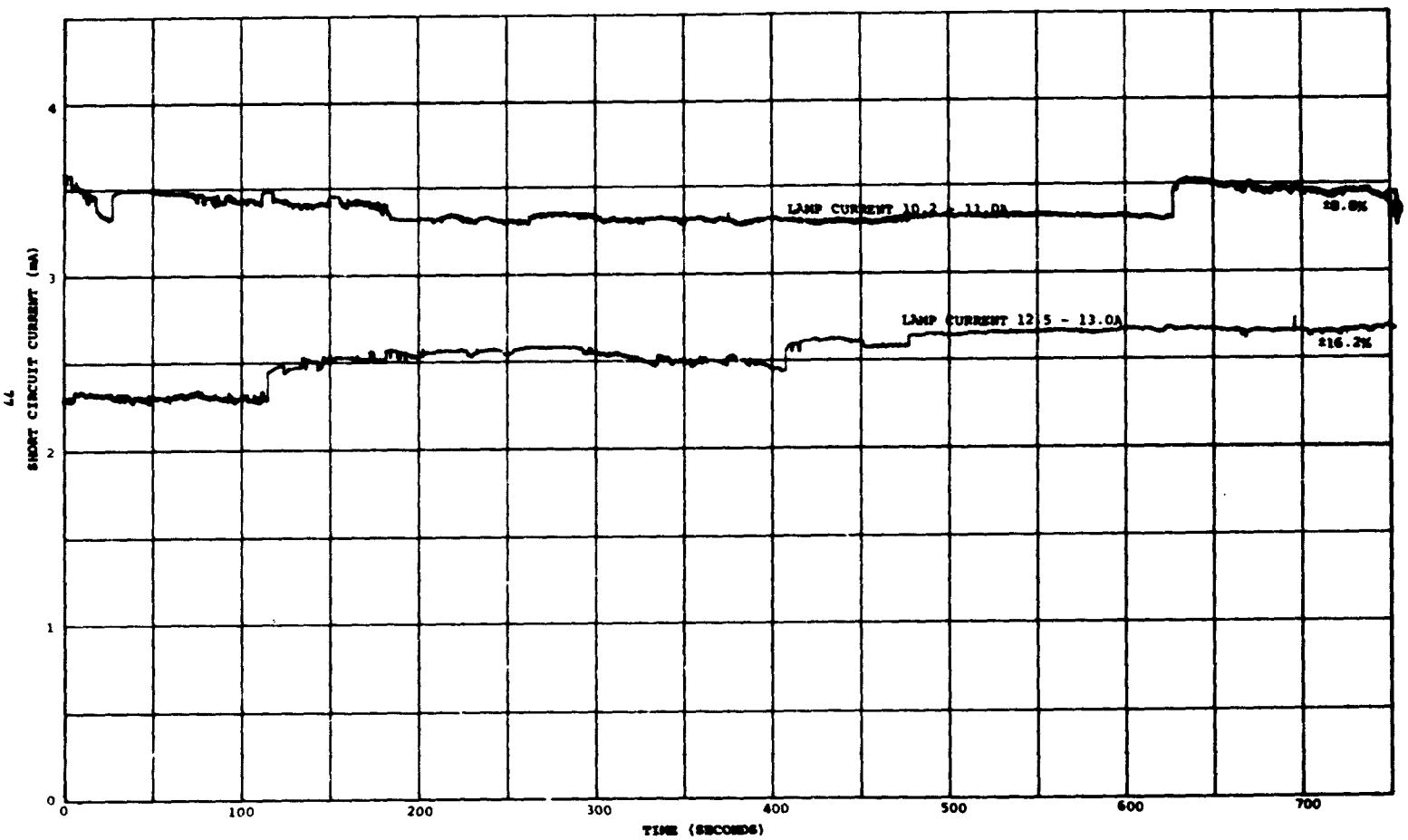

FIGURE 42 HANOVIA 537B AC XENON-MERCURY ARC STABILITY TEST

this A.C. arc and curves taken with tungsten is identical to that shown in Fig. 16.

2.5.0 CARBON ARC

Carbon arc studies were carried out with a Strong Electric Company UHI lamp. A thorough study of carbon arcs is covered in the "Fiat Final Report"[7].

2.5.1 SPECTRAL DISTRIBUTION

Different portions of the carbon arc have different color temperatures. The spectral distribution published for the "blown" type of arc is shown in Fig. 43. This spectrum is more blue than sunlight above the atmosphere. The spectral distribution published by the National Carbon Company[8] (carbon rod manufacturer) for the H. I. 13.6 mm bare carbon arc is shown in Fig. 44. The latter spectrum is more red than sunlight above the atmosphere. For the purposes of this contract, a Strong Electric Company UHI carbon arc lamp was measured without any lenses at a current of approximately 150 amps. The results of this measurement are shown in Fig. 45. The fine resolution details are questionable due to intensity variations during the measurement.

2.5.2 POWER REQUIREMENT

The power required for the selenium rectifier system supplied with the arc lamp is 220 volts three phase at 49 amperes.

---

(7) Finkelnburg, W. "The High Current Carbon Arc" Fiat Final Report No. 1052. Office of Military Government for Germany (US), Field Information Agency Technical

(8) Gibson, D. W. & Weinard, J., "The Absolute Spectral Energy Distribution of Different Light Sources", Proceedings at the Solar Working Group Conference, Section 12, Interagency Advanced Power Group PIC-SOL 209/2.1. April 1962.

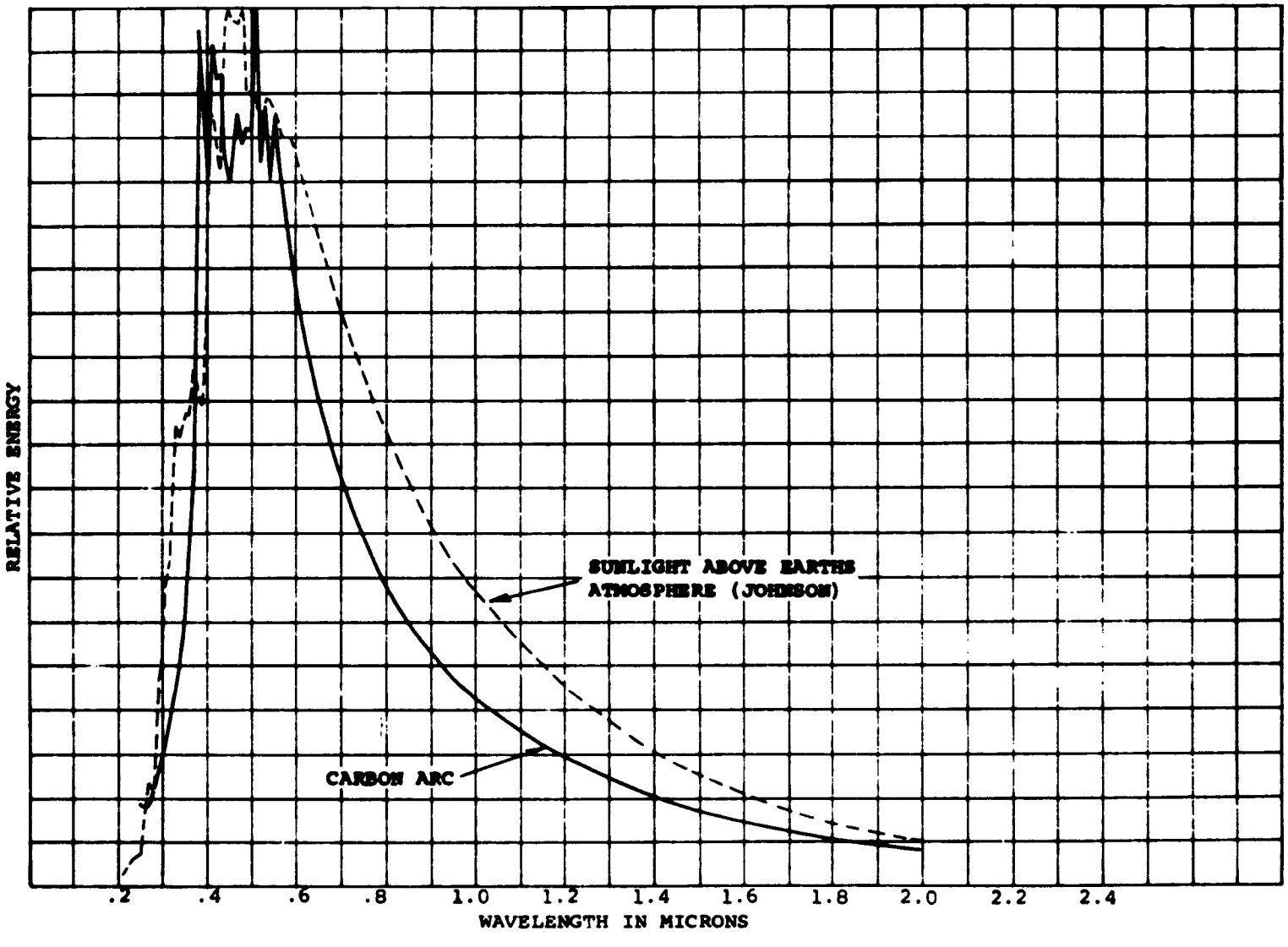

FIGURE 43 SPECTRAL ENERGY DISTRIBUTION

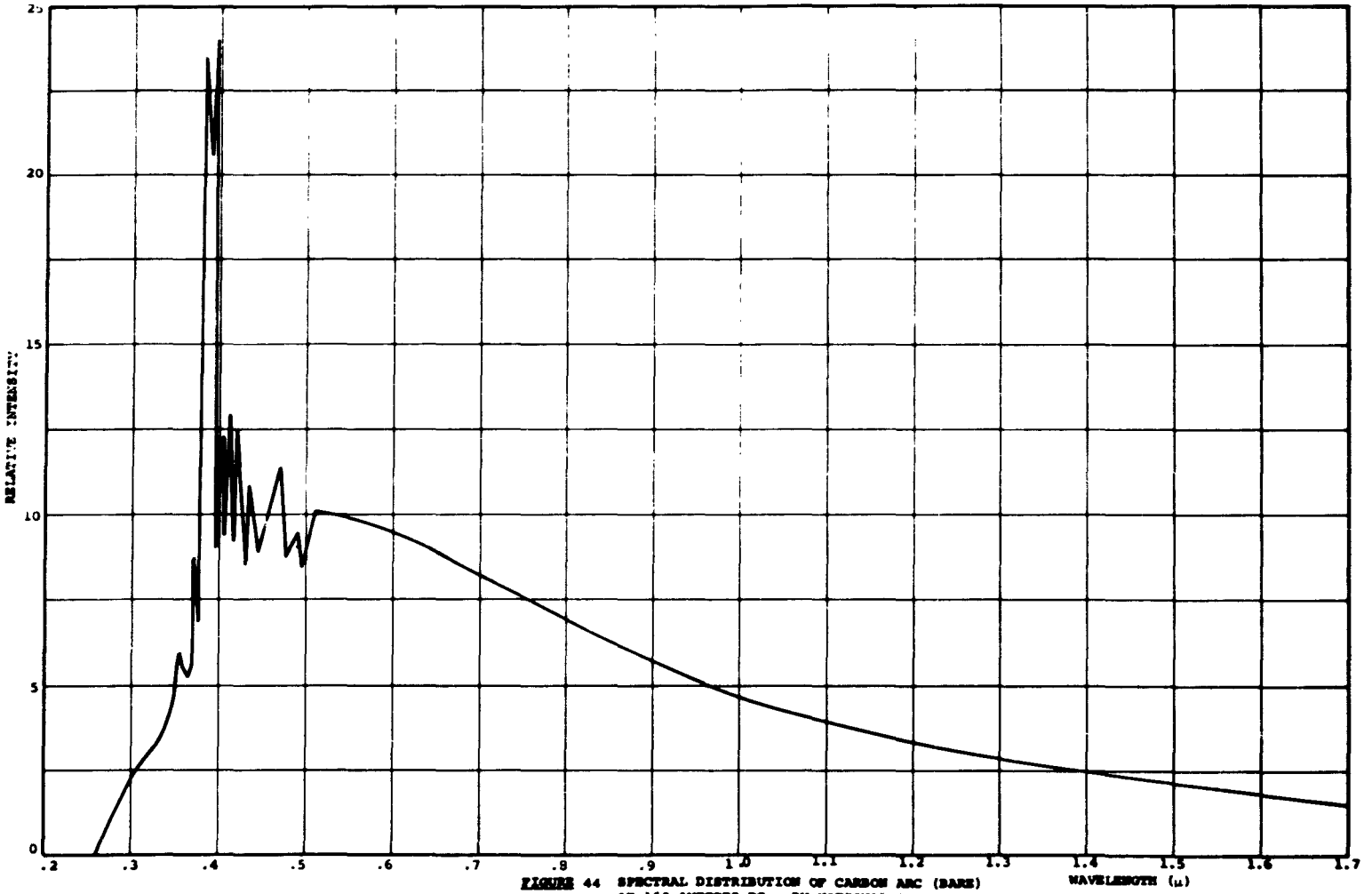

FIGURE 44 SPECTRAL DISTRIBUTION OF CARBON ARC (BARE) AT 160 AMPERES DC - BY NATIONAL CARBON CO.

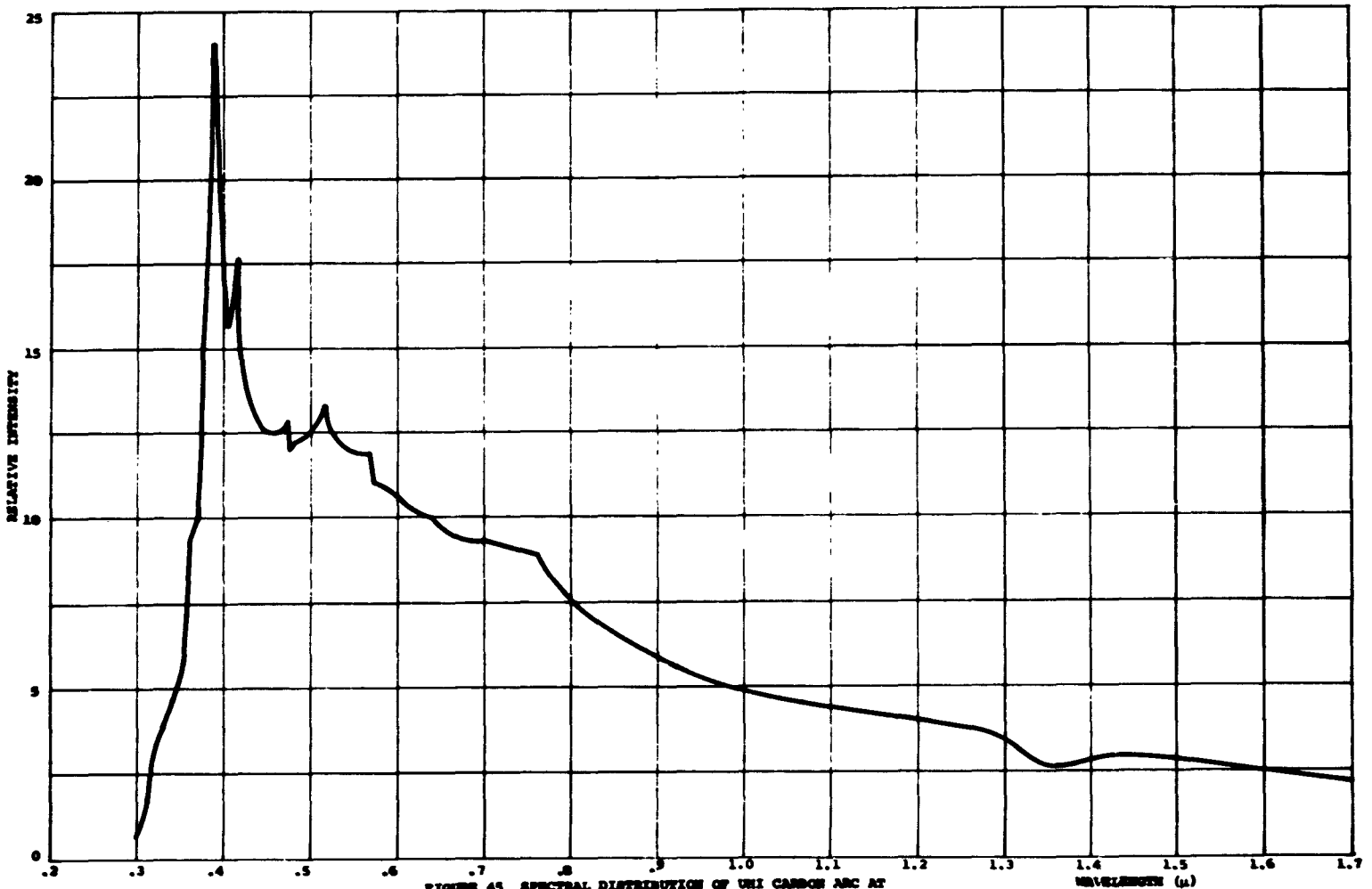

FIGURE 45 SPECTRAL DISTRIBUTION OF UHI CARBON ARC AT APPROXIMATELY 150 AMPERES DC

2.5.3 DISTANCES FROM LAMP AT REQUIRED INTENSITY AND UNIFORMITY OF ILLUMINATION

Because the lamp is supplied with a reflector, intensity measurements were made in the same manner as with the tungsten lamps. The required intensity occurred at approximately 15 feet. The intensity varied more than 10% with time and prevented measuring the 95% iso-intensity line. It is estimated that the area of 95% intensity uniformity is approximately 8 inches in diameter.

Other carbon arcs are sold with lens system having various influences upon uniformity.

2.5.4 LONG-TERM VARIATIONS

The intensity of the arc operating at approximately 152 amperes was measured with a solar cell reading short circuit current. A plot of intensity vs. time is shown in Fig. 46. The regular pattern of the intensity fluctuations coincides with the speed of rotation of the positive carbon (approximately 10 seconds). The fluctuation of longer period (approximately 150 seconds) is probably due to the tracking of the servo which drives the carbons. In approximately 20 minutes the positive carbon burns up and the lamp must be shut down for carbon rod replacement.

2.5.5 SHORT-TERM VARIATIONS

The carbon arc, like other arcs, depends upon the power supply ripple which influences the light intensity. The lamp tested was operated on three phase power and as a result did not show ripple. An I-V curve was drawn of a solar cell and is shown in Fig. 47. The long-term fluctuations caused the variations of the heavy curve. Several minutes were required to scan the load resistance range for making this plot. Two curves are

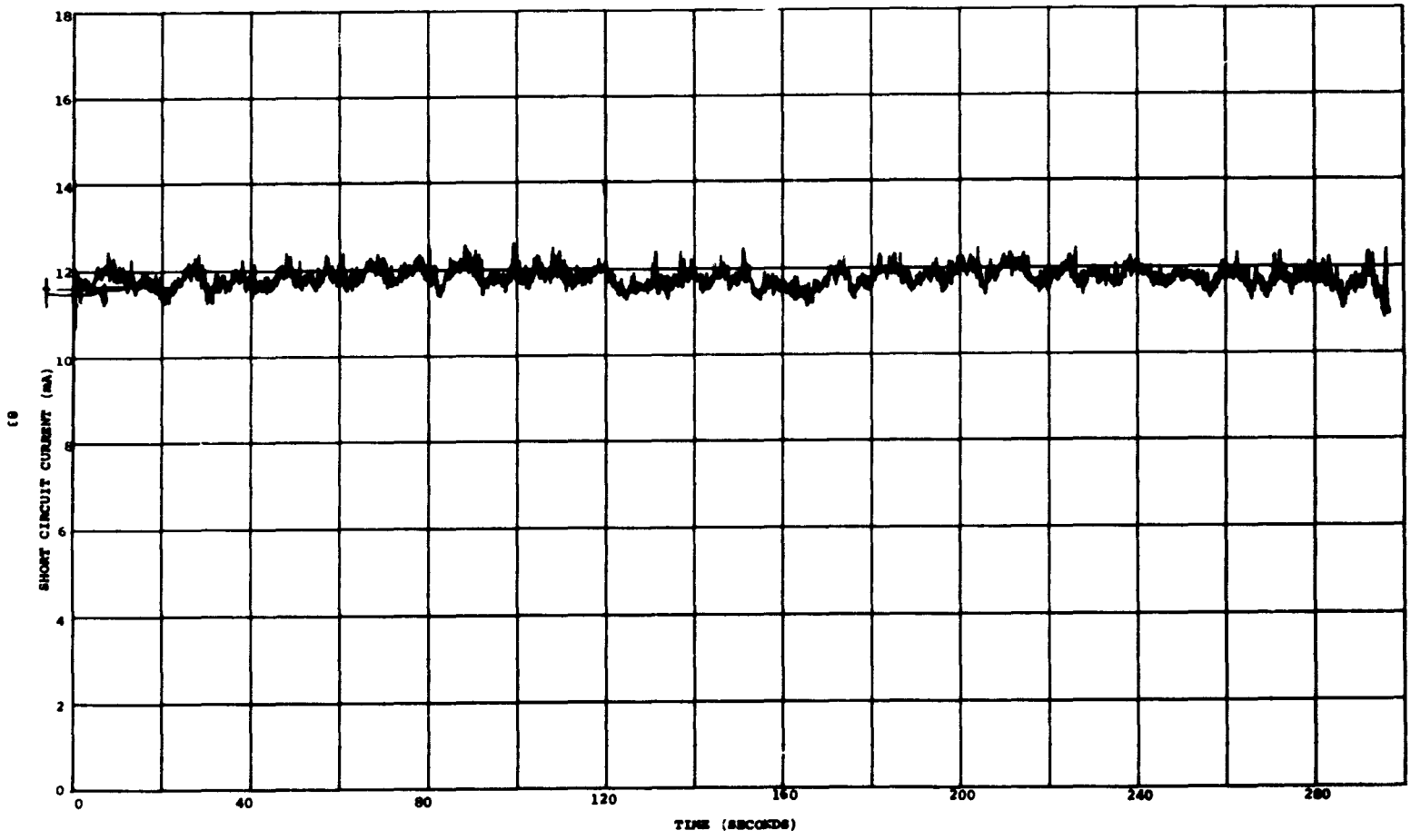

FIGURE 46 CARBON ARC STABILITY TEST

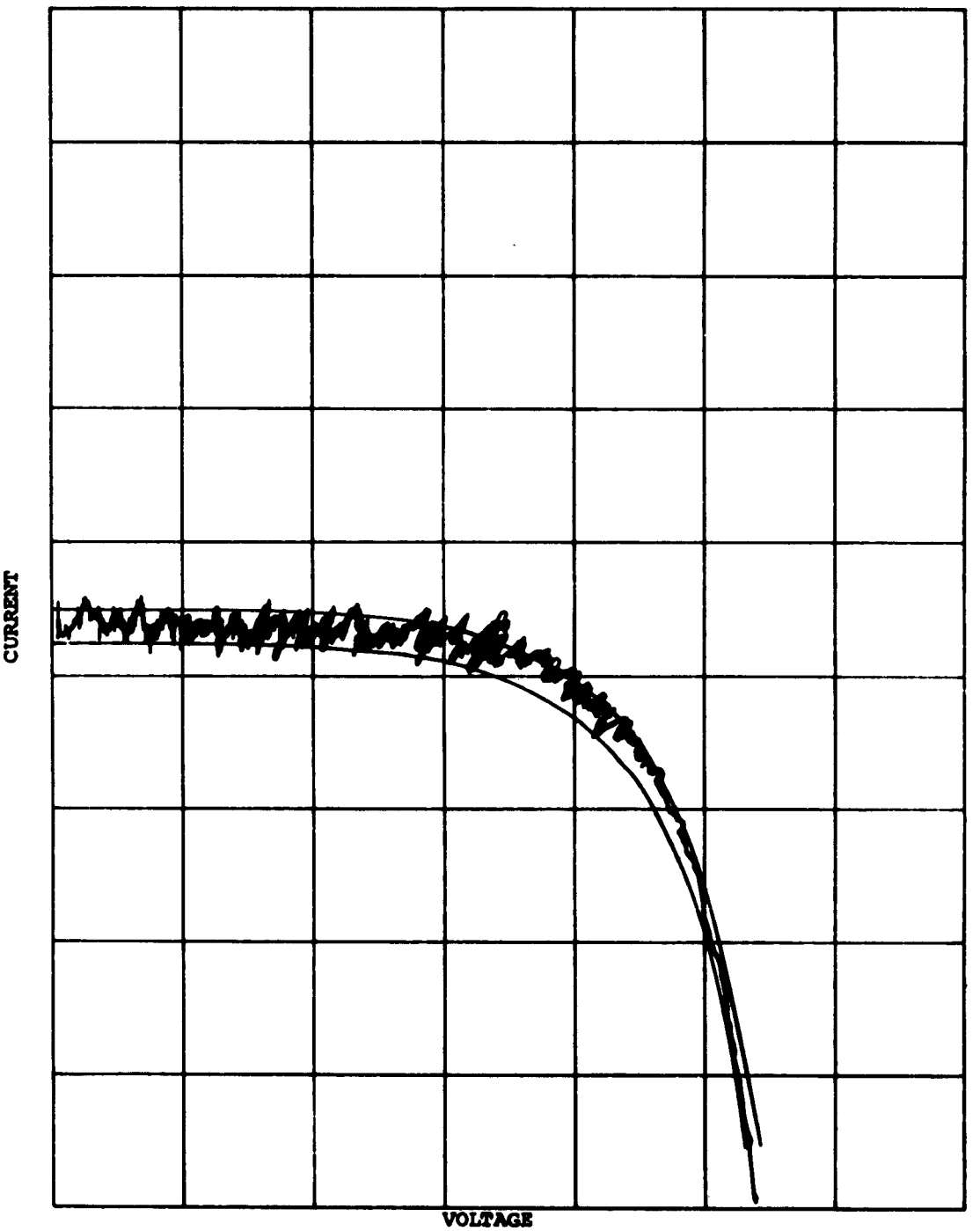

FIGURE 47 SOLAR CELL CHARACTERISTICS WITH CARBON ARC AND WITH TUNGSTEN

superimposed near the extremes of the variation. These two curves were drawn at two different intensities with a tungsten lamp. It can be seen that, eliminating the long-term variation, the carbon arc does not exhibit any short-term degradation as is shown in Fig 16.

2.6.0 COMBINATIONS AND MODIFICATIONS OF LIGHT SOURCES

Several combinations and modifications of light sources have been investigated for the testing of solar cells for space use. These light sources are used as simulators of the sun's radiation. Much work has been done in an effort to specify this type of a simulator.

2.6.1 SPECIFICATIONS FOR SUNLIGHT SIMULATORS

Preliminary specifications for solar simulators have been set forth by the AIEE. These specifications are reproduced below:

The mean solar constant in space near earth shall be assumed to be 139.5 mW/cm^2. In the spectral region between 3,000 and 12,000 Angstroms, the integrated energy shall be assumed to be 109.4 mW/cm^2.

Throughout the 3,000 to 12,000 Angstrom spectral region, the total energy in any wavelength band shall not deviate from that in the same band under the Naval Research Lab. Johnson curve (Journal of Meteorology, 1954) by more than the following indicated percentages in every elemental area (one centimeter square) of the test region:

Specification #	$\Delta\lambda$	$\pm$ %
1A	200Å	20
1B	400Å	15
1C	600Å	10
1D	1000Å	5

The integrated energy output shall be 109.5 mW/cm^2 between 3000 and 12000 Angstroms subject to the following tolerances:

2. Maximum drift between calibrations ± 1%

3. Intensity uniformity ± 2% (for a 1cm^2 area or 10% of the test area, whichever is smaller)

4. Allowable ripple 2% (peak to peak)

5. Collimation ±6°

6. Precision of setting 1/2%

2.6.2 AVAILABLE SOLAR SIMULATORS

Following are some of the more popular solar simulators available today. This list of light sources is based upon a literature survey for all but the Hoffman simulator.

2.6.2.1 SPECTROLAB

Two solar cell test simulators manufactured by Spectrolab Division, Textron Electronics, Inc., are known as the Spectrosun© Models D-1203 and D-1206. These units are identical except for the illuminated areas, the former test area being 12 x 3 cm and the latter 12 x 6 cm. Each incorporates a single compact xenon arc as a source in conjunction with interference filters. The instrument uses the single lamp in order to minimize the spectral difficulties resulting from balancing two sources.

The specifications 2, 3, 4, and 6 are met over the specified test areas. The collimation angles of 2° x 6° and 4° x 6° for the two instruments, respectively, exceed specification 5. Intensity may be continuously varied ± 20% from the nominal 140mW/cm^2, with additional provisions for an increase of the Model D-1203 intensity in steps to 300 mw/cm^2. Specification 1 is not met. No data has been shown for the simulator with regard to its compliance to specification 1a, and the published data is now obsolete for specifications 1b and 1c. Current data was not available at the time of publication of this report.

Maximum deviation of specification 1d taken from the 1000 Angstrom integrations and their locations are listed below:

1d (±5%)	Spectral Band	Deviation
	$\lambda \leq .36\ \mu$	$\geq$ 5% becoming 100% deficient .30μ
	$.36\mu < \lambda < .89\ \mu$	$< \pm 5\%$
	$.89\mu \leq \lambda \leq .94\ \mu$	$< \pm 10\%$
	$.94\mu < \lambda < 1.00\ \mu$	$< \pm 5\%$
	$1.00\mu < \lambda < 1.07\ \mu$	$< \pm 10\%$
	$1.07\mu < \lambda < 1.12\ \mu$	$< \pm 5\%$
	$1.12\mu < \lambda < 2.00\ \mu$	$< \pm 10\%$

The spectral distribution curve for the Spectrosun Model D-1203 Solar Simulator vs. NRL air-mass-zero distribution for a resolution of 1000 Angstroms is shown in Fig. 48.

2.6.2.2 OPTICAL COATING LABORATORY

The Optical Coating Laboratory, Inc. has constructed a solar simulator to meet the AIEE specifications. The simulator avoids the complex filtering problem of a xenon single source by eliminating the troublesome portion of the xenon compact arc spectrum with interference filters and filling in the remainder with a filtered tungsten lamp(9). The unit meets specifications 2 and 3 over an area of 1 x 3", in addition to meeting 5 and 6. AC ripple is listed as ± 4%. Deviations from specification 1 are listed as follows:

Spec.	λ Range	% Deviation
1A (±20%)	<.310μ	---
1B (±15%)	<.320μ	---
1C (±10%)	<.320μ	---
1D (±5%)	<.340μ	---
	.91 - .92μ	+5.3%

The spectral distribution of this simulator vs. the NRL air mass zero curve is shown in Fig. 49.

---

(9) Apfel, J. H. and Thelen, A. J., "A Solar Simulator", Proceedings of the Solar Working Group Converence, Section 7, Inter-agency Advanced Power Group PIC-SOL 209'2.1, February 1962.

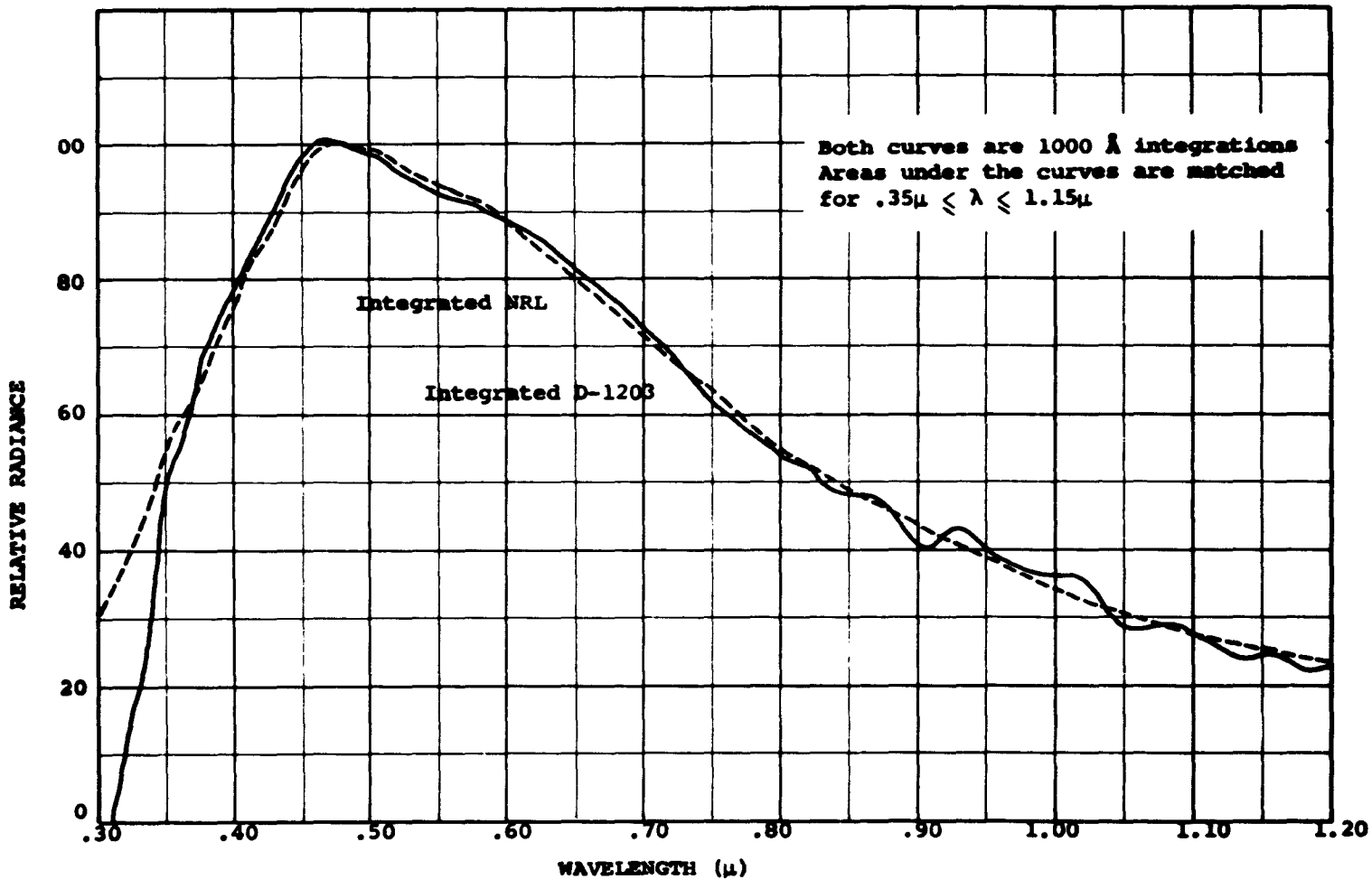

FIGURE 48 SPECTROSUN[R] MODEL D-1203 - TYPICAL SPECTRAL RADIANCE VS. NRL SOLAR RADIANCE

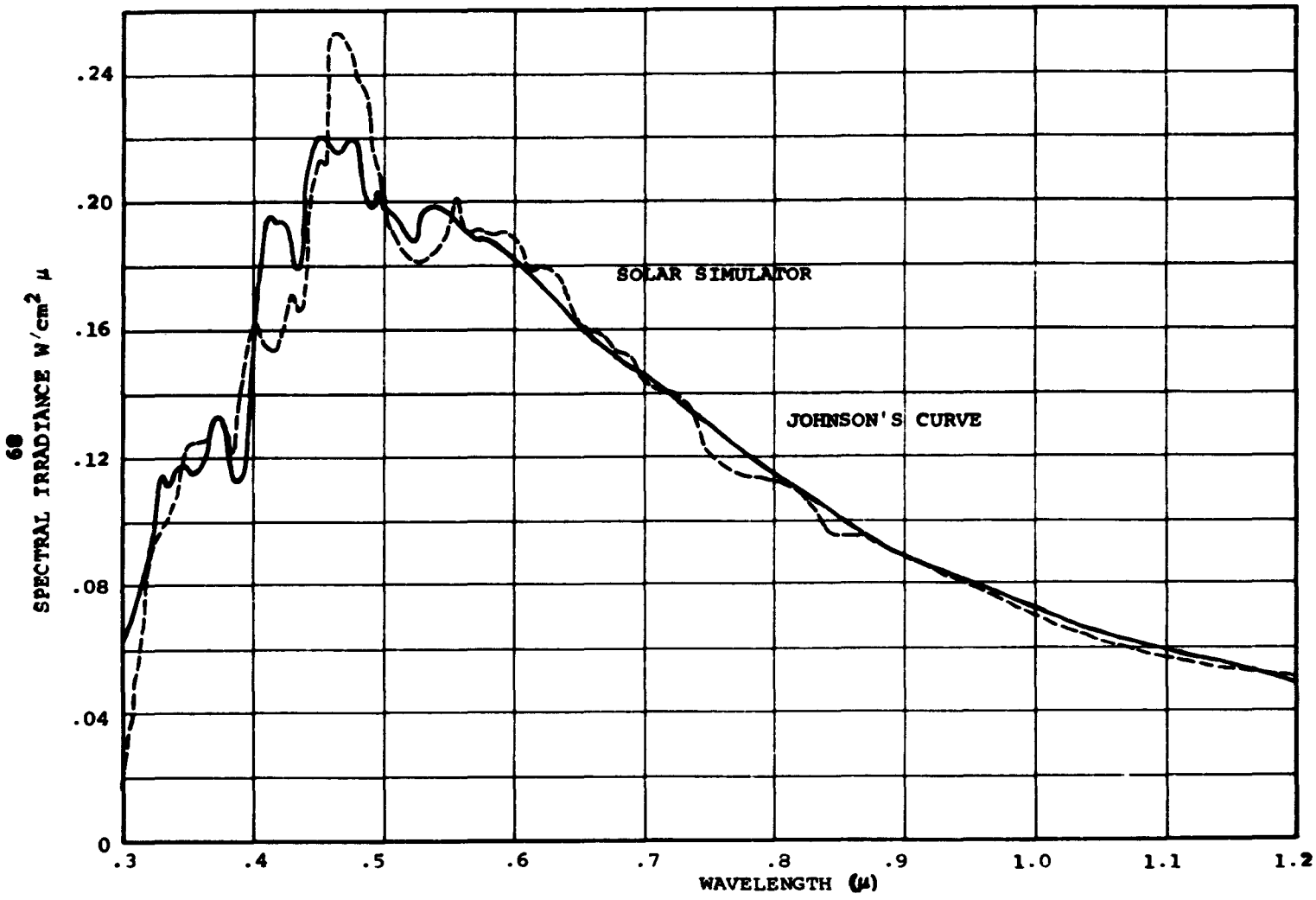

FIGURE 49 SPECTRAL DISTRIBUTION OF OCLI SOLAR SIMULATOR OUTPUT COMPARED TO JOHNSON'S CURVE

2.6.2.3 HOFFMAN ELECTRONICS CORPORATION

Hoffman Electronics Corp., Semiconductor Division, has also constructed a solar simulator for the purpose of testing silicon solar cells[10]. This unit also combines a xenon arc with a tungsten lamp, but uses a water-cooled line arc with absorption filters. This unit does not meet specification 5, having a collimation half-angle of ±20°. Specifications 2, 4 and 6 are all met. Specification 3 is exceeded over a 1x3" area. Deviations from specification 1 are listed below:

Spec.	λ Range	% Deviation
1A (±20%)	.452-.472μ	+27%
	<.375μ	---
1B (±15%)	<.375μ	---
1C (±10%)	<.380μ	---
	1.020 - 1.080	-12%
1D (±5%)	<.380μ	---
	.600 - .750μ	+7.1%
	1.00 - 1.100	-11.4%

The spectral distribution of this unit is shown in Fig. 50 as compared with the NRL zero air mass curve.

---

(10) Bickler, Donald, "The Hoffman Solar Simulator", Proceedings of the Solar Working Group Conference, Section 6, Inter-agency Advanced Power Group PIC-SOL 209/2.1, February 1962.

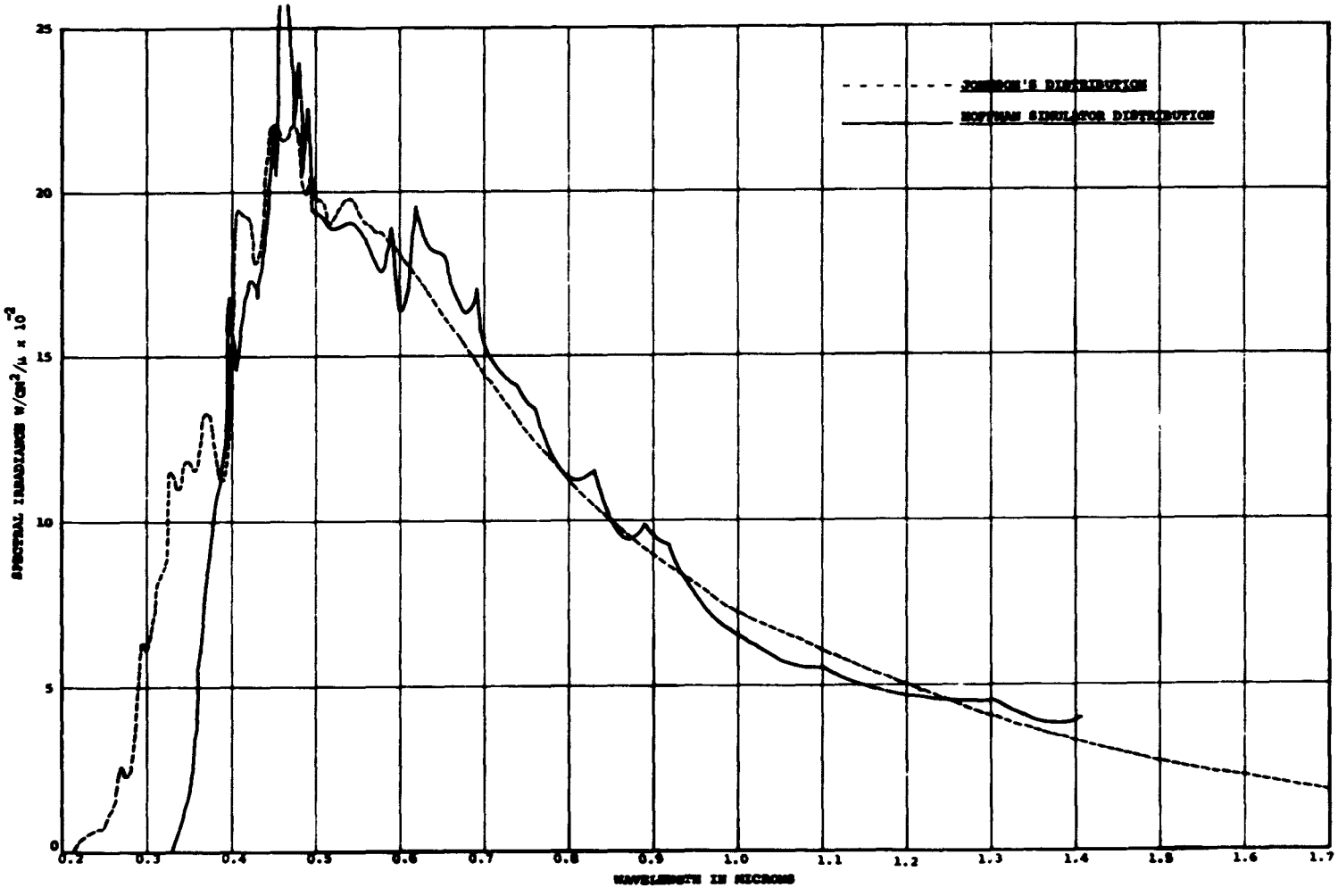

FIGURE 50 HOFFMAN SOLAR SIMULATOR SPECTRAL DISTRIBUTION COMPARED TO NRL (JOHNSON'S) SPACE DISTRIBUTION

APPENDIX IV

PROCEDURES AND INSTRUMENTATION CONSIDERATIONS IN DETERMINING THE OUTPUT OF SILICON SOLAR CELL POWER SUPPLIES

1.0 SOLAR CELL POWER SUPPLY OUTPUT MEASUREMENTS

The preferred means of determining the output of silicon solar cell power supplies is from the illuminated forward current-voltage characteristics. To accomplish this, an X-Y recorder is used, in conjunction with suitable current sensing resistors and a variable load, to plot the I-V curve. A schematic diagram of such a system is shown in Fig. 51, and a typical I-V curve is shown in Fig. 52.

1.1 THE X-Y RECORDER

The X-Y recorder chosen for tracing the I-V characteristics of solar cells and solar cell power supplies is a self balancing voltmeter type with an accuracy of ± 0.2% of full scale. The most sensitive range of the instrument is 0.5 mV/in. and is used for current sensing on the axis with a 10" full scale deflection.

Using a 10" scale length and a desired full scale current of 100 mA, the required resistance value is 50 mΩ and for 1 amp full scale the resistance is 5 mΩ. These current sensing resistors should be accurate to within 0.1% and should maintain this tolerance at any power level required.

1.1.1 CURRENT SENSING

The recorder has an input impedance of 200kΩ/volt on the lower ranges. For .5mV/in with a scale length of 10 inches, the input impedence will be 1kΩ. Then any current sensing resistor up to 1Ω will contribute a maximum of 0.1% error. Since the input impedence of the voltage channel is 200kΩ, all of the current output from the solar cell power supply flows through the current sensing resistor and X-Y recorder. Thus, the anticipated maximum error in current readings is ±0.5%.

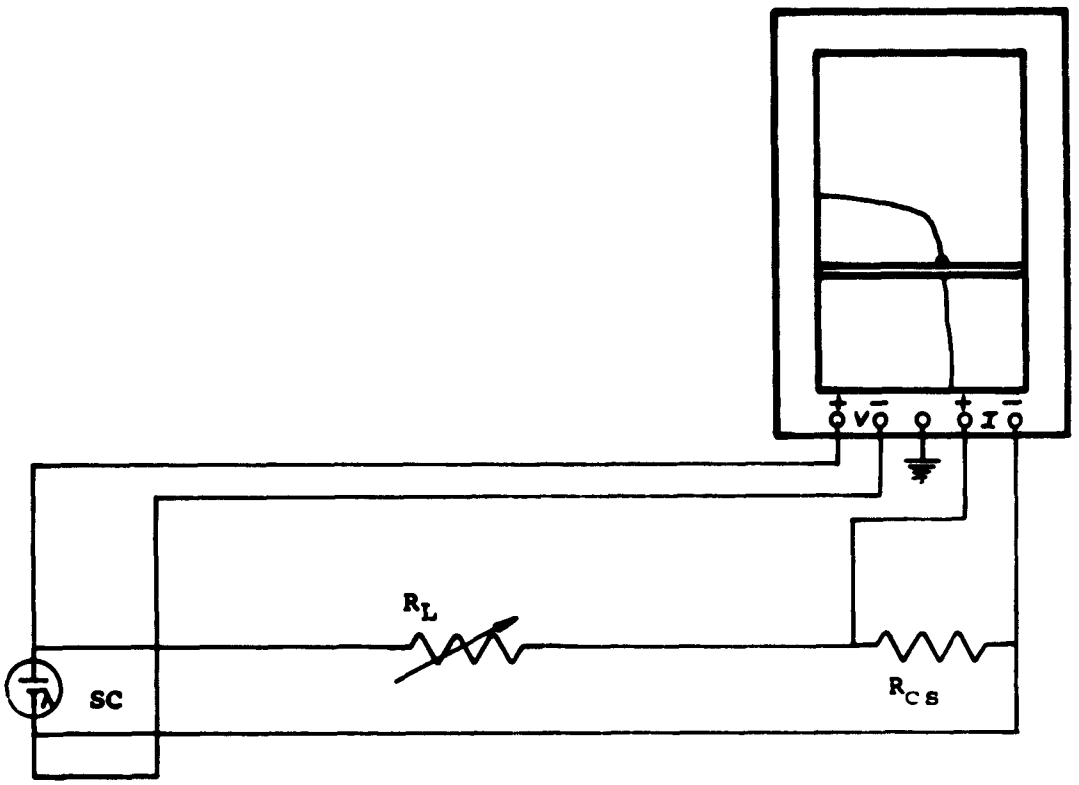

SC = solar cell

R_L = variable load resistance 0- ∞ Ω

R_{CS} = current sensing resistance

FIGURE 51 I-V CURVE-TRACER

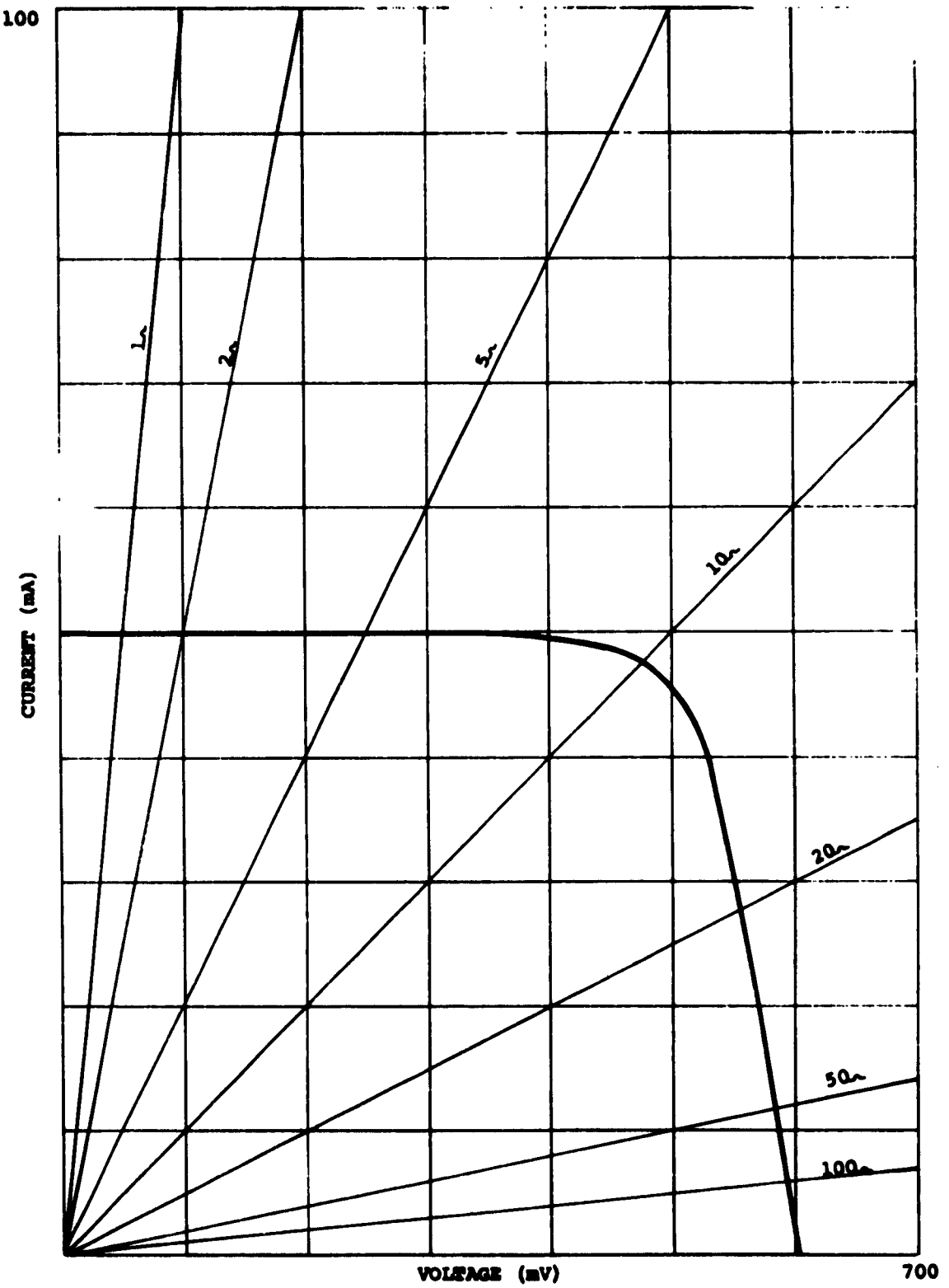

FIGURE 52 I-V CHARACTERISTIC CURVE

1.1.2 VOLTAGE SENSING

The minimum range used for voltage measurements is 100mV/in. The input impedence on this range is 200kΩ/volt. Considering a scale length of 10", the total impedence is then 200kΩ. At a voltage level of 500mV, the total current drain from the solar cell power supply is 2.5×10^{-6} amps. The difference between the voltage at this current and true open circuit voltage is negligible.

1.2 THE VARIABLE LOAD

The variable load may be based upon several techniques. A potentiometer may be used for R_L if certain conditions are met. The "zero" resistance must be low enough to give an accurate short circuit current reading and the "open circuit" resistance must be high enough to give an accurate open circuit voltage reading. Referring to Fig. 52 (the curve of a single cell), it is seen that one portion of the curve is drawn by varying the resistance from 0 to 10Ω and the remainder of the curve from 10Ω to ∞.

To keep the speed of the pen of the recorder under 5"/sec, required for maximum accuracy, either a ten-turn potentiometer or a non-linear potentiometer must be used. A typical potentiometer value for single cell testing is 500Ω. This may be turned slowly enough during the first revolution of 50Ω to yield an accurate curve. A non-linear potentiometer could be used with a total resistance of 1000Ω and a logarithmic resistance characteristic.

To allow operation with higher output powers, a resistive load in the form of a rheostat, either hand operated or motor driven may be used. However, this arrangement is somewhat bulky and cumbersome. A more desirable solution is to absorb the power in transistors. This system may be made lightweight and compact. Another advantage of using transistor circuitry is the low power control circuit required to drive the transistors which may be operated through a potentiometer, a capacitive-charge circuit or may be programmed through the use of operational amplifiers.

If the capability of the load does not include resistances of less than 1Ω, it is desirable to incorporate a separate power supply capable of passing the entire solar cell current and having sufficient voltage to bias the cell in the reverse direction. A more accurate determination of short-circuit current may thus be made.

Four wires connecting the load box to the panel are required to maintain high accuracy. One pair of wires serves the voltage measuring circuit, the other pair serves the current measuring circuit. This procedure prevents the voltage drops across the current carrying wires from influencing the voltage readings. The current flowing through the voltage leads will ordinarily be sufficiently small that any practical wire size may be used. The wires carrying the current should be large enough so that the voltage drop along them is of the same order of magnitude as the voltage drop across the current sensing resistor. The greater the voltage drops in these wires, the greater will be the error in recording short-circuit current. Contact resistances throughout the current-carrying system must likewise be held to a minimum.

A convenient means to locate the maximum power point on a graph is to plot the curve on a chart which has hyperbolic lines of constant power imprinted upon it. These lines may be labeled for power output or for efficiency for any set of scales, particular size of converter and given illumination. Fig. 53 shows graph paper of this type for 1 x 2 cm cells having 1.8 cm^2 of active area with 100mW/cm^2 sunlight equivalent incident radiation.

In order to provide a rational basis for solar cell and panel extrapolation, the liberty is taken to briefly digress into the realm of solar cell device engineering.

The crudest model of the solar cell as a two-terminal black-box gives rise to the DC equivalent circuit pictured in Fig. 54.

As shown, a generator G provides a current I_L which is shunted by a diode D. The current I into the load impedance R_L is simply

$$I = I_L - I_D \qquad (1)$$

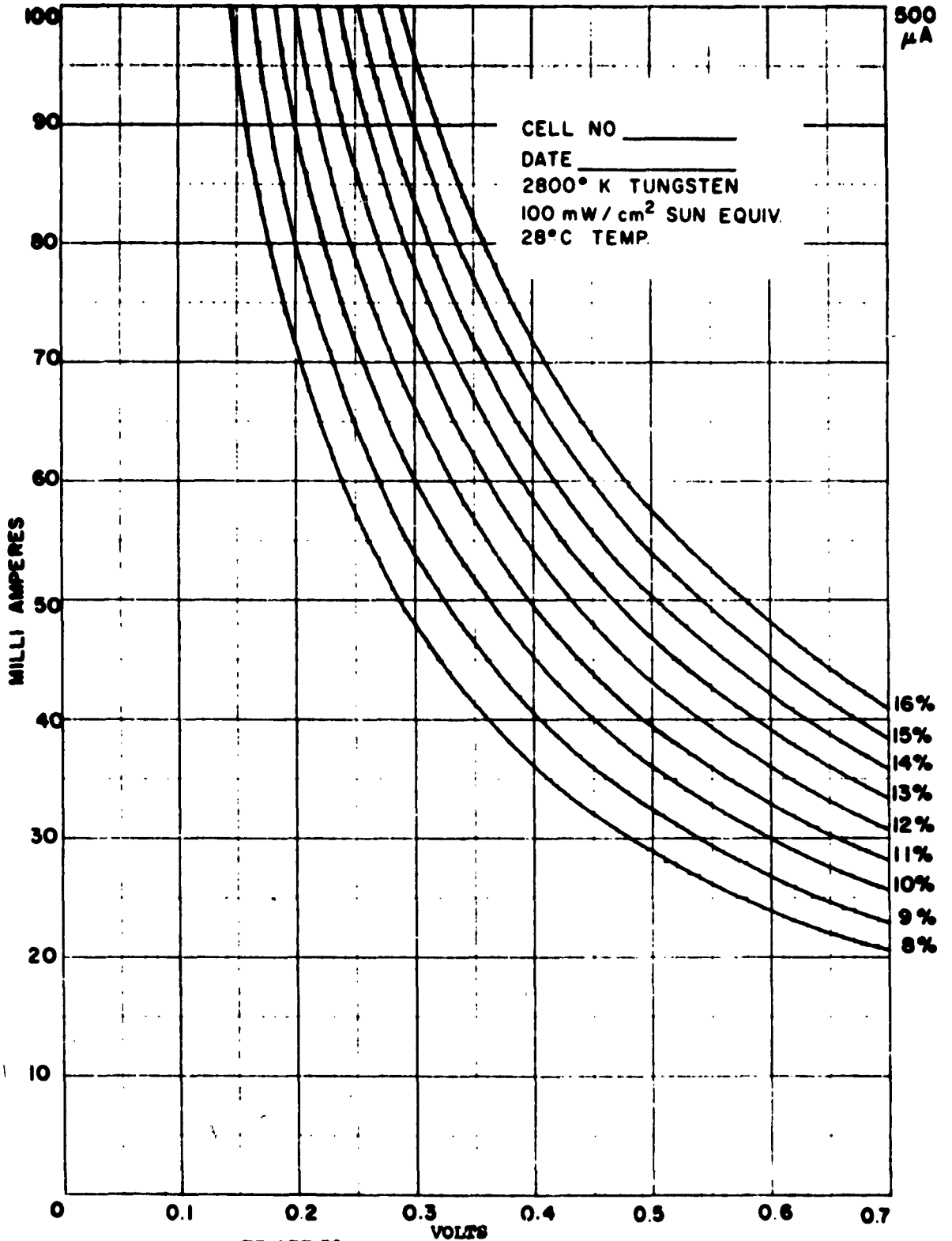

FIGURE 53 SOLAR CELL EFFICIENCY PAPER

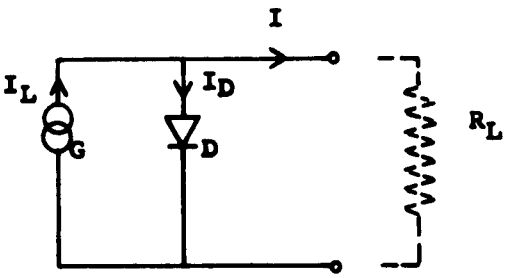

FIGURE 54 SIMPLEST SOLAR CELL DC EQUIVALENT CIRCUIT

Since D is a PN junction diode, I_D is a strong function of voltage, and we have according to Shockley[1].

$$I_D = I_o \left(\exp \frac{qV}{kT} - 1\right) \qquad (2)$$

where I_o = Saturation current of a PN junction

q = Electronic charge

k = Boltzmann constant

T = Absolute temperature

The solar cell I-V curve may now be synthesized from an ideal diode curve I_D subtracted from a constant current I_L as shown in Fig. 55.

When this curve is compared with a real solar cell characteristic, several discrepancies arise. It is noted that I_D is by no means a true exponential. This has been acknowledged by insertion of a "constant" (A)[2] in the exponential of equation (3)

$$I_D = I_o \left(\exp \frac{qV}{AkT} - 1\right) \qquad (3)$$

The quotation marks indicate a rather variable voltage dependent "constant". The value of A varies from as high as 4 or 5 in some units near the origin to between 1 and 2 near V_{oc}. This factor alone would not jeopardize an extrapolation. If we draw a second generator current I_{L_2} we find the available load current still by subtracting the diode curve, which, neglecting temperature effects, retains its curve shape independent of current. The short circuit current of this solar cell is

---

(1) Shockley, W., Bell Syst. Tech. Jour. 29, 436

(2) Sah, C. T., Noyce, R. N., and Shockley, W., Proc. IRE 45, p. 1228, (Sept. 1957).

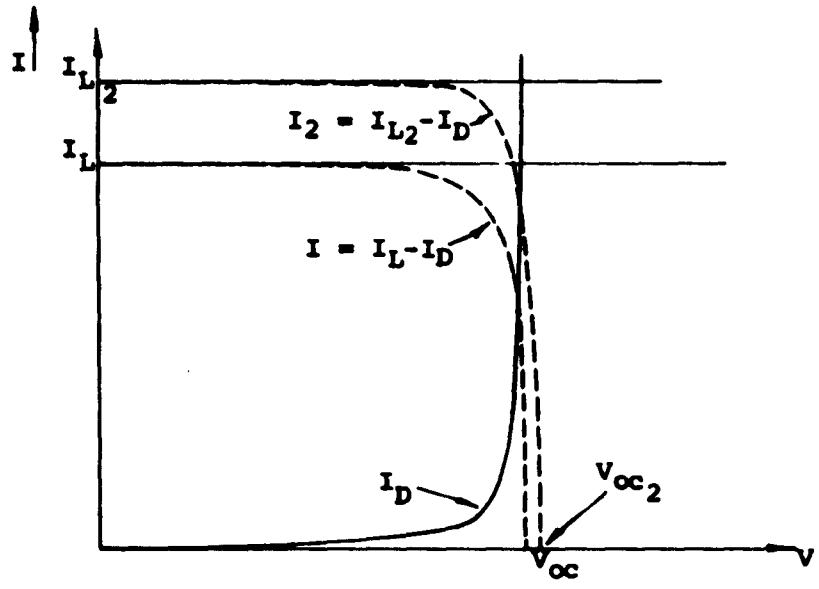

FIGURE 55 IDEAL SOLAR CELL CHARACTERISTIC

$$I_{sc} = I_L - I_o \left(\exp \frac{qV}{AkT} - 1\right) = I_L \qquad (4)$$

and for I_{L_2} $\qquad I_{sc2} = I_{L_2}$ $\qquad (5)$

since for any power conversion application

$$I_{sc} \gg I_o \quad \text{and letting} \quad \frac{q}{AkT} = V_o^{-1}$$

one obtains

$$I = I_{sc} - I_o \exp \frac{V}{V_o} \qquad (6)$$

To find V_{oc}

$$I = 0 = I_{sc} - I_o \exp \frac{V_{oc}}{V_o} \qquad (7)$$

$$V_{oc} = V_o \ln \frac{I_{sc}}{I_o} \qquad (8)$$

For an increase in light intensity to I_{sc_2}

$$\frac{I_{sc_2}}{I_{sc_1}} \quad I_o \exp \frac{V_{oc_2} - V_{oc_1}}{V_o} \qquad (9)$$

$$V_{oc_2} = V_{oc_1} + V_o \ln \frac{I_{sc_2}}{I_{sc_1}} \qquad (10)$$

In order to approximate the real solar cell more closely, one may redraw the equivalent circuit of Fig. 54 as shown in Fig. 56. In Fig. 56 two resistances were introduced. R_s is a series resistance and is due to the sheet resistance of the thin diffused layer, the thickness of the bulk semiconductor material, the contact resistance of the metal-semiconductor joints and any lead resistance that might be present. It is typically from 1/4 - 1/2Ω in gridded solar cells. In ungridded cells, it is

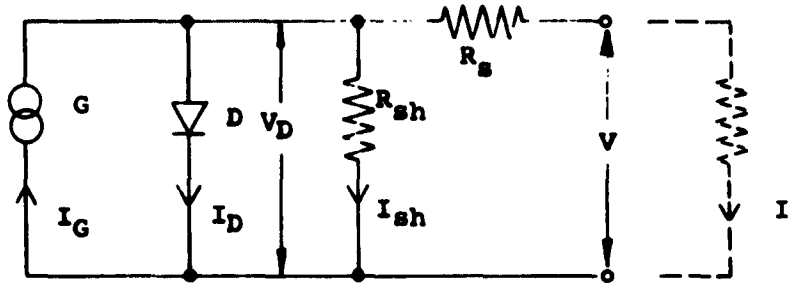

FIGURE 56 LESS SIMPLE SOLAR CELL DC EQUIVALENT CIRCUIT

one order of magnitude larger. R_{sh} represents a shunt resistance across the diode D. It is caused by inversion or conducting layers, moisture, etc. In good cells R_{sh} is from 10KΩ to 100KΩ.

The equation for this solar cell is

$$I_L = I_D + I_{sh} + I \tag{11}$$

$$I = I_L - I_D - I_{sh} = I_L - I_o \exp\left(\frac{V+IR_s}{V_o}\right) \quad \frac{V+IR_s}{R_{sh}} \tag{12}$$

This is a transcendental equation, the current I appearing in the dependent variable and in the argument of the exponential function. It cannot be explicitly evaluated. Since the shunt resistance R_{sh} is so large it can usually be neglected.

The actual solar cell model appears to be even more complicated. This was first noted by Shockley[1] in his "Patch Effect in P-N Junctions" (It may be noted that this work was done five years before the invention of the solar cell). A recent paper by M. Wolf and H. Rauschenbach[3] elaborates on the complexity of the actual solar cell model as a distributed matrix of resistance linked diodes. It is the author's belief that the situation is even more complex in that it involves a two-dimensional matrix. Wolf et al (Ibid) were able to show considerable improvement by going to a second order lumped constants model. However, for purposes of practical field tests, such a method proves far too cumbersome.

Returning to Fig. 55, it is evident that the diode curve shape is no longer independent of the current I and an extrapolation by a simple shift of the voltage axis can no longer be accomplished. However, an extrapolation may still be made based upon establishment of the series resistance of the cell or panel[4]. This will be referred to as Swanson's method and is reproduced here.

---

(3) Wolf, M. and Rauschenbach, H., Conference paper, General Meeting of the AIEE, Salt Lake City, Utah, Aug. 23-25, 1961.

(4) L. D. Swanson, & L. W. Schmidt, Internal publication, Hoffman Semiconductor Division.

The I-V characteristic for the cell or panel is plotted at two arbitrary light intensities I_{L_α} and I_{L_β}. See Fig. 57. No knowledge of these light levels is required. Now a current increment ΔI is chosen and subtracted from the short circuit current of both curves. The voltages corresponding to these currents is measured. The difference in voltages $V_\beta - V_{oc}$ divided by the difference in the new current, $I_\alpha - I_\beta$ gives the desired series resistance R_s. This comes about as follows: The incremental current $I_{oc} - I_\beta$ is the current component I_D shunted through the diode. Therefore, the ideal diode voltage (V_D in Fig. 56) must be identical for the two cases.

In accordance with Fig. 56 and neglecting R_{sh}

$$I = I_D = I_o \exp \frac{V_D}{V_o} = I_o \exp \frac{V + I_\alpha R_s}{V_o} \tag{13}$$

$$I_\alpha = I_{L_\alpha} - I_o \exp \frac{V + I_\alpha R_s}{V_o} \text{ since } I_{L_\alpha} - I_\alpha = \Delta I \text{ and} \tag{14}$$

$$I_{L_\beta} - I_\beta = \Delta I$$

$$\Delta I = I_o \exp \frac{V_\alpha + I_\alpha R_s}{V_o} = I_o \exp \frac{V_\beta + I_\beta R_s}{V_o} \tag{15}$$

$$\therefore V_\alpha + I_\alpha R_s = V_\rho + I_\rho R_s \tag{16}$$

$$R_s = \frac{V_\beta - V_\alpha}{I_\alpha - I_\beta} \tag{17}$$

The coarse extrapolation of solar cells and panels neglecting series resistance was described as a simple shift downward of the voltage axis by the difference between the measured short circuit current and the space short circuit current. In order to make the series resistance correction, one may proceed as follows: The method illustrated above is carried through. Light levels may be adjusted by use of filters, wire screens, light source power adjustment and inverse square law manipulation, or by tilting the solar panels.

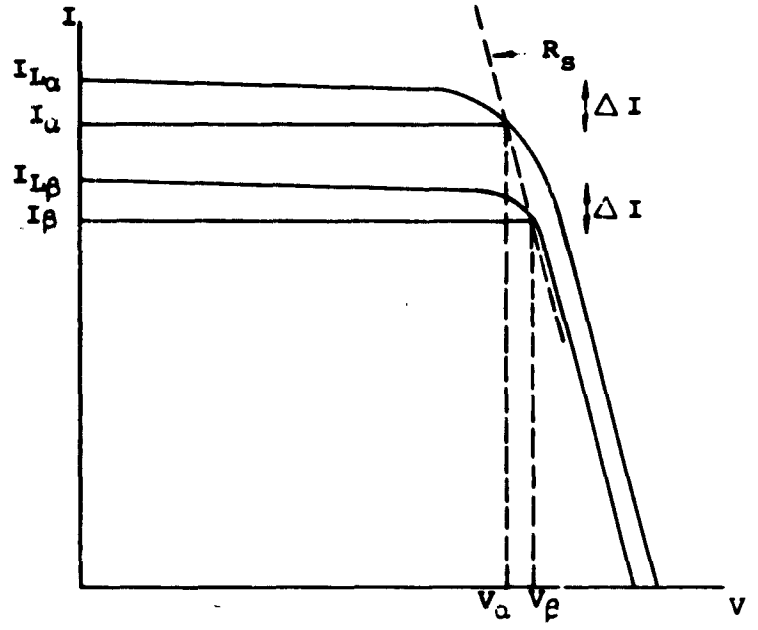

FIGURE 57 SERIES RESISTANCE MEASUREMENT

Assume an I-V curve has been plotted for a panel under earth sunlight giving short circuit current I_{sc_1}, open circuit voltage V_{oc_1}. By use of the tester described in another section of this report, or by other means, an extrapolated value for space short circuit current I_{sc_2} has been obtained. The axis is now shifted on the original I-V plot in order to give the rough extrapolated curve.

The voltage of any corrected point (I_C, V_C) is obtained from the rough extrapolated curve (I_R, V_R) and the measured curve (I_u, V_u)

$$V_C = V_R - (I_R - I_u)R_s \tag{18}$$

The method of extrapolation is now briefly summarized.

1. Obtain I-V curve from X-Y recorder under existing light source.

2. Extrapolate short circuit current under test conditions to air mass zero using the computer.

3. Translate the voltage axis in accordance with the new short circuit current for air mass zero as if dealing with an ideal PN junction converter. (Rough extrapolation). If the series resistance of the converter is sufficiently low, this curve may be used as the space I-V curve, and the extrapolation is complete. If the series resistance is a significant factor, the actual space I-V characteristic will be flattened compared with the ideal curve and a lower maximum power point will result. In that case 4, 5 and 6 below must be carried out or the extrapolated space power will be over optimistic.

4. Obtain a second I-V curve under a different illumination level. The light level need not be specified either spectrally or in intensity.

5. Obtain the converter series resistance by Swanson's method.

6. Correct any desired point on the rough extrapolation curve by making the series resistance correction as outlined above (corrected extrapolation).

If the solar cell power supply output is desired at some temperature other than the test temperature, it may be calculated by application of the proper coefficients. The current shift is determined from the absolute spectral response vs. temperature. The short circuit current coefficient is calculated as follows:

$$f = \frac{\int_\lambda DR d\lambda}{\int_\lambda D_T R_T d\lambda} \qquad (20)$$

where f = Temperature coefficient
D = Spectral distribution of source
R = Spectral response of cell
sub T = Parameters at test temperature
No sub = Parameters at desired temperature

This procedure is quite tedious and must be done for cells illuminated with 2800°K tungsten because the coefficient is of the order of 0.5%/°C in the temperature range of 0°C to 80°C. For sunlight measurements, it may be disregarded since the total change is only approximately 0.5% for the entire range of 0°C to 80°C.

The voltage shift is determined from the I-V characteristics vs temperature. Fig. 58 shows the change in open circuit voltage per change in temperature as a function of temperature for a typical solar cell. For practical applications, this curve is valid for all current values from open circuit voltage to a point beyond the maximum power point. The voltage shift is calculated as follows:

$$V_\rho + N(T_T - T)\ \Delta V_{OC}/\Delta T$$

where

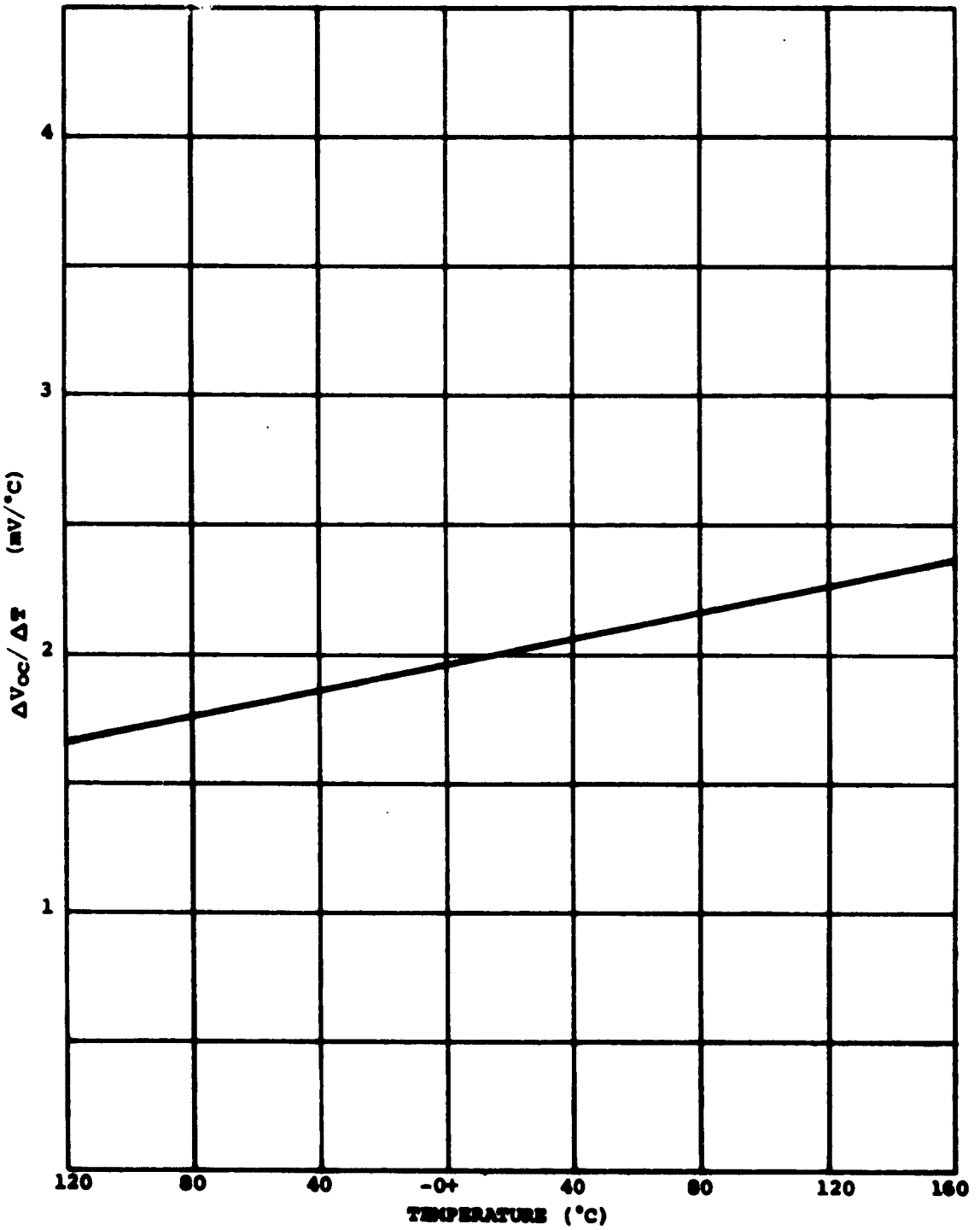

FIGURE 58 VARIATION OF $\Delta V_{OC}/\Delta T$ WITH TEMPERATURE

V_ρ = power point voltage

N = number of cells in the series string

T_T = temperature of panel at test

T = temperature at which panel output is desired.

$\Delta V_{OC}/\Delta T$ is read from the graph at the mean temperature between T_T and T.

APPENDIX V

PROCEDURES AND INSTRUMENTATION CONSIDERATIONS IN STANDARDIZATION OF SOLAR CELL EFFICIENCY MEASUREMENT

1.0 DEFINITION OF EFFICIENCY

The maximum efficiency of a solar cell converter is defined as the ratio of maximum available power output to total incident radiant power[1].

If a solar cell would have a flat spectral response over a given spectral range, then its efficiency would be the same for all light sources within this range provided its output is linear with intensity. However, since solar cells do not have a flat response, and since the spectral response is not the same for all cells, the spectral distribution of the light is a very important factor. For instance, a high-quality silicon solar cell will have an efficiency of nearly 25% for a line source near .9μ but will have an efficiency of zero for a line source at 1.4μ.

2.0 STANDARDIZATION OF MEASUREMENT CONDITIONS

Since the efficiency depends upon the spectral distribution of the incident radiation, the incident radiation must be standardized in order to correlate these measurements. The majority of solar cells manufactured at this time are produced for applications in space. The spectral curve that has been adopted is that of NRL [2].

3.0 MEASUREMENTS IN TUNGSTEN

---

(1) Solar Cell Measurement Standardization, Lockheed Aircraft Corp. LMSD-288184, p.4-2 (1960).

(2) Johnson, F.S. "The Solar Constant", J. Meterol. 11, No. 6, 431 (1954)

3.1 HISTORICAL

In the past, solar cells were measured in tungsten light to determine their efficiencies independent of weather conditions. A tungsten lamp was set to an arbitrarily chosen color temperature of 2800°K and to an intensity of "100 mW/cm^2 solar radiation equivalent" as determined by the short circuit current of a specially calibrated solar cell. An instrument was designed and built to permit setting of tungsten lamps to a given color temperature with good reproducibility. This instrument will be described at the end of this paragraph. The specification of 100 mW/cm^2 sunlight equivalent is based upon the output that a given standard cell would have in sunlight at 100 mW/cm^2. This calibration was originally done in Evanston, Illinois. Cells later produced in El Monte, California were found to produce more output in tungsten light but relatively 10% to 20% less output in sunlight, while cells from the earlier production measured almost the same output under both conditions at sea level[3]. A slightly reduced output of the old cells was expected and found, when the measurements were performed on Table Mountain (7,400 feet altitude). The spectral distribution of the solar radiation there had a peak energy near 0.5μ compared to a peak near 1.2μ for 2800°K tungsten, causing a decrease in cell efficiency.

The color temperature meter is a specially designed portable self-contained laboratory instrument for measuring the color temperature of tungsten lamps. It operates as a two-channel comparator bridge using matched pairs of silicon solar cells. A basic diagram of the instrument is shown in Fig. 59.

The color temperature meter target is a sensing unit consisting of two pairs of matched cells with selective filters arranged in a checkerboard manner, as shown in Fig. 60. The spectral transmission characteristics of the filters are shown in Fig. 61. The resistors R_1 and R_2 are adjusted such that the null meters M_1 and M_2 show null. This condition requires that the voltage across the solar cells is zero, which is equivalent to short circuit current. Then the solar cell

---

(3) Final Technical Engineering Report "Pilot Line Production of High Efficiency Solar Cells" Contract AF33(600)-40497 Hoffman Electronics Corp. (1961)

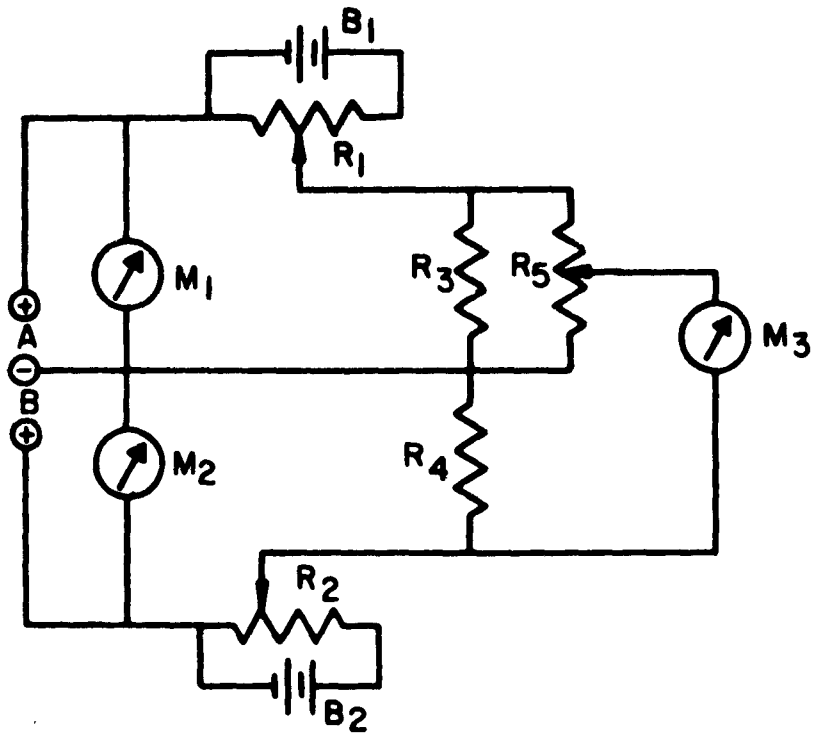

FIGURE 59 Color Temperature Meter Schematic

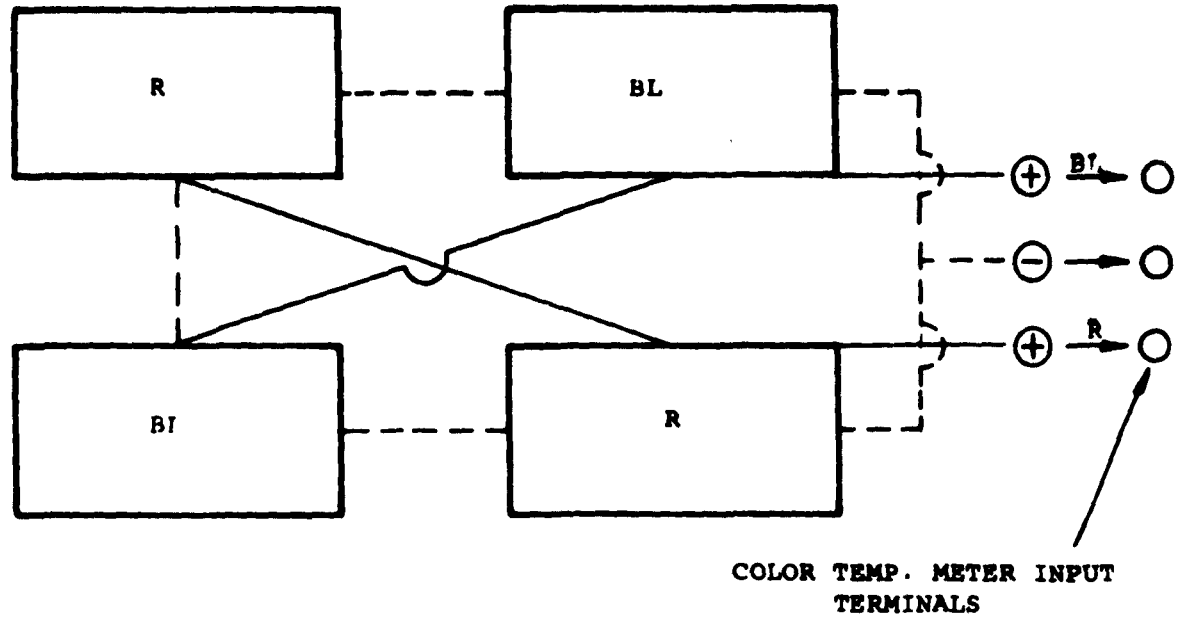

FIGURE 60 Block Diagram Color Temperature Target

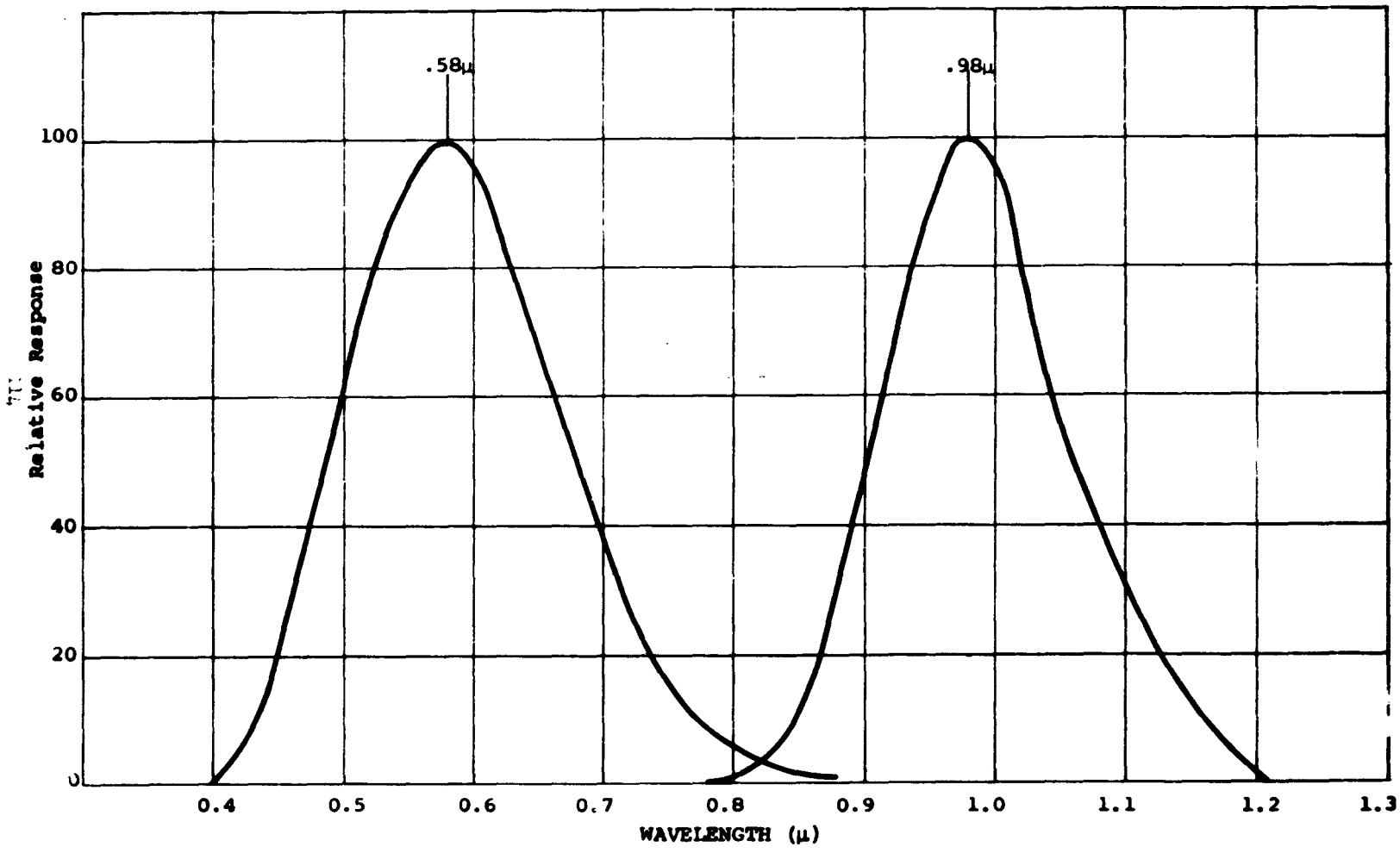

FIGURE 61 SPECTRAL RESPONSE - COLOR TEMPERATURE TARGET "B"

currents flow through the current sensing resistors R_3 and R_4, and R_5 is adjusted until null is shown on meter M_3. A calibrated dial on R_5 gives a reference reading. The target and readout is calibrated with secondary standard color temperature bulbs. Using these bulbs, color temperature vs. dial reading is plotted to obtain the calibration.

The characteristics of the meter are as follows:

RANGE: 1800°K to 3200°K tungsten.

ACCURACY: Short circuit current ±0.1% of full scale. Color temperature ±20°K with temperature control, performed to calibrated standards.

STABILITY: Short circuit current ±0.5% of full scale short and long term; color temperature ±10°K short and long term.

Early in 1960 the AIEE formed a measurements standardization committee composed of workers in the solar energy conversion field. This committee emphasized standard solar cells, measurement under laboratory light sources, and measurements in sunlight. The laboratory light source decided upon was tungsten, set at 2800°K ±50°K with an intensity of 100 mW/cm^2 sunlight equivalent as determined with a standard reference solar cell.

3.2 DISADVANTAGES OF TUNGSTEN AS A STANDARD LIGHT SOURCE

If the spectral responses of all cells were identical or the cells were to be used only under 2800°K tungsten, this would be a valid standard. The cells, however, are manufactured primarily for use in space sunlight and the ratio of sunlight output to tungsten output may vary as much as 20%. Therefore, each cell with a different spectral response requires its own "Sunlight equivalent" in tungsten and measurement repeatability is greatly jeopardized.

Variations in solar cell tungsten-to-space output ratios may be demonstrated by measuring solar cells under a tungsten source set at 2800°K, 100 mW/cm^2 sunlight equivalent with a standard cell and by measuring the same cells under a solar

simulator set at 140 mW/cm^2. The ratios between the efficiencies in tungsten to the efficiencies in sunlight vary from 1.0 to 1.3.

4.0 DERIVATION OF CELL EFFICIENCY IN SPACE

4.1 DETERMINATION OF OUTPUT FROM ABSOLUTE SPECTRAL RESPONSE

The output of a silicon solar cell may be determined as shown in Appendix IV. It is only necessary to know the I_{SC} in space and the I-V curve under any light source.

If the absolute spectral response of the desired cell is known, it may be multiplied, at each wavelength, by the NRL space spectral distribution and integrated to obtain the desired space I_{SC}. This procedure is used for this program and is described in Appendix I.

4.2 CALIBRATION IN SUNLIGHT

4.2.1 SPECTRAL DISTRIBUTION MEASUREMENT

This method of extrapolation is based on the measurements of the spectral distribution of the incident solar radiation. The curve of Fig. 62 is multiplied point for point by the average spectral response of the desired solar cells.

The product is shown as Curve A in Fig. 63 and represents the solar cell output versus wavelength when illuminated with the radiation as shown. The same multiplication is performed on the curve of solar radiation in space and the spectral response of the cells. This product, curve B in Fig. 63, shows the cell output versus wavelength in space.

The area under the curve of Fig. 62 corresponds to the pyrheliometer reading; the area under NRL's curve corresponds to $140mW/cm^2$. The area under curve A of Fig. 63 is proportional to the actually measured short circuit current of the cell, while the area under curve B of Fig. 63 is proportional to the current output in space. The ratio of the areas under the latter two curves gives the direct increase in current output at the load voltage and, therefore, the direct increase in power output from the measured value to the space value.

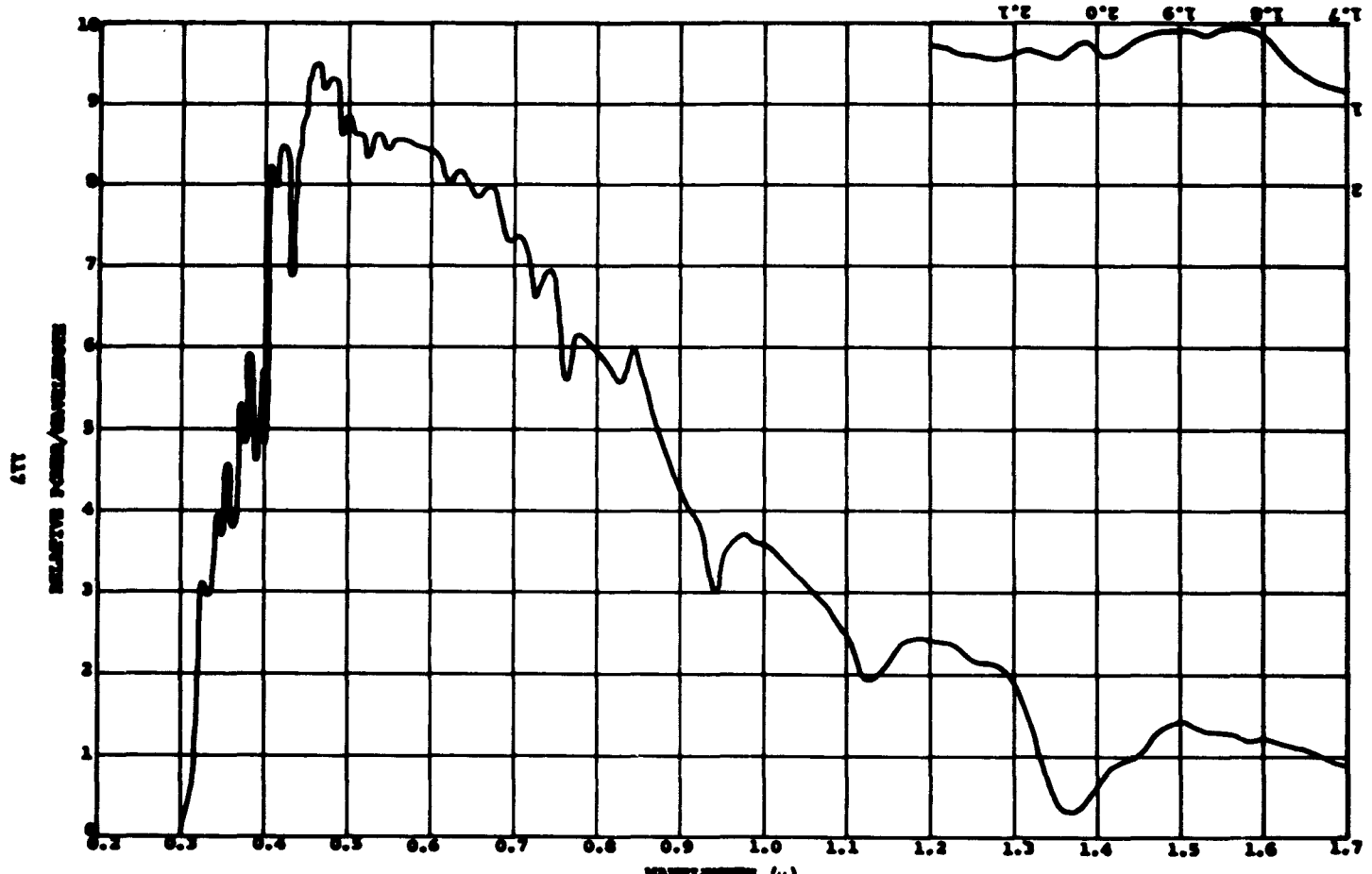

FIGURE 62 INCIDENT SOLAR RADIATION SPECTRAL DISTRIBUTION - TABLE MT., CALIF. 6-22-60

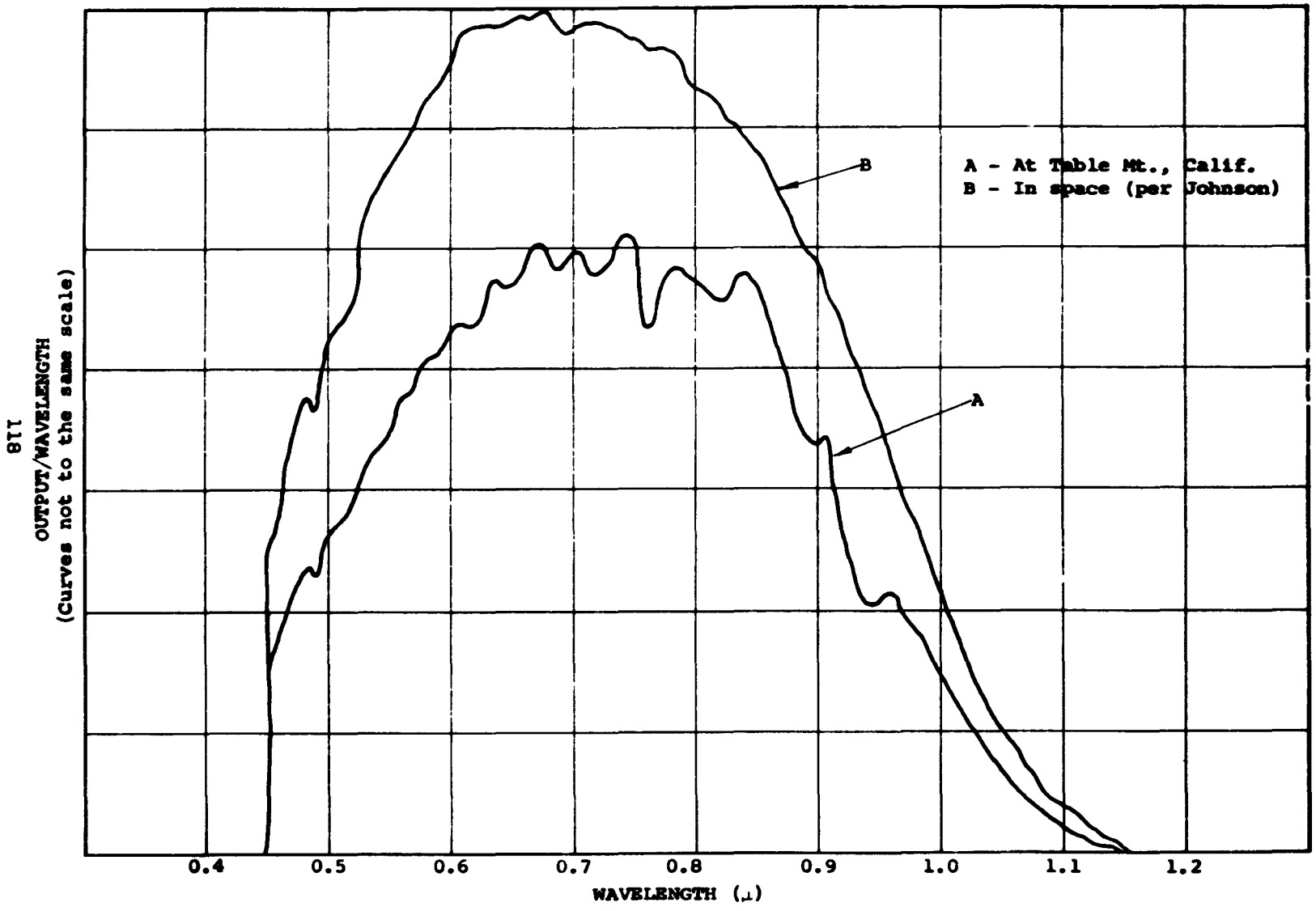

FIGURE 63 SOLAR CELL OUTPUT WITH UV FILTER

The primary objections to this method concern the measurement of the total incident radiation and the measurement of the incident spectral distribution. Pyrheliometric measurements generally show repeatability to within 2% over long periods of time. The accuracy of pyrheliometric measurements is dependent upon the work of the Smithsonian Institution. Later, the Smithsonian Institution revised their pyrheliometric scales, and in 1956 a compromise was chosen by the International Radiation Commission for the standard pyrheliometric scale[4]. If the assumption that the IPS (International Pyrheliometric Scale) is correct, then we may expect a variation of ±2% from this factor alone.

The measurement of spectral distribution is difficult. The spectral distribution must be measured with a calibrated spectroradiometer. The calibration need only be relative, as the resultant curve may be made absolute through the use of the pyrheliometer. The calibration procedure is quite difficult, however. The usual means of calibrating a spectroradiometer consists of focusing a source of known spectral distribution, either a black-body or a calibrated tungsten lamp on the entrance slit. By plotting the output of the detector vs the incident energy, the instrumental transfer function may be found. Most of these sources have insufficient energy in the shorter wavelengths to yield an adequate calibration. In addition, if stray radiation effects are present, the instrumental transfer function will be different for the low temperature source and for sunlight. A slight variation on this method has been proposed by Smits[5].

4.3.2 SPECTRAL DISTRIBUTION CALCULATION

A means of determining the spectral distribution by calculations based upon absorption and scattering coefficients of the atmospheric constituents is described in Appendix VII. If the curve derived by this method is multiplied by the

---

(4) Drummond, etal IGV Instruction Manual, Part VI, Radiation Instruments & Measurements Pergammon Press, 378, 1958

(5) Smits, F.M., etal. "A Method for Terrestrial Determination of Solar Cell Short Circuit Current under Outer Space Solar Illumination", Paper 7/3 Wescon 1961.

spectral response of the cell and is integrated, and the procedure is repeated for Johnson's curve, a ratio of short-circuit currents between the measurement site and space is derived. This factor is then multiplied by the I_{sc} measured, and the I_{sc} in space is then known.

This procedure has the same difficulties with the pyrheliometer as in 4.2.1 but eliminates the difficulties with the spectroradiometer. In addition, it cancels possible errors in calibration on the equipment which produced the NRL curve, by referring test site light distributions directly to the space distribution.

4.4 TESTER

The portable tester described in section 2.0 of this report is capable of determining the efficiency of a solar cell in space from terrestrial measurements. Using this instrument, the power output of the cell per active area is divided by Johnson's energy of 140 mW/cm^2.

APPENDIX VI

CHARACTERISTICS OF SILICON SOLAR CELLS

1.0 EFFICIENCY CORRELATION

1.1 TEST CONDITIONS

The following cells were measured under a 2800°K tungsten source set at 100 mW/cm^2 sunlight equivalent with a standard reference solar cell and under the Hoffman Solar radiation simulator set at 140 mW/cm^2:

Manufacturer	Efficiency	Type
#1	8	P/N
	9	P/N
	10	P/N
	11	P/N
	12	P/N
	13	P/N
#2	9	P/N
	10	P/N
	11	P/N
	12	P/N
	13	P/N
	14	P/N

Manufacturer	Efficiency	Type
#3	11	P/N
	12	P/N
	13	P/N
#4	9	P/N
	12-13	P/N
#5	8-10	N/P
	10-12	N/P
	12	N/P

1.2 TEST RESULTS

It was desired to correlate the efficiencies as measured under both sources. The cell efficiencies as stated by the manufacturer are generally the lower limit for a group of cells. In Table 1, the following data is shown:

Manufacturer
Stated Efficiency
Tungsten Efficiency
Solar Simulator Efficiency

The efficiencies were averaged over the entire sample for each efficiency group.

TABLE 1

MFG	Stated Efficiency	Tungsten Efficiency	Solar Simulator Efficiency
No. 1	8%	10.2	8.7
	9	10.9	9.5
	10	11.7	9.9
	11	12.2	10.3
	12	13.0	10.5
	13	13.3	10.7
No. 2	9%	10.9	9.4
	10	11.6	9.7
	11	12.6	10.3
	12	13.8	11.0
	13	14.6	11.3
	14	14.9	11.8
No. 3	11%	11.5	10.4
	12	12.1	10.8
	13	12.4	11.0
No. 4	9%	10.3	7.8
	12-13	12.8	9.9
No. 5	8-10%	9.0	7.9
	10-12	10.8	8.8
	12	12.5	9.8

2.0 SPECTRAL RESPONSE

2.1 TEST CONDITIONS

The following types of cells were subjected to a spectral response analysis:

Manufacturer	Type	Efficiency %
#1	P^+/N	8
	P^+/N	9
	P^+/N	10
	P^+/N	11
	P^+/N	12
	P^+/N	13
#2	P^+/N	9
	P^+/N	10
	P^+/N	11
	P^+/N	12
	P^+/N	13
	P^+/N	14
#3	P^+/N	11
	P^+/N	12
	P^+/N	13
#4	P^+/N	9
	P^+/N	12-13

Manufacturer	Type	Efficiency %
#5	N^+/P	8-10
	N^+/P	10-12
	N^+/P	12

From the relative spectral response data on each group of cells (each efficiency group considered separately), the following characteristics were recorded:

% Response at 0.56μ relative to peak response

% Response at 1.04μ relative to peak response

The wavelengths 0.56μ and 1.04μ were chosen as being the most sensitive wavelengths for determining relative shifts in the blue and red portions of the spectrum respectively.

2.2 TEST RESULTS

The mean relative responses at 0.56μ and 1.04μ and the wavelength at peak response for the cells are shown in Table 2. The wavelength at peak response for all P/N cells in a given efficiency range was $\pm$0.03μ from the mean. The N^+/P cells have peaks at shorter wavelengths, averaging 0.07μ shorter. In Fig. 64, a typical 12% cell from each manufacturer is shown.

One additional series of measurements were made. It was expected that a shift in spectral response toward the red would occur when a cell is operated at angles other than normal incidence. This phenomena was expected because of the increased distance from surface to junction at angles other than normal (effective P-layer thickness). Cells were measured for their spectral response characteristics at normal incidence (90°), 75°, 60°, 45°, and 30°. No significant change was found because all variations were less than the instrumental error.

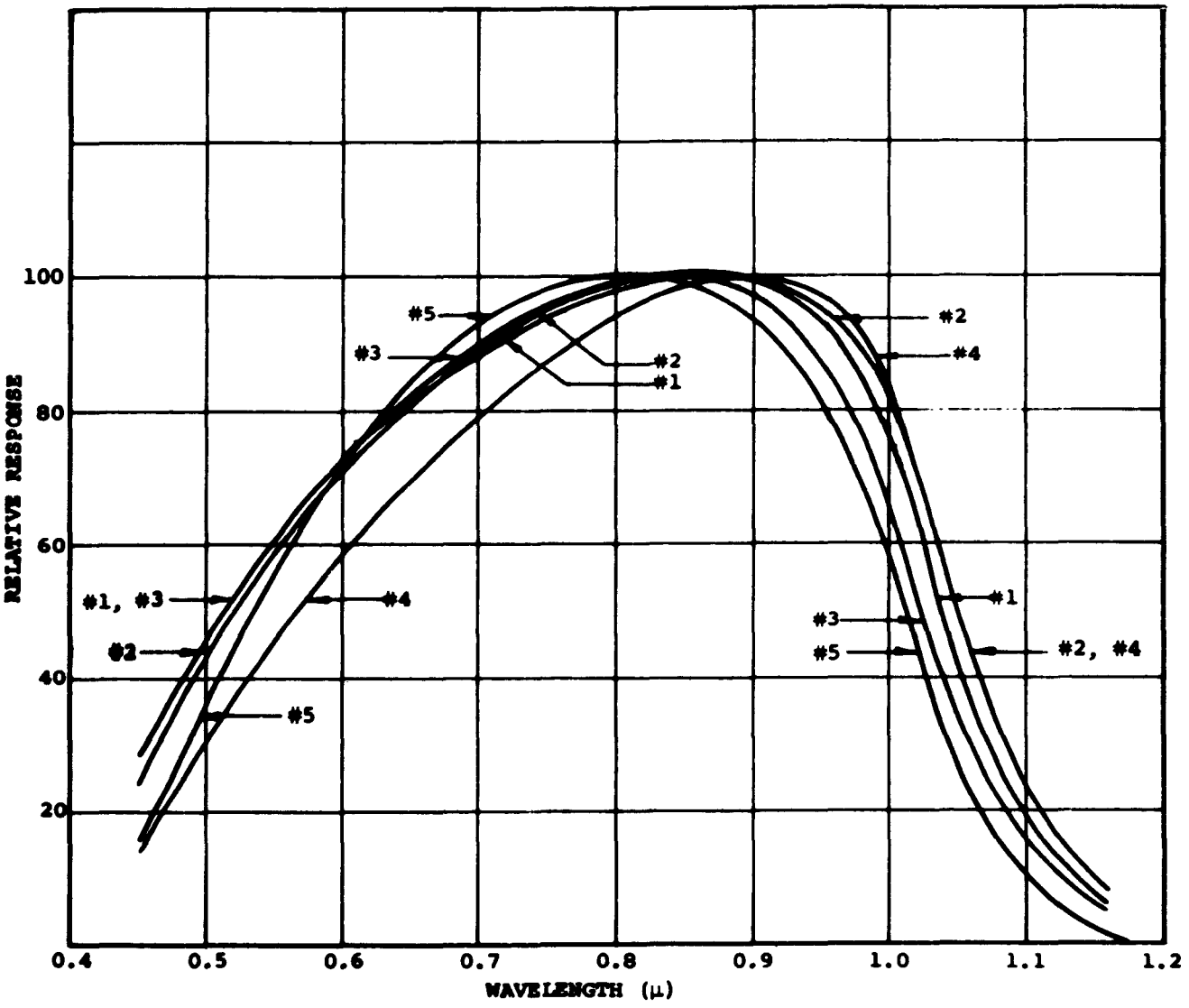

FIGURE 64 COMPARISON OF 12% CELLS FROM DIFFERENT MANUFACTURERS

TABLE 2

Manufacturer	% Efficiency	Response At 0.56μ	Response at 1.04μ	Wavelength of Peak Response
#2	9	.635	.435	.836
	10	.610	.513	.860
	11	.606	.458	.856
	12	.610	.543	.836
	13	.600	.547	.889
	14	.604	.591	.884
#3	11	.605	.374	.844
	12	.630	.418	.846
	13	.621	.450	.856
#4	9	.473	.645	.884
	12-13	.498	.618	.896
#5	8-10	.625	.281	.784
	10-12	.627	.295	.788
	12	.567	.359	.816

TABLE 3

Manufacturer	% Efficiency	0.56 μ Min.	0.56 μ Max.	1.04 μ Min.	1.04 μ Max.
#1	8	.577	.750	.267	.653
	9	.530	.757	.276	.683
	10	.599	.707	.288	.571
	11	.584	.718	.293	.589
	12	.573	.691	.389	.604
	13	.545	.677	.447	.633
#2	9	.591	.710	.269	.534
	10	.570	.627	.488	.567
	11	.576	.636	.383	.497
	12	.600	.617	.493	.587
	13	.570	.627	.502	.547
	14	.533	.644	.575	.615
#3	11	.555	.651	.210	.508
	12	.590	.677	.360	.491
	13	.580	.666	.356	.553
#4	9	.428	.518	.397	.645
	12-13	.479	.526	.474	.618
#5	8-10	.524	.730	.190	.367
	10-12	.548	.732	.208	.392
	12	.510	.615	.184	.528

3.0 TEMPERATURE CHARACTERISTICS

3.1 TEST CONDITIONS

I-V curves were recorded vs. temperature for a total of 180 cells.

The illumination used was simulated solar radiation. Some cells were measured through the range from -100°C to 160°C and the others were measured from 30°C to 160°C. Temperature control was provided by liquid nitrogen, flowing water and a Calrod heater. Temperature was measured using two calibrated copper-constantan thermocouples referenced with an ice bath and measured with a DC amplifier and a digital voltmeter.

3.2 TEST RESULTS

Parameters investigated were open circuit voltage, short circuit current, spectral response, maximum power and series resistance, all versus temperature.

3.2.1 OPEN CIRCUIT VOLTAGE VS. TEMPERATURE

The open circuit voltage varies with temperature approximately at the rate of -2 mV/°C. This coefficient varies with temperature, being larger at higher temperatures. Ten cells were used to determine the characteristic shown in Fig 65. Due to the difficulty in obtaining sufficient resolution with the readout instrumentation, a great deal of scatter was present. The method of least squares was used to obtain the best straight line fit. The average $\Delta V_{OC}/\Delta T$ for all cells at 16°C was 2.0086, whereas the maximum and minimum values were 2.139 and

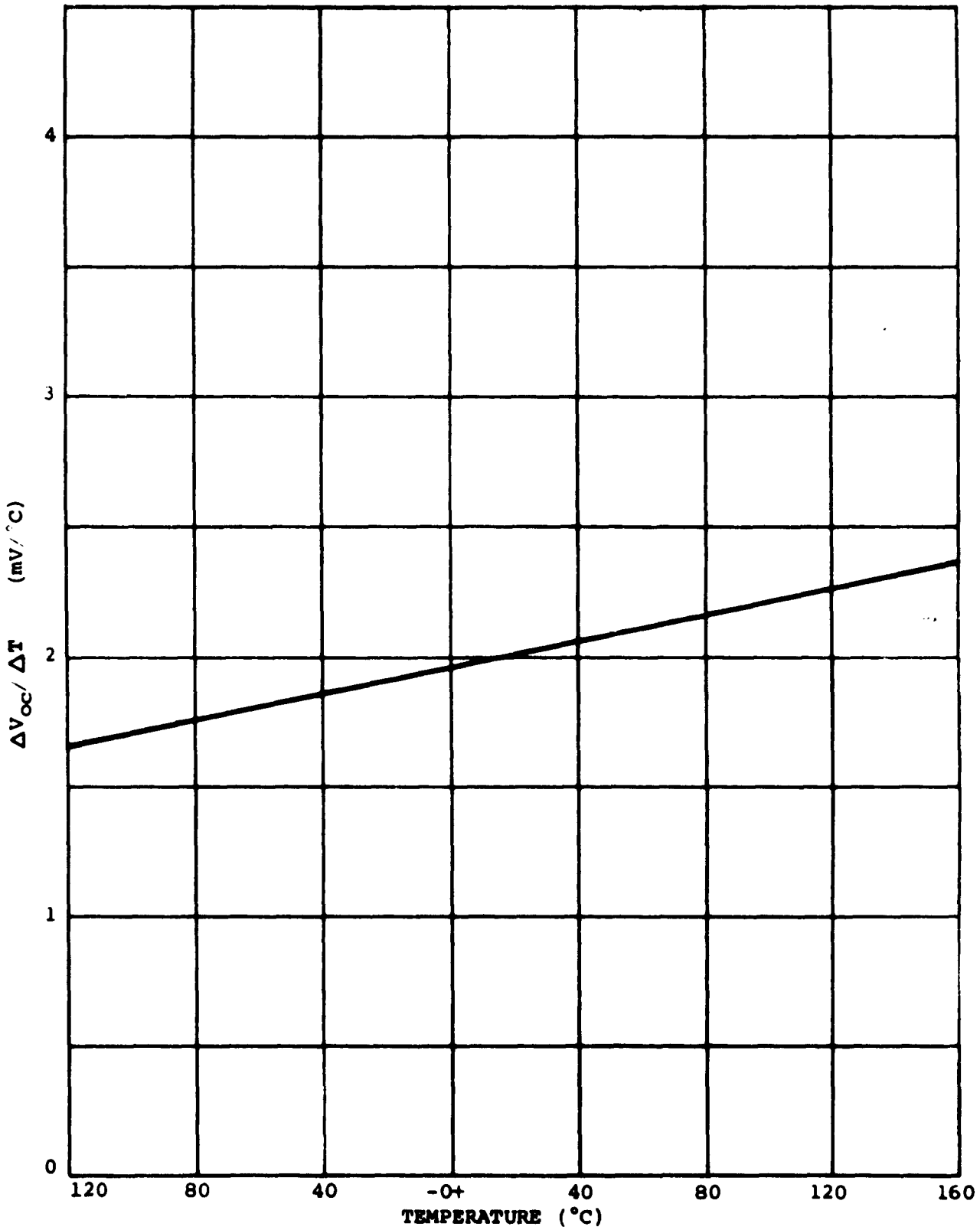

FIGURE 65 VARIATION OF $\Delta V_{oc}/\Delta T$ WITH TEMPERATURE

and 1.859 respectively. The coefficients for the other cells, from 30 to 160°C, were compared to the data from the ten cells. The average temperature for the other cells was 95°C, and this point was chosen for comparison. The ten cells had an average of 2.20mV/°C. The averages of the other cells varied from 2.11mV/°C to 2.33mV/°C. There was no measured dependence of this coefficient upon the efficiency of the cells.

3.2.2 SHORT CIRCUIT CURRENT VS. TEMPERATURE

The short circuit current vs. temperature characteristics are dependent upon the incident spectral distribution. The light source chosen was the solar simulator (see Appendix III, Section 2.6.2.4) due to the space orientation of most solar cell applications. The function is expressed in % $\Delta I_{sc}/\Delta T$. The results of the tests of 9 cells are shown in Fig. 66. This graph shows the average I_{sc} for the 9 cells versus temperature over the range from -100 to +160°C. Under solar irradiation, there is less than 1% I_{sc} over the temperature range from -30 to 110°C. The equivalent cells from the other manufacturers showed similar properties.

3.2.3 SPECTRAL RESPONSE VS. TEMPERATURE

The variation in spectral response of a solar cell vs. temperature is shown in Fig. 67. The change in the wavelength range shorter than 0.9μ is negligible, but the relative output for wavelengths longer than 0.9μ increases with increasing temperatures. As a result, the I_{sc} in sunlight is almost invariant with temperature, whereas the I_{sc} increases with increasing temperature under a low temperature incandescent source.

3.2.4 MAXIMUM POWER VS. TEMPERATURE

The variation of maximum available power as a function of temperature is rather complex and is best determined empirically. The $\Delta V_{mp}/\Delta T$ characteristics are very similar to the $\Delta V_{oc}/\Delta T$ characteristics with a slightly smaller coefficient. The coefficient is nearly 1.8 mV/°C at 20°C. for more efficient cells. If the cell has significant series resistance, this function may change in either direction and by unpredictable amounts. The

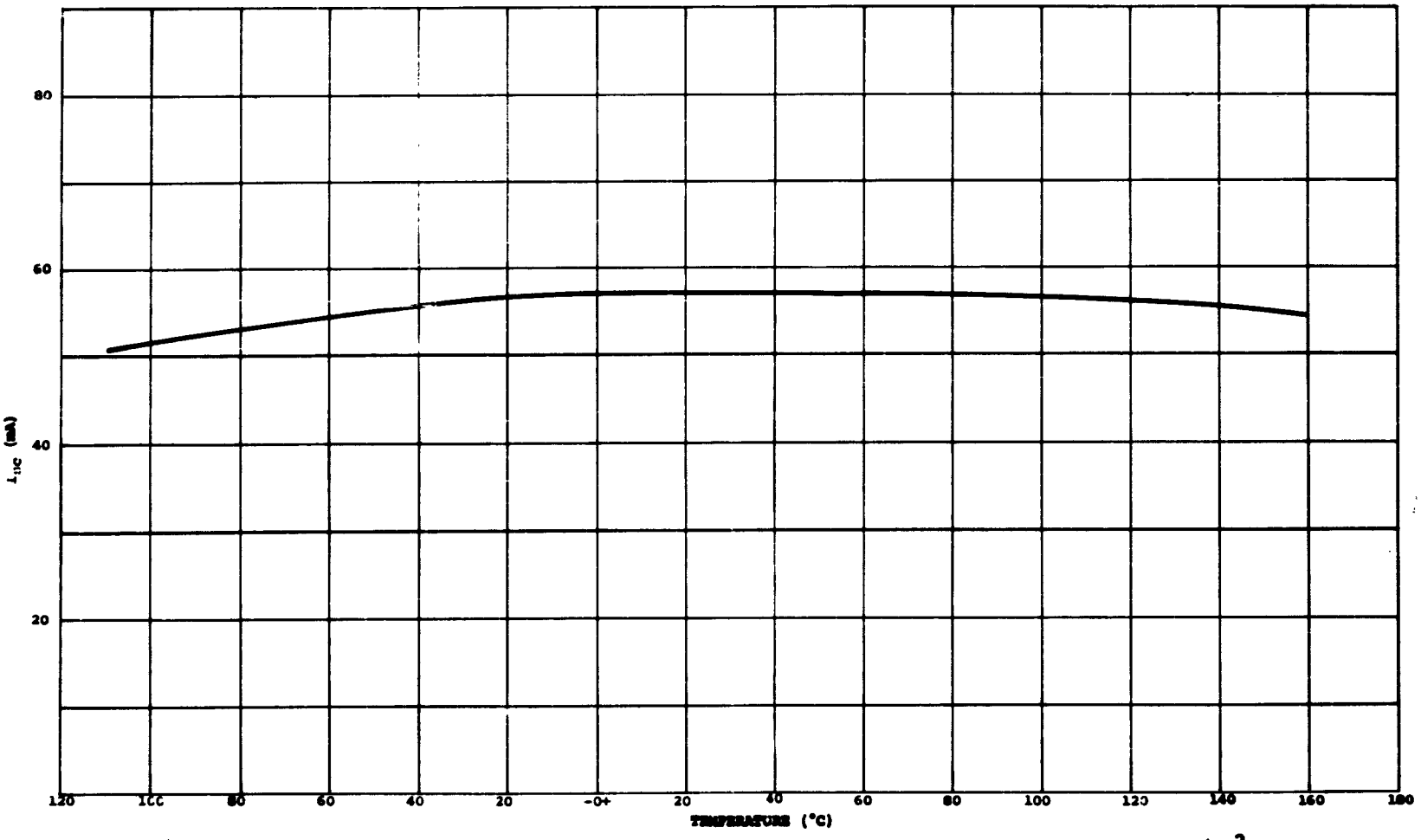

FIGURE 66 VARIATION OF SHORT CIRCUIT CURRENT WITH TEMPERATURE AVG. 9 CELLS 140 mW/cm^2 M = O

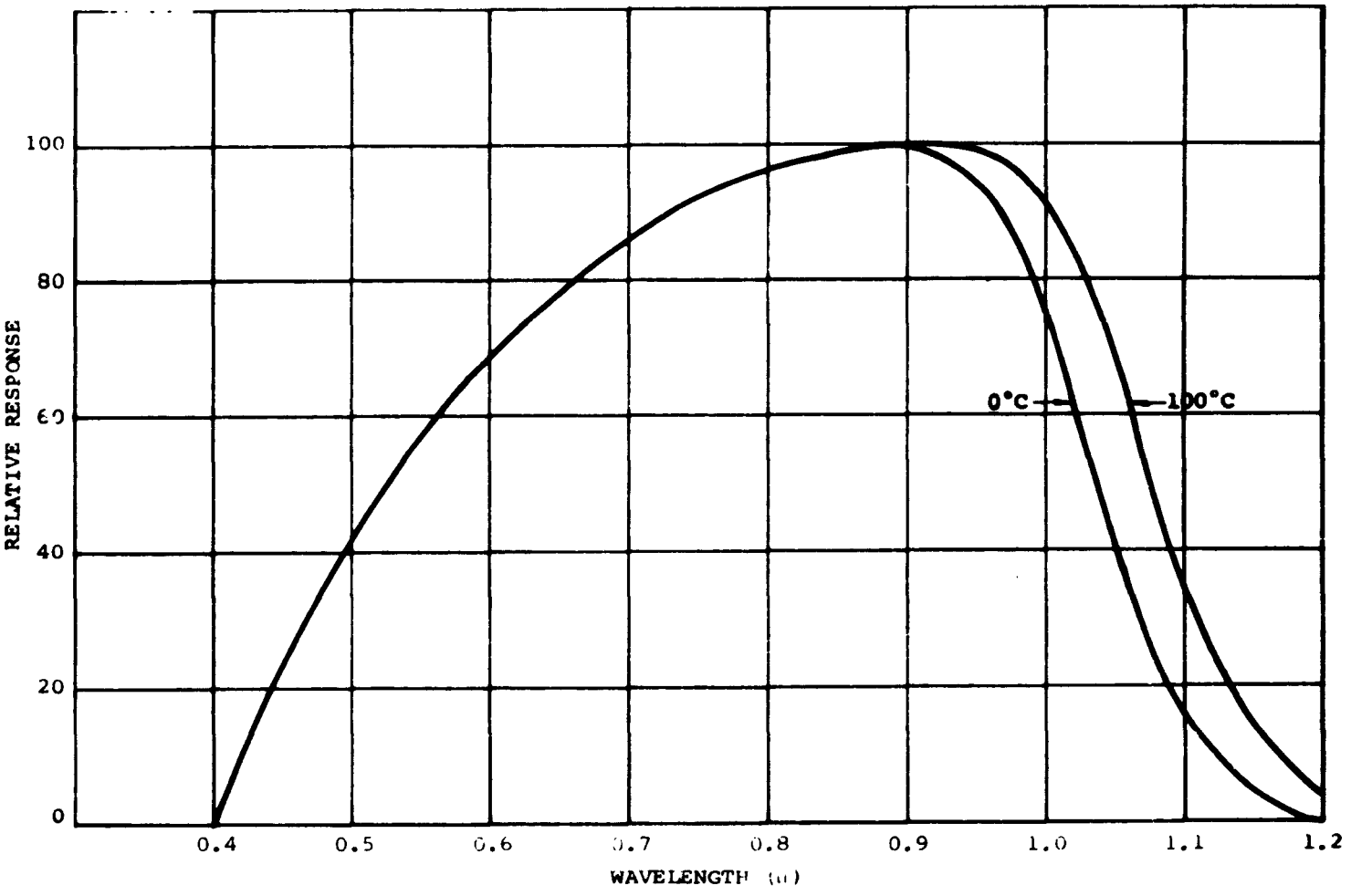

FIGURE 67 VARIATION OF SPECTRAL RESPONSE VS. TEMPERATURE

variation in I_{mp} is also impredictable from the I_{sc} characteristics. In order to obtain conservative results it has been common practice to use 2.0 to 2.1 mV/°C for both open circuit voltage and maximum power point degradation as a function of temperature for solar cell panels.

3.2.5 SERIES RESISTANCE VS. TEMPERATURE

The change of series resistance vs. temperature is shown in Fig. 79. This is essentially constant from -40 to 120°C. This curve is the average of the characteristics of 7 cells.

An example of the complete characteristics of a cell vs. temperature is shown in Fig. 69.

4.0 RADIATION DAMAGE

Solar cell output degradation as a function of nuclear or Van Allen belt radiation damage has been the subject of a number of studies [1-14].

---

(1) P. Rappaport, J. J. Loferski and E. G. Linder, "The Electron-Voltaic Effect in Germanium and Silicon P-N Junctions," RCA Review, Vol. XVII, No. 1, (March 1956).

(2) A. B. Francis, W. W. Happ, "Photovoltaic Solar Energy Converters for Space Vehicles--Present Capabilities and Objectives," AIEE, Paper No. 60-985.

(3) J. J. Loferski, P. Rappaport, "The Effect of Radiation on Silicon Solar Energy Converters," RCA Review, Vol. XIX, No. 4, (December 1958).

(4) F. A. Junga, G. M. Enslow, "Radiation Effects in Silicon Solar Cells," IRE Transactions on Nuclear Science, Vol. NS-6, (June 1959).

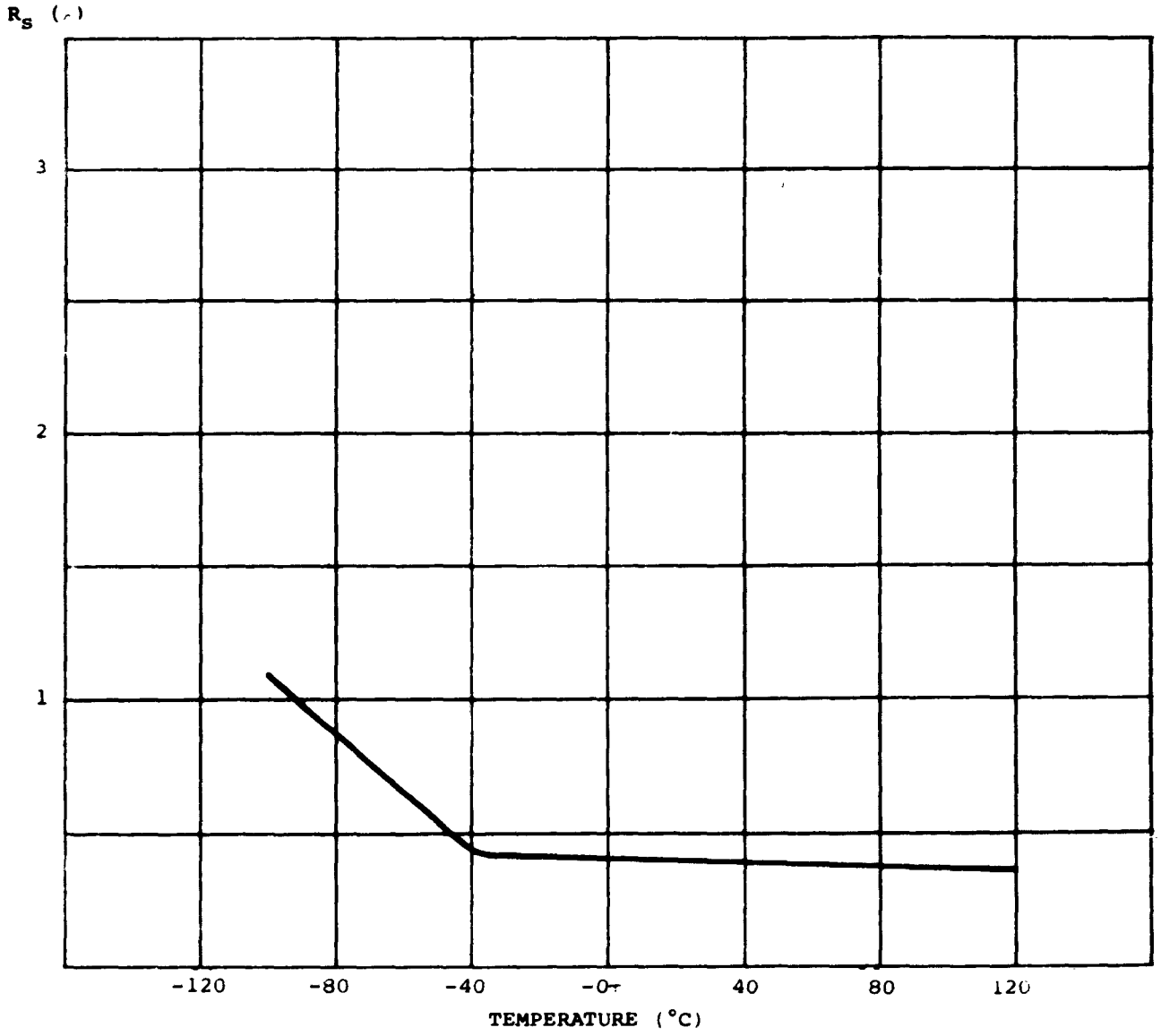

FIGURE 68 AVERAGE VARIATION OF SERIES RESISTANCE VS. TEMPERATURE

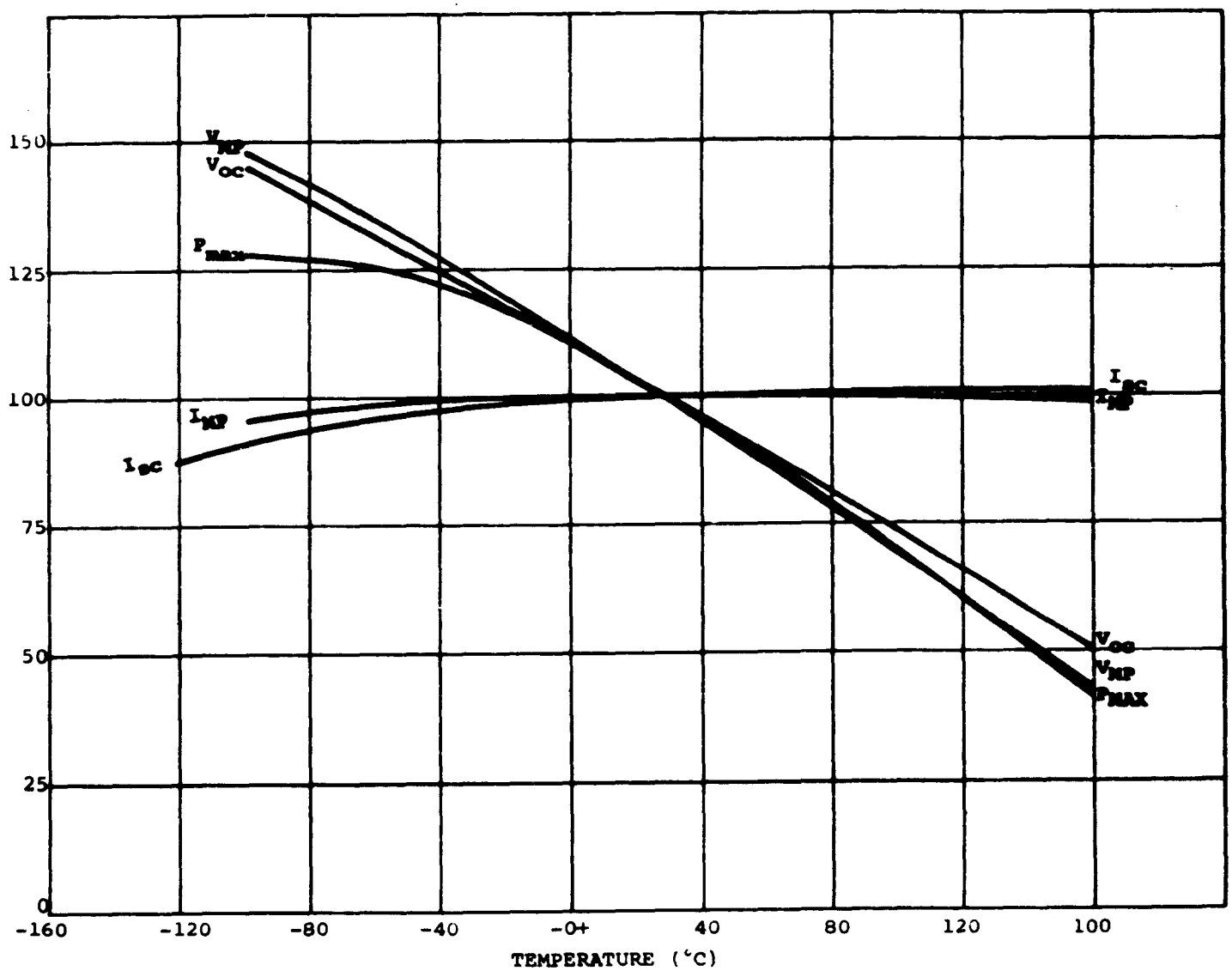

FIGURE 69 TEMPERATURE CHARACTERISTICS OF TYPICAL 11% SOLAR CELL

(5) "Radiation Effects in Silicon Solar Cells," Lockheed Aircraft Corporation, Missile Systems Division, Palo Alto, California, Report LMSD-48351.

(6) G. Enslow, F. Junga, W. W. Happ, "Gamma Radiation Effects in Silicon Solar Cells," Lockheed Aircraft Corporation, Missile Systems Division, Palo Alto, California, Report LMSD-5137.

(7) G. Mandelkorn, C. McAfee, J. Kesperis, L. Schwartz, W. Pharo, "A New Radiation Resistant High Efficiency Solar Cell," USASRDL Technical Report 2162, (October 1960).

(8) W. L. Brown, G. L. Pearson, "Proton Radiation Damage in Silicon Solar Cells," Bell Telephone Laboratories, Inc., (June 1960).

(9) R. G. Downing, "Electron Bombardment of Silicon Solar Cells," STL/TR-60-0000-04057, (February 1960).

(10) J. J. Loferski, P. Rappaport, "Radiation Damage Study of Silicon Solar Energy Converters," RCA Report, (April 1957) - Contract No. DA 36-039 SC-64643.

(11) J. W. Oliver, "Charged Particle Radiation Damage in Semiconductors II," STL Report 8987-0001 RU001.

(12) J. M. Denney, R. G. Downing, S. R. Lackman, J. W. Oliver, "Estimate of Space Radiation Effects on Satellite Solar Cell Power Supplies," STL Report EM 10-21.

(13) J. M. Denney, R. G. Downing, "Spacecraft Radiation Damage Experiments," STL Report 8653-6002 TU-000.

(14) "Radiation Damage to Semiconductor Solar Devices," Vol. 1, Proc. of the Solar Working Group Conference, Interagency Power Group, Washington, D.C., (February 27 and 28, 1962).

It is a theoretically predicted and experimentally observed fact that the diffusion length of minority carriers decreases as a function of radiation damage. This has two distinct effects upon solar cell operation: The long wavelength response is decreased and the saturation current (I_o) is increased. For severe dosages additional degradation may occur affecting the series resistance (R_s) and the A factor in the solar cell equation. A first order approximation of the effect of irradiation may be made by setting the absolute spectral response on the computer corresponding to a given radiation dose. A sample absolute spectral response curve corresponding to a representative dosage is illustrated in Fig. 81. The spectral response corresponding to a given dosage may also be calculated from the diffusion length degradation[11]. When dealing with a solar converter panel, predictability is made more complex due to the statistical spread in output degradation on large numbers of cells exposed to the same dosage. Since most solar cell panels employ series-parallel circuit configurations, those portions of the panel in the series circuit will show the degradation of the most seriously degraded cell. For this reason the panel circuitry is an important factor in the degradation of power output due to high energy irradiation.

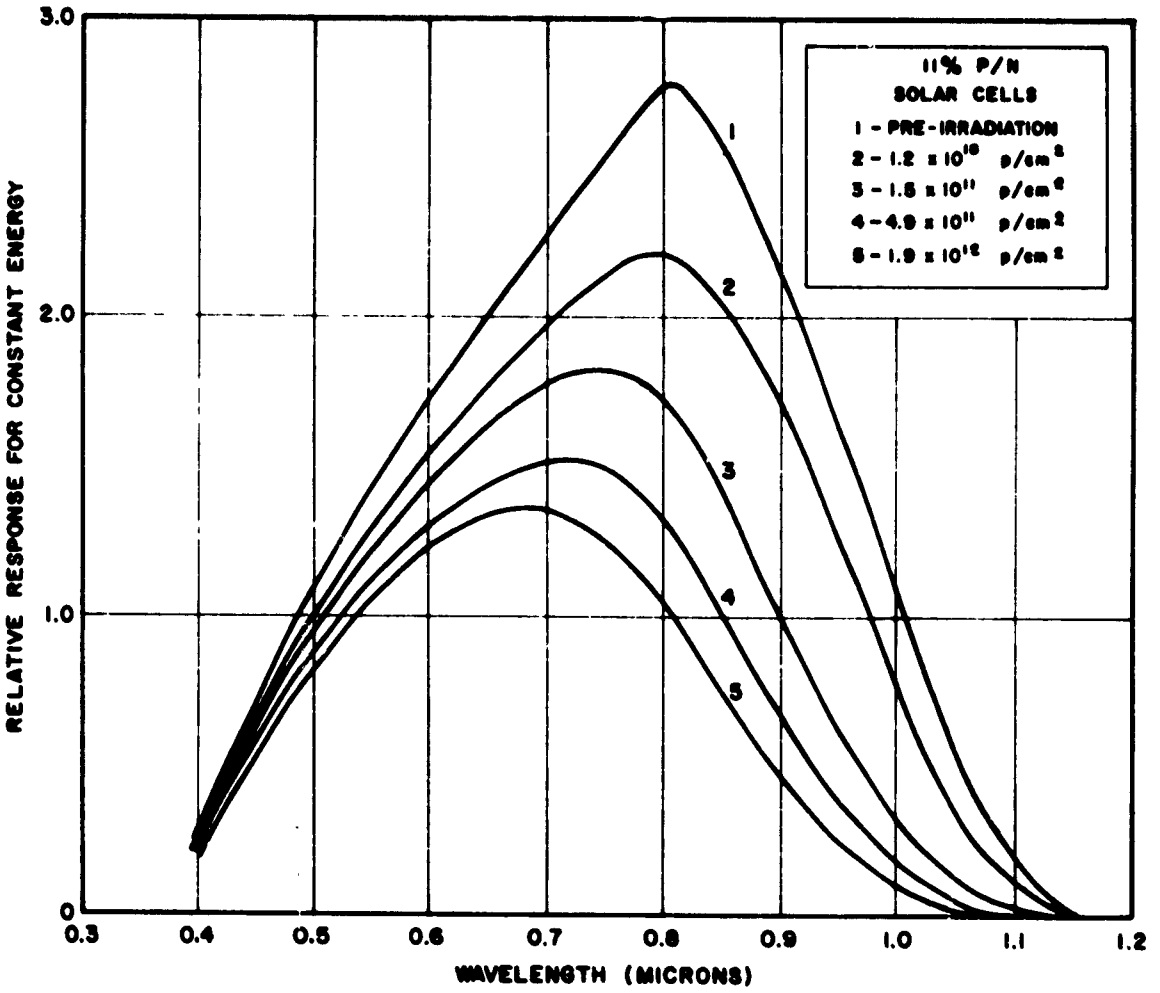

FIGURE 70 - SPECTRAL RESPONSE DEGRADATION OF SILICON SOLAR CELLS VS. ENERGETIC PROTON DOSAGE (450 MEV) AS MEASURED BY J. M. DENNEY AND R. G. DOWNING, SPACE TECHNOLOGY LABORATORIES, REPRODUCED WITH THEIR KIND PERMISSION.

APPENDIX VII

A PROCEDURE FOR CALIBRATING REFERENCE SOLAR CELLS UNDER SUNLIGHT

1.0 TEST SITE

The performance testing of solar cells and panels in natural sunlight demands a knowledge of the incident spectral distribution in order to compute power outputs in free space. A set of curves is also invaluable for the calibration of standard solar cells.

Table Mountain, California has been the most popular site for making measurements under solar irradiation. Table Mountain is within 100 miles from Los Angeles and has excellent facilities. An observing station of the Smithsonian Institution was located there, which had complete spectrobolometric and pyrheliometric facilities. The geographical coordinates of this station are 34° 22'N and 117° 41'W. The elevation is 7400 ft. The atmosphere, through variable, is reasonably free from contamination. The curves to be presented are representative for Table Mountain; however, they may possibly be applied to similar locations.

2.0 THE SOLAR CONSTANT

The solar constant is defined as the rate of energy arrival upon a unit surface, normal to the sun's direction, in free space at the earth's mean distance from the sun[1]. The Smithsonian Institution has undertaken the determination of the solar constant in great detail over a period of nearly 30 years, and the mean value is 1.94 cal cm^{-2} min^{-1}[2]. The

---

(1) Johnson, F. S., "The Solar Constant," J. Meteorol. 11, No. 6, 431, (1954).

(2) Aldrich, L. B., & Hoover, W. H., "The Solar Constant, Science 116, 3, (1952).

most recent revision of the Smithsonian value was proposed by Johnson[1] upon adding high-altitude rocket data in the ultraviolet spectrum. He obtained a value of 2.00 cal cm^{-2} min^{-1}. The National Bureau of Standards[3] gives a preliminary value of 2.05 cal cm^{-2} min^{-1}.

Johnson's value of 2.00 cal cm^{-2} min^{-1}, is considered the best estimate. His spectral distribution curve is discussed in the next section. The Smithsonian value is definitely too low in the light of the high-altitude rocket data, and the NBS value is taken from data run only one, and has not been thoroughly substantiated by further measurements.

3.0 SOLAR SPECTRAL IRRADIANCE

The work done by the Smithsonian Institution in the determinations of the solar constant included spectrobolometric measurements of sunlight. These curves may be extrapolated to a curve that represents the spectral distribution of sunlight in free space[4].

Moon[5] synthesized a curve which he proposed as a standard curve for illumination engineers, based primarily upon the work of the Smithsonian Institution. The deviations from the Smithsonian results are most noticeable in the infrared spectrum beyond 1.25μ, where a 6000°K Plankian curve was used, and at wavelengths shorter than 0.4μ, where he used

---

(3) Stair, R., & Johnston, R. G., "Preliminary Spectroradiometric Measurements of the Solar Constant", J. Res. NBS 57, No. 4, 205, (1956).

(4) Abbot, C. G., Fowle, F. E., & Aldrich, L. B., "The Distribution of Energy in the Spectra of the Sun and Stars," Smithsonian Misc. Coll., 74, No. 7, 15, (1923).

(5) Moon, P., "Proposed Standard Solar-Radiation Curves for Engineering Use," J. Franklin Inst., 230, 583, (1940).

values from Pettit[6].

In 1954, Johnson[1] applied the recent rocket findings to change the curve at wavelengths shorter than 0.318μ. He favored the data from Dunkelman & Skolnik[7] from 0.318 to 0.60μ, and took the data from Moon for the remainder of the spectrum.

Stair[3] et al, has measured the spectral distribution of the sun at Sunspot, N. M., and has obtained a curve whose shape is quite different from the older curves. The curves of Abbot, Moon, Johnson, and Stair are shown in Fig. 71.

The curve of Johnson has been selected as the best available data at this time. The Stair data has not been thoroughly substantiated, and the Moon and Smithsonian data are obsolete in the ultraviolet.

4.0 AIR MASS CONCEPT

The usual definition of "unity air mass" is the optical path length through the atmosphere at a solar elevation of 90° at sea level. Air mass, denoted by m, is computed from the cosecant of the solar elevation, i.e., solar elevation = 30°, m = 2. This definition is adequate for solar elevations from 15° to 90°. When working at a different altitude, such as Table Mountain, the correction has been assumed to be linear with barometric pressure[8]. For example, the mean barometric pressure on Table Mountain is 585 mm of Hg. For a solar elevation of 30° at M.S.L., the air mass reduction has been $\frac{585}{760}$,

---

(6) Pettit, E., "Measurements of Ultraviolet Solar Radiation," Astrop. J., 75, 185, (1932).

(7) Dunkelman, L., & Skolnik, R., "Solar Spectral Irradiance and Vertical Atmospheric Attenuation in the Visible and Ultraviolet," J. Opt. Soc. Amer. 49, 356, (1959).

(8) Solar Cell Measurement Standardization, Lockheed Aircraft Corp., Report LMSD-288184, 2-23, (1960).

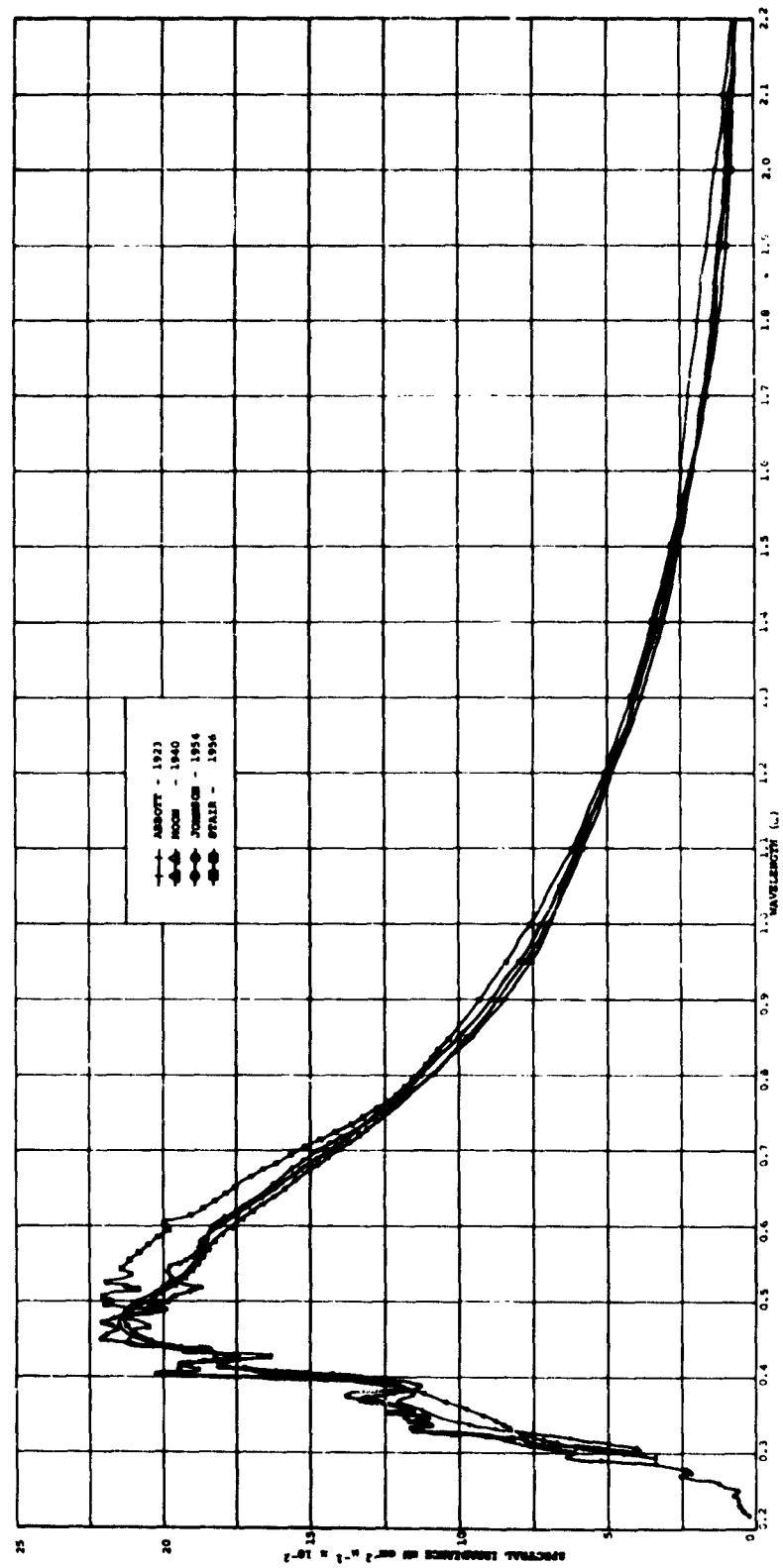

FIGURE 71 SPECTRAL DISTRIBUTION OF THE SUN IN SPACE

yielding a value of m = 1.54 for Table Mountain under these conditions. The foregoing assumes that the constituents in the atmosphere are equally distributed throughout the atmosphere. It is known that this assumption is false. For instance, ozone is primarily concentrated in a layer located approximately 30 kilometers above the earth's surface[9].

For the purpose of this work, it is necessary to retain the method used by the Smithsonian Institution on Table Mountain. By definition, $m_T = 1$ is the optical air mass with the sun at 90° elevation at Table Mountain, and $m_T = 2$ corresponds to a solar elevation of 30°. In this way, one can avoid the ambiguity of barometric pressure corrections.

5.0 ATMOSPHERIC SCATTERING

The direct radiation from the sun is attenuated principally by three atmospheric constituents; the air molecules, water vapor molecules, and dust particles. These effects will be discussed in order.

Moon[5] has shown that the atmospheric scattering transmission factor can be represented by the equation

$$\tau_{a\lambda} = 10^{-k_{a\lambda}} \qquad (1)$$

where $k_{a\lambda}$ is a function of wavelength. This equation is valid for Mt. Wilson, California (p = 623 mm of Hg). The values of $k_{a\lambda}$, which are shown in Table 4, are from Fowle[10] for Mt. Wilson. It has been assumed that the differences between the values of $k_{a\lambda}$ for Mt. Wilson and Table Mountain are negligible.

Scattering due to water vapor is of a similar nature to

---

(9) United States Air Force, Handbook of Geophysics, 8-5, Macmillan, (1960).

(10) Fowle, F. E., "Avogadro's Constant and Atmospheric Transparency," Astrop. J., 40, 435, (1914).

TABLE 4

ATMOSPHERIC SCATTERING COEFFICIENTS VS. WAVELENGTH[10]

ρ = 585 mm Hg

$\lambda\mu$	$k_{a\lambda}$	$\tau_{a\lambda}$	$\lambda\mu$	$k_{a\lambda}$	$\tau_{a\lambda}$
0.24	0.82	0.234	0.55	0.034	0.964
0.26	0.61	0.344	0.60	0.023	0.972
0.28	0.49	0.440	0.65	0.016	0.977
0.30	0.38	0.526	0.70	0.012	0.983
0.32	0.29	0.605	0.75	0.0093	0.986
0.34	0.22	0.677	0.80	0.0072	0.988
0.36	0.16	0.739	0.85	0.0055	0.990
0.38	0.14	0.791	0.90	0.0044	0.992
0.40	0.12	0.833	0.95	0.0034	0.994
0.42	0.098	0.869	1.00	0.0029	0.995
0.44	0.078	0.898	1.10	0.0020	0.996
0.46	0.066	0.920	1.20	0.0014	0.997
0.48	0.059	0.939	1.30	0.0010	0.997
0.50	0.046	0.953			

that of air molecules. The equation used is that from Fritz[11]:

$$\tau_\lambda = e^{-S_{w\lambda} W_{mt}} \qquad (2)$$

where: m_t = air mass

W = precipitable water vapor

and S_w = scattering factor = $0.00865\ \lambda^{-2}$

Since the occurrence of dust particles in the atmosphere is principally below elevations of 1000 m[5], its effect will be neglected here.

6.0 ATMOSPHERIC ABSORPTION

The principal absorption of solar radiant energy in the earth's atmosphere occurs in the ozone bands at short wavelengths and in the water vapor bands in the infrared. Ozone absorbs strongly at wavelengths shorter than 0.29μ and weakly in the Chappius band centered around 0.59μ[12]. Some typical values of ozone concentration in the southwest are:

Tucson, Arizona	-	1.8 mm[6]
Tucson, Arizona	-	2.0 mm[7]
Mt. Whitney, Calif.	-	1.8 mm[5]
Sunspot, N.M.	-	2.3 mm[3]
Sacramento Peak, N.M.	-	2.1 mm[3]
Mauna Loa, Hawaii	-	2.4 mm[13]

---

(11) Fritz, S., "Transmission of Solar Energy Through the Earth's Clear and Cloudy Atmosphere," Transactions of the Conference of The Use of Solar Energy, Vol. I, 17, (1955).

(12) Wulf, O. R., "The Determination of Ozone by Spectrobolometric Measurements," Smithsonian Misc. Coll. 85, No. 9, 9, (1931).

(13) Stair, R., & Johnston, R. G., "Some Studies of Atmospheric Transmittance on Mauna Loa," J. Res. NBS, 61, No. 5, 419, (1958).

List[14] gives a value of 2.5 mm as representative for the middle latitudes, and this is the value that is chosen here. The transmission coefficients are given by Wulf[12] and are shown in Table 5 along with the calculated transmissions for the chosen value of 2.5 mm.

The method employed for the calculation of water vapor absorption is by use of the Bouquer relationship as used by Moon. The quantity of water vapor in the atmosphere above the test site is measured by a monochromator fitted with a heliostat. The sun's image is partially focused at the monochromator entrance slit by means of the clock driven heliostat mirrors. The spectral distribution is plotted by an X-Y recorder. This method of spectral measurement is subject to errors from the standards used for calibration, the errors in the calibration process and errors from stray radiation. For these reasons, combined with the questionability of the actual sun spectrum, the measured spectrum is not used as the absolute test spectrum. The monochromator can, however, quite accurately measure the water vapor absorption bands. This measurement is used to determine the quantity is proportional to the transmission factors for water vapor plotted on a logarithmic scale.

The transmission factor for water vapor is shown in Fig. 72 (data from Fowle[15]). This data was given for a precipitable water vapor of 20 mm. The Bouquer law is used to vary the transmission factor such that it corresponds to the measured precipitable water vapor.

7.0 FINAL IRRADIATION CURVES

Data is now available for the calculation of solar spectral irradiance curves for Table Mountain conditions. There are:

---

(14) List, R. J., Ed., Smithsonian Meteorological Tables, 6th Rev. ed., p. 429, (1951).

(15) Fowle, F. E., "The Transparency of Aqueous Vapor," Astrop. J., 42, 394, (1915).

TABLE 5

ABSORPTION COEFFICIENT AND TRANSMISSION FOR OZONE[12]

2.5 mm LAYER

$\lambda\mu$	α	τ_λ	$\lambda\mu$	α	τ_λ
0.290	1.65	0.0000752	0.325	0.0180	0.901
0.291	1.46	0.000226	0.330	0.0092	0.949
0.292	1.29	0.000597	0.335	0.0048	0.973
0.293	1.11	0.00168	0.340	0.0025	0.986
0.294	1.00	0.00318	0.345	0.0013	0.992
0.295	0.89	0.00598	0.350	0.0008	0.995
0.296	0.79	0.0106			
0.297	0.70	0.0188	0.48		1.000
0.298	0.61	0.0298	0.49		0.999
0.299	0.52	0.0500	0.50		0.997
0.300	0.460	0.0705	0.51		0.995
0.301	0.405	0.0971	0.52		0.993
0.302	0.360	0.1261	0.53		0.989
0.303	0.315	0.1631	0.54		0.986
0.304	0.275	0.205	0.55		0.982
0.305	0.241	0.249	0.56		0.977
0.306	0.213	0.295	0.57		0.973
0.307	0.190	0.335	0.58		0.969
0.308	0.164	0.389	0.59		0.966
0.309	0.144	0.436	0.60		0.969
0.310	0.126	0.484	0.61		0.973
0.311	0.112	0.525	0.62		0.977
0.312	0.099	0.567	0.63		0.982
0.313	0.087	0.605	0.64		0.986
0.314	0.076	0.645	0.65		0.989
0.315	0.066	0.684	0.66		0.993
0.316	0.057	0.720	0.67		0.995
0.317	0.050	0.749	0.68		0.997
0.318	0.044	0.777	0.69		0.999
0.319	0.039	0.802	0.70		1.000
0.320	0.0345	0.820			

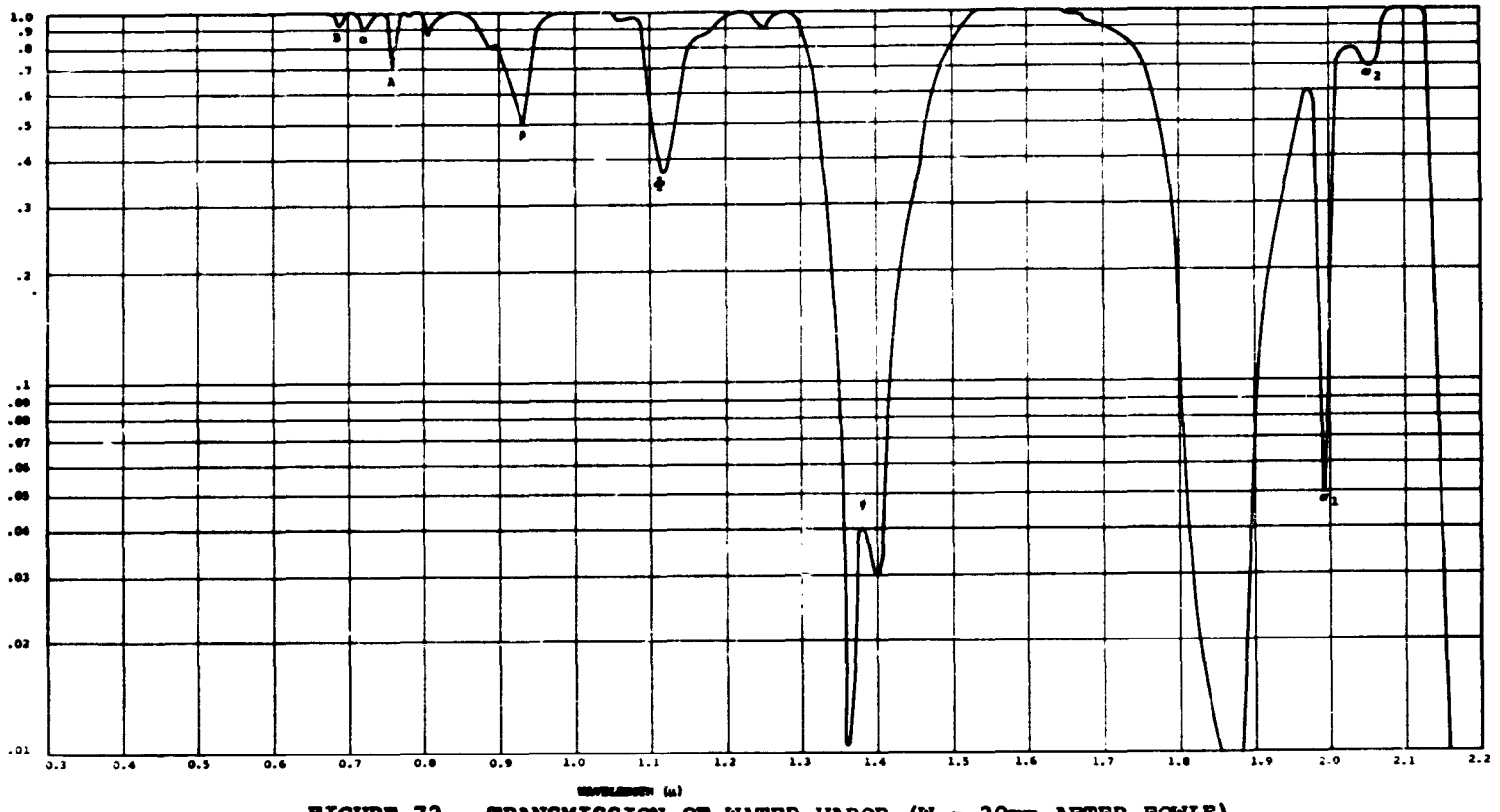

FIGURE 72 TRANSMISSION OF WATER VAPOR (W = 20mm AFTER FOWLE)

p = barometric pressure at time of test

w = inches of precipitable water at time of test

d = 0

O_3 = 2.5 mm

m_T = cosecant of solar elevation

Applying these factors to Johnson's curve of solar radiation yields the solar spectral irradiance for $m_T = 1$. The total transmission factor used to obtain the $m_T = 1$ curve is then multiplied by the $m_T = 1$ curve to obtain the $m_T = 2$ curve, corresponding to a solar elevation of 30°. Virtually all measurements on solar cell arrays are made between solar elevations of 30° and 90° so that these two curves will be sufficient. The final curves are shown in Fig. 73. Table 6 lists the values for $m_T = 1$ and $m_T = 2$.

As a check on the validity of these curves, the area underneath them was integrated, with the aid of a planimeter, yielding a power per unit area. Pyrheliometric observations at or near the solar elevations on typical days at Table Mountain have yielded values very near to the integrated curves. The curves have proven quite useful in predicting space power outputs for solar cells, as well as general curves representing Table Mountain.

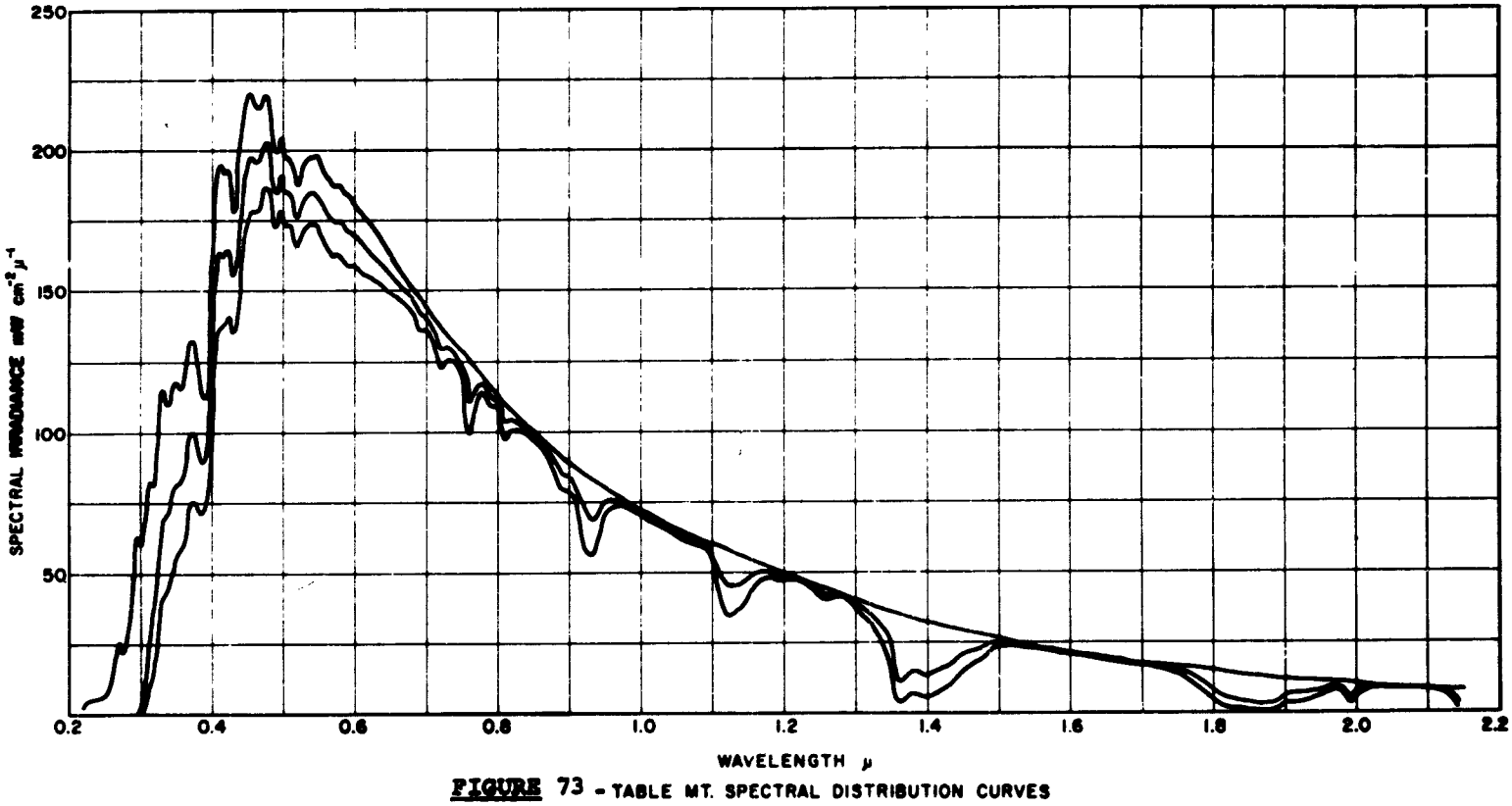

FIGURE 73 - TABLE MT. SPECTRAL DISTRIBUTION CURVES

TABLE 6

SOLAR SPECTRAL IRRADIANCE CURVES FOR TABLE MT., CALIF.

λ_μ	$H_{mt}=1$	$H_{mt}=2$	λ_μ	$H_{mt}=1$	$H_{mt}=2$	λ_μ	$H_{mt}=1$	$H_{mt}=2$
0.290	0	0	0.475	.2026	.1868	0.710	.1361	.1315
0.295	.0002	0	0.480	.1998	.1849	0.720	.1292	.1220
0.300	.0022	.0001	0.485	.1884	.1749	0.730	.1296	.1252
0.305	.0089	.0012	0.490	.1852	.1724	0.740	.1273	.1246
0.310	.0203	.0054	0.495	.1905	.1779	0.750	.1230	.1191
0.315	.0320	.0125	0.500	.1853	.1733	0.760	.1112	.0992
0.320	.0394	.0190	0.505	.1847	.1730	0.770	.1153	.1085
0.325	.0560	.0307	0.510	.1840	.1729	0.780	.1161	.1140
0.330	.0687	.0410	0.515	.1777	.1670	0.790	.1121	.1091
0.335	.0695	.0435	0.520	.1759	.1653	0.800	.1107	.1086
0.340	.0723	.0471	0.525	.1802	.1692	0.810	.1034	.0973
0.345	.0785	.0527	0.530	.1829	.1717	0.820	.1042	.1012
0.350	.0815	.0563	0.535	.1846	.1730	0.830	.1027	.1006
0.355	.0820	.0579	0.540	.1853	.1736	0.840	.1008	.0991
0.360	.0833	.0598	0.545	.1851	.1731	0.850	.0987	.0972
0.365	.0948	.0696	0.550	.1822	.1705	0.860	.0962	.0947
0.370	.0995	.0745	0.555	.1793	.1675	0.870	.0929	.0906
0.375	.0996	.0752	0.560	.1775	.1658	0.880	.0889	.0848
0.380	.0952	.0737	0.565	.1761	.1642	0.890	.0852	.0795
0.385	.0905	.0711	0.570	.1742	.1622	0.900	.0846	.0788
0.390	.0896	.0717	0.575	.1741	.1620	0.910	.0788	.0712
0.395	.0970	.0785	0.580	.1740	.1618	0.920	.0726	.0618
0.400	.1258	.1029	0.585	.1719	.1597	0.930	.0686	.0565
0.405	.1560	.1294	0.590	.1709	.1586	0.940	.0711	.0619
0.410	.1632	.1373	0.595	.1704	.1588	0.950	.0752	.0705
0.415	.1626	.1377	0.600	.1694	.1587	0.960	.0757	.0730
0.420	.1639	.1400	0.610	.1661	.1560	0.970	.0754	.0739
0.425	.1629	.1406	0.620	.1642	.1551	0.980	.0743	.0733
0.430	.1551	.1351	0.630	.1613	.1532	0.990	.0731	.0725
0.435	.1595	.1398	0.640	.1586	.1514	1.00	.0719	.0713
0.440	.1792	.1584	0.650	.1552	.1488	1.01	.0701	.0696
0.445	.1909	.1694	0.660	.1530	.1471	1.02	.0686	.0681
0.450	.1969	.1761	0.670	.1499	.1449	1.03	.0671	.0666
0.455	.1972	.1778	0.680	.1466	.1422	1.04	.0658	.0653
0.460	.1959	.1776	0.690	.1418	.1360	1.05	.0643	.0634
0.465	.1958	.1783	0.700	.1401	.1365	1.06	.0629	.0617
0.470	.1987	.1820						

TABLE 6 (Cont'd.)

λ_μ	$H_{mt}=1$	$H_{mt}=2$	λ_μ	$H_{mt}=1$	$H_{mt}=2$	λ_μ	$H_{mt}=1$	$H_{mt}=2$
1.07	.0619	.0608	1.43	.0173	.0097	1.79	.0101	.0066
1.08	.0612	.0603	1.44	.0198	.0130	1.80	.0085	.0048
1.09	.0605	.0597	1.45	.0213	.0153	1.81	.0062	.0025
1.10	.0547	.0493	1.46	.0223	.0171	1.82	.0058	.0023
1.11	.0498	.0417	1.47	.0230	.0186	1.83	.0052	.0019
1.12	.0452	.0350	1.48	.0238	.0204	1.84	.0048	.0016
1.13	.0455	.0362	1.49	.0252	.0234	1.85	.0044	.0014
1.14	.0462	.0380	1.50	.0253	.0240	1.86	.0041	.0012
1.15	.0482	.0422	1.51	.0252	.0244	1.87	.0041	.0012
1.16	.0498	.0458	1.52	.0250	.0246	1.88	.0042	.0013
1.17	.0503	.0476	1.53	.0248	.0246	1.89	.0049	.0018
1.18	.0500	.0480	1.54	.0244	.0243	1.90	.0072	.0040
1.19	.0491	.0472	1.55	.0239	.0238	1.91	.0074	.0043
1.20	.0490	.0479	1.56	.0235	.0234	1.92	.0075	.0046
1.21	.0486	.0481	1.57	.0231	.0230	1.93	.0079	.0051
1.22	.0479	.0476	1.58	.0227	.0226	1.94	.0083	.0057
1.23	.0467	.0462	1.59	.0223	.0222	1.95	.0088	.0066
1.24	.0452	.0443	1.60	.0219	.0218	1.96	.0097	.0082
1.25	.0437	.0423	1.61	.0215	.0214	1.97	.0100	.0088
1.26	.0426	.0411	1.62	.0211	.0210	1.98	.0093	.0077
1.27	.0425	.0416	1.63	.0207	.0206	1.99	.0062	.0035
1.28	.0422	.0420	1.64	.0203	.0202	2.00	.0080	.0059
1.29	.0409	.0403	1.65	.0199	.0198	2.01	.0093	.0082
1.30	.0389	.0371	1.66	.0194	.0192	2.02	.0096	.0089
1.31	.0373	.0349	1.67	.0187	.0183	2.03	.0096	.0090
1.32	.0357	.0326	1.68	.0183	.0178	2.04	.0093	.0085
1.33	.0329	.0284	1.69	.0180	.0174	2.05	.0090	.0081
1.34	.0302	.0244	1.70	.0177	.0171	2.06	.0094	.0090
1.35	.0237	.0154	1.71	.0173	.0167	2.07	.0095	.0094
1.36	.0116	.0039	1.72	.0169	.0161	2.08	.0095	.0095
1.37	.0132	.0049	1.73	.0165	.0156	2.09	.0093	.0093
1.38	.0152	.0068	1.74	.0160	.0150	2.10	.0092	.0092
1.39	.0145	.0063	1.75	.0154	.0141	2.11	.0090	.0090
1.40	.0136	.0056	1.76	.0147	.0131	2.12	.0088	.0088
1.41	.0151	.0071	1.77	.0136	.0114	2.13	.0077	.0068
1.42	.0167	.0088	1.78	.0117	.0086	2.14	.0048	.0027

Aeronautical Systems Division, Dir/Aerome-chanics, Flight accessories Lab, Wright-Patterson AFB, Ohio.
Rpt Nr ASD-TDR-62-882. SOLAR ENERGY MEASUREMENT TECHNIQUES. Final report, Jan 63, 167p. incl illus., tables, 56 refs.

Unclassified Report

This report describes a broad investigation which has been made of the subject of solar cell measurements. A portable tester has been designed and built which will enable an operator to determine the output of a solar cell power supply in space by analyzing output under conditions existing at either laboratory or field test sites. Painstaking

(over)

experimentation and analysis of many alternatives has resulted in recommended optimum instrumentation and procedures for measuring solar cells and for performing the calibrations required. Calibrated primary standard solar cells have been provided in terms of their absolute spectral response. Data has been accumulated on the operational parameters of many solar cells using optimized measurement procedures.

1. Solar energy
2. Cell measurement techniques
3. Portable testers
I. AFSC Project 8173, Task 817301-12
II. Contract AF 33 (616)-7946
III. Hoffman Electronics Corp., El Monte, Calif.
IV. Dr. B. Ross, D. B. Bickler
V. Aval fr OTS
VI. In ASTIA collection

Aeronautical Systems Division, Dir/Aerome-chanics, Flight accessories Lab, Wright-Patterson AFB, Ohio.
Rpt Nr ASD-TDR-62-882. SOLAR ENERGY MEASUREMENT TECHNIQUES. Final report, Jan 63, 167p. incl illus., tables, 56 refs.

Unclassified Report

This report describes a broad investigation which has been made of the subject of solar cell measurements. A portable tester has been designed and built which will enable an operator to determine the output of a solar cell power supply in space by analyzing output under conditions existing at either laboratory or field test sites. Painstaking

(over)

experimentation and analysis of many alternatives has resulted in recommended optimum instrumentation and procedures for measuring solar cells and for performing the calibrations required. Calibrated primary standard solar cells have been provided in terms of their absolute spectral response. Data has been accumulated on the operational parameters of many solar cells using optimized measurement procedures.

1. Solar energy
2. Cell measurement techniques
3. Portable testers
I. AFSC Project 8173, Task 817301-12
II. Contract AF 33 (616)-7946
III. Hoffman Electronics Corp., El Monte, Calif.
IV. Dr. B. Ross, D. B. Bickler
V. Aval fr OTS
VI. In ASTIA collection